Canada - Ontario Mineral Development Agreement

Entente Canada - Ontario sur l'exploration minérale

Canada

Ontario

CANADA - ONTARIO

MINERAL DEVELOPMENT AGREEMENT

SIMULATION OF BULK MINING AT DEPTH WITH BACKFILL IN ONTARIO MINES

Final Report - Volume 2

MATHEMATICAL FORMULATION AND CODE DEVELOPMENT

by

Mines Research Department
INCO Limited

March, 1991

198pp

Work on the project was conducted under the auspices of Canada Centre for Mineral and Energy Technology, Energy, Mines and Resources Canada under the Canada/Ontario Mineral Development Agreement.

DSS File No. 14SQ.23440-6-9033
DSS Contract Serial No. 23440-6-9033/01-SQ
CANMET Project No. 6-9033
CANMET Scientific Authority: Y.S. Yu

MICROMEDIA

ABSTRACT

This report details the mathematical formulations developed for the implementation of localized plastic behaviour and multiple material behaviour into the boundary element technique. The report presents the findings of investigations on the suitability of various representations for these components in a three-dimensional formulation. The development was first conducted for a two-dimensional formulation which was embodied in the numerical program MINE2D. The findings from testing of this development were then used as a basis for the three-dimensional formulation and development of program MINE3D. Testing was then performed on the three-dimensional components. Example analyses are presented which demonstrate the accuracy of each of the various formulations in MINE2D and MINE3D.

Continuous, piecewise linear strength elements were required rather than discontinuous, constant strength elements because constant elements were found to behave poorly for large plastic deformations, whereas linear elements demonstrated reasonable accuracy and behaved well for plastic yield. The use of linear elements necessitated the implementation of a special algorithm to handle the singular surface stress integral at surface nodes. For the three-dimensional formulation, an offset node algorithm was developed which calculates the integral at a small distance from the surface node measured along the average normal at the node.

The elastoplastic character of the medium was modelled using an initial stress formulation. This was found to be a reasonable scheme provided that only very localized regions of plastic yield are analyzed. The approach requires extensive discretization or higher-order elements to provide an accurate calculation for displacement fields involving large-scale plastic collapse. This, however, is not feasible for three-dimensional analysis within present computer memory constraints.

Different algorithms were investigated to model multiple materials. In two dimensions, volume elements were used to represent different materials as well as plastic regions. A more efficient approach was developed for the three-dimensional formulation whereby different materials were treated as separate boundary element domains with interactions only through their boundaries.

Finally, the development of the three-dimensional formulation in MINE3D required a significant variation from the two-dimensional formulation in order to reduce storage requirements for the boundary element coefficients. The conventional formulation used in MINE2D would use an enormous amount of computer memory if extended to a three-dimensional formulation for plasticity, making the solution of mine-scale size problems essentially impossible for computer hardware systems typically available to mining organizations. An alternative approach, used for MINE3D, was to restrict the geometric shape of the boundary elements to

parallelepiped shapes. This results in a significant reduction in the memory requirement. Unfortunately, an investigation of typical hardware systems found that even for the parallelepiped scheme, present systems have a substantial degradation of performance rate when accessing the required memory for coefficient storage. The consequence of this finding is that the size of problem which can be solved with the three-dimensional formulation in MINE3D is still quite restrictive (smaller than approximately 2000 boundary element nodes). MINE3D can only be used on a practical basis when larger core memory or faster disk hardware becomes available.

RÉSUMÉ

Ce rapport présente les formulations mathématiques développées pour le couplage de la technique des éléments frontières avec le comportement plastique de matériau et la modélisation de matériaux multiples. Ce rapport présente aussi les résultats de recherches sur les représentations appropriées de ces techniques dans le cadre d'une formulation en trois dimensions. Le développement fut tout d'abord réalisé pour une formulation en deux dimensions, à savoir de programme MINE2D. Les résultats des tests de ce programme ont servit de bases pour la formulation en trois dimensions, et ont conduit au développement du programme MINE3D, puis aux tests de celui-ci. Des exemples d'analyses sont présentés, lesquels démontrent la pertinence de chacune des deux formulations de MINE2D et MINE3D.

Des éléments à la résistance linéaire continue par intervalle ont été utilisés plutôt que des éléments à la résistance discontinue et constante par intervalle, ceux-ci n'étant pas satisfaisants pour représenter les larges déformations plastiques, au contraire des premiers plus précis. L'utilisation de ces éléments a nécessité le développement d'un algorithme particulier permettant de tenir compte de la singularité des contraintes aux noeuds de surface. Pour le cas de la formulation en trois dimensions, un algorithme de reject de noeud a été développé pour calculer l'intégrale à une courte distance de noeud de surface mesurée le long de la normale moyenne au noeud.

L'élastoplasticité du milieu a été modélisée par une formulation du type de contraintes initiales. Cette approche est justifée dès que l'analyse plastique porte sur des régions trés localisées. Elle requiert néanmoins une discrétisation trés élévée ou des éléments d'un ordre supérieur pour permettre un calcul précis dans le cas de champs de déplacements impliquant une plasticité de grande échelle. Ceci n'est cependant pas possible dans une analyse en trois dimensions sans problème de mémoire d'ordinateur.

Plusieurs algorithmes ont été envisagés pour modéliser les matériaux multiples. En deux dimensions, des éléments de volume ont été utilisés pour représenter tant les différents matériaux que les régions plastiques. Une méthode plus efficace a été développée pour la formulation tridimensionnelle, dans laquelle les différents matériaux ont été représentés comme autant de domaines d'éléments frontières distincts, interagissant seulement au travers de leur frontières.

Finalement, de développement de la formulation tridimensionnelle de MINE3D a nécessité des changements significatifs de la formulation bidimensionnelle, afin de minimiser la mémoire allouée aux coefficients des éléments frontières. La formulation conventionnelle de MINE2D, étendue à MINE3D, serait prohibitive en terme de mèmoire d'ordinateur, rendant impossible la modélisation de problèmes à l'échelle d'une mine pour le type d'ordinateurs usuel aux mines. Une alternative fut de restreindre la forme

géométrique des éléments frontières à celle de parallépipèdes. Le résultat fut une réduction trés signifcative de la mémoire requise. Néammoins, un examen des systèmes d'ordinateurs montra que même cette alternative réduisait encore largement les performances par la mémoire importante toujours requise.

La conséquence de ce résultat est que la taille d'un problème qui peut être étudié par la formulation tridimensionnelle de MINE3D est encore trés restrictive (inférieure à environ 2000 noeuds d'éléments frontières). MINE3D pourra seulement être utilisé sur une base pratique guand des mémoires plus étendues ou disques plus rapides seront disponibles.

PREFACE

This project entitled "Simulation of Bulk Mining at Depth in Ontario Mines with Backfill" consists of two major components: the development of a numerical model, and field verification of the model. The project, which began in 1986, was expected to take four years ending in September 1990 but was extended until March 1991. This report is the second of six volumes which describes the results of the project.

The work was initiated by INCO Limited and is partially funded through the MDA Program (joint Canada-Ontario Mineral Development Agreement, DSS file 14SQ.23440-6-9033). The project is administered by Canmet and their assistance is greatly appreciated.

NOMENCLATURE

A_{ij}^{q}	global to local coordinate transformation matrix for point q
A_{ij}^{qp}	global to local coordinate rotation matrix for face p of element q
C_{ijk}	fundamental singular solution for stresses (due to a point force)
$C_{ijk}^{'}$	fundamental singular solution for stresses due to a displacement discontinuity
Cd	Green's function for stresses due to displacement discontinuity
Cd_{ijk}^{q}	Green's function for stresses due to displacement discontinuity at point q
Cd_{ijk}^{qp}	Green's function for stresses at point p due to displacement discontinuity at point q
$Cd_{ijk}^{'qp}$	Green's function for stresses at point p due to displacement discontinuity at point q in local coordinates
$Cd_{ijk}^{'qp}$	Green's function for stresses due to surface forces
Cs_{ijk}^{q}	Green's function for stresses due to surface forces at point q
Cs_{ijk}^{qp}	Green's function for stresses at point p due to surface forces at point q
$Cs_{ijk}^{'qp}$	Green's function for stresses at point p due to surface forces at point q in local coordinates
Cv	Green's function for stresses due to initial stresses
Cv_{ijk}^{q}	Green's function for stresses due to initial stresses at point q
Cv_{ijk}^{qp}	Green's function for stresses at point p due to initial stresses at point q
$Cv_{ijk}^{'qp}$	Green's function for stresses at point p due to initial stresses at point q in local coordinates
C_{o}	uniaxial compressive strength
C_{o}	peak uniaxial compressive strength
C_{o}	residual uniaxial compressive strength
d	prefix indicating increment in value
$D_{Interface}$	elastic stress-strain relations for interface material
e	permutation symbol
E	Young's modulus
g_{ij}	fundamental singular solution for displacements (due to a point force)
$g_{ijk}^{'}$	fundamental singular solution for displacements due to a displacement discontinuity
G	Shear modulus
Gb_{ij}^{qp}	Green's function for displacements at point p due to body forces at point q
$Gb_{ij}^{'qp}$	Green's function for displacements at point p due to body forces at point q in local coordinates
Gd	Green's function for displacements due to displacement discontinuity
Gd_{ij}^{q}	Green's function for displacements due to displacement discontinuity at point q
Gd_{ij}^{qp}	Green's function for displacements at point p due to displacement discontinuity at point q

Gd'^{qp}_{ij}	Green's function for displacements at point p due to displacement discontinuity at point q in local coordinates
Gs	Green's function for displacements due to surface forces
Gs^{q}_{ij}	Green's function for displacements due to surface forces at point q
Gs^{qp}_{ij}	Green's function for displacements at point p due to surface forces at point q
Gs'^{qp}_{ij}	Green's function for displacements at point p due to surface forces at point q in local coordinates
Gv	Green's function for displacements due to initial stresses
Gv^{q}_{ij}	Green's function for displacements due to initial stresses at point q
Gv^{qp}_{ij}	Green's function for displacements at point p due to initial stresses at point q
Gv'^{qp}_{ij}	Green's function for displacements at point p due to initial stresses at point q in local coordinates
I	identity matrix
	superscript indicating state I
	superscript indicating state II
M	total number of nodal points
N	total number of nodal points
N^{0qp}	coefficients for a constant variation due to a distribution over element q at point p
N^{1qp}	coefficients for a linear variation due to a distribution over element q at point p
N^{2qp}	coefficients for a quadratic variation due to a distribution over element q at point p
p	normal surface stress
p'	normal surface stress acting on an elastic-plastic interface
p_i	normal surface stress acting on an internal surface
p'_i	normal surface stress acting on an elastic-plastic interface
p_o	far field stress
P	surface force
q	parameter in the Mohr-Coulomb failure criterion
Q	plastic potential function
Q_o	strength parameter
r	subscript indicating radial component
r	radial position
R	radius of excavation surface
R'	radius of elastic-plastic interface
R''	radius of elastic-plastic interface
s	surface region indicating excavation surfaces
s'	surface region indicating fault surfaces
S_o	cohesion
S_o	peak cohesion
S_o	residual cohesion
t^q	surface stress components in local coordinates
T_o	tensile strength
T_o	peak tensile strength
T_o	residual tensile strength
tan	tangent function
u	displacement

v	volumetric region
V	volume
V_m	volume excavated
W_b	energy used in the deformation of backfill
W_c	change in stored elastic strain energy
W_e	work done during the deformation surfaces due to loads in excess of the support pressure
W_f	plastic work done during fault slip
W_k	excess energy
W_p	work done in plastic deformation of material
W_s	work done during the deformation of surfaces due to support pressure
W_t	total visco-plastic work done
W_v	work done is viscous deformation of material
X	rigid body displacements
z	coordinate in volumetric region
o	superscript indicating state 0
β	dilation rate
Γ	displacement discontinuity
γ	viscous parameter
γ_1	linear viscous parameter
γ_2	quadratic viscous parameter
δ	Kronecker delta
δ^{qp}	substitution tensor
Δ	prefix indicating change in value
ϵ_{ij}	total strain
ϵ^0_{ij}	initial strain
λ	parameter
ν	Poisson's ratio
θ	angle of solid material
ξ	cartesian coordinate
π	pi
σ	stress
σ'	stress component due to frictional element
σ^o	initial stress
σ^T	pre-existing field stress in host material
$\sigma^{T'}$	pre-existing field stress in host material in local coordinates
σ_{Host}	pre-existing field stress in host material
$\sigma_{Interface}$	pre-existing field stress in interface material
σ^p	stress state in the host material at point p
Σ	symbol indicating summation
ϕ	surface force or friction angle
ϕ'	peak friction angle
ϕ''	residual friction angle
Φ	elastic strain energy density
ψ	body force
∂	differential

TABLE OF CONTENTS

		page
1.0	INTRODUCTION	1-1
2.0	GENERAL THEORETICAL BASIS.	2-1
	2.1 Initial Stresses - Strain Suppression	2-1
	2.2 Indirect Boundary Element Method.	2-3
	2.2.1 Constant Strength Surface Elements - Field Stresses	2-5
	2.2.2 Constant Strength Surface Elements - Boundary Stresses.	2-7
	2.3 Discretization of Integrals for Discontinuous, Constant Strength, Initial Stresses	2-8
	2.3.1 Constant Strength Interior Elements - Field Stresses	2-8
	2.3.2 Constant Strength Interior Elements - Boundary Stresses.	2-11
	2.3.3 Suitability of Constant Strength Interior Elements	2-13
	2.4 Discretization of Integrals for Continuous, Piecewise Linear Strength, Initial Stresses	2-13
	2.4.1 Linear Strength Interior Elements - Field Stresses	2-14
	2.4.2 Linear Strength Interior Elements - Boundary Stresses.	2-18
	2.4.3 Suitability of Linear Strength Interior Elements	2-18
	2.5 Evaluation of Integrals for Singular Points	2-19
	2.6 The Theory of Incremental Plasticity.	2-20
	2.6.1 Strength of Material - Failure Criterion	2-21
	2.6.2 Dilation of Material - Plastic Potential Function	2-22
	2.6.3 Details of Plastic Behaviour	2-24
	2.7 Plasticity in the Boundary Element Method	2-28
	2.7.1 Stress-Strain Characteristics of Internal Elements	2-28
	2.7.2 Plastic Solution Technique	2-29
3.0	TWO-DIMENSIONAL FORMULATION (Program MINE2D)	
	3.1 Introduction.	3-1
	3.2 Quadrilateral Elements.	3-1
	3.3 Corners	3-3
	3.4 Multiple Materials.	3-8
	3.5 Backfill Placement - Mining Steps	3-10
	3.6 Elasto-Visco-Plastic Behaviour.	3-13
	3.6.1 Elasto-Visco-Plastic Theory.	3-13
	3.6.2 Elasto-Visco-Plastic Examples.	3-15
	3.7 Fault Slip - Seam Mining Simulation	3-18
	3.7.1 Displacement Discontinuities	3-18
	3.7.2 Strength of Material - Failure Criterion	3-21
	3.7.3 Details of Plastic Behaviour	3-24
	3.7.4 Gouge or Seam Material	3-25

TABLE OF CONTENTS (continued)

page

3.8 Displacements 3-27
3.9 Energy Release. 3-30
3.9.1 Work Done on the Surface of the Elastic Host Material. 3-31
3.9.2 Work Done on Displacement Discontinuities. 3-34
3.9.3 Work Done on Volume Element. 3-35
3.10 Verification Analyses 3-36
3.10.1 Square-shaped Drift. 3-37
3.10.2 Two Rectangular Drifts with a Weak Pillar. 3-39
3.10.3 Circular Tunnel in a Homogeneous Stress Field. 3-47

4.0 THREE-DIMENSIONAL FORMULATION (PROGRAM MINE3D)
4.1 Introduction. 4-1
4.2 Overview of Basic Equations 4-1
4.2.1 Equations for Elastoplasticity 4-2
4.2.2 Discretization: Parallelepiped Grid. . . . 4-4
4.2.3 Boundary Element Approximation: Linear Elements. 4-5
4.2.4 System of Equations. 4-6
4.3 Evaluation of Integrals 4-6
4.3.1 Saving Scheme: Parallelepiped Grid 4-6
4.3.2 Numerical Integration. 4-8
4.3.3 Handling of Corners. 4-10
4.4 Plasticity Formulation. 4-12
4.5 Multiple Materials. 4-16
4.5.1 Principle of Solution. 4-16
4.6 Sequential Mining 4-17
4.6.1 Mining Steps and Plasticity. 4-17
4.7 Solution Process. 4-18
4.7.1 Algorithm of Resolution. 4-19
4.7.2 Method of Solution: Successive Overrelaxation (SOR) 4-20
4.8 Energy Release. 4-20
4.8.1 Case 1: Elastic Host Rock 4-20
4.8.2 Case II: Elastic Host Rock Mass, Excavation Occurs in Plastic Material. . . 4-24
4.9 Verification Analyses 4-29
4.9.1 Square-shaped Drift. 4-30
4.9.2 Rectangular Drifts Separated by a Weak Pillar 4-43
4.9.3 Destress Slot in Large Crown Pillar. . . . 4-57
4.10 Computer Hardware and Run Time Assessment 4-65
4.10.1 Coefficient Storage Requirements 4-65
4.10.2 Run Time Evaluation. 4-67
4.10.3 Speed Enhancement Studies. 4-68
4.11 Conclusions and Recommendations 4-69

TABLE OF CONTENTS (continued)

		page
5.0	REFERENCES	5-1
6.0	APPENDICES	
	APPENDIX I — Point Force Applied in an Infinite Medium	
	APPENDIX II — Distributed Forces in an Infinite Medium	
	APPENDIX III — Coordinate Transformation	
	APPENDIX IV — Shape Functions for Linear Variation	
	APPENDIX V — Corners and Edges of Potemtial Functions	
	APPENDIX VI — Indicial Notation	
	APPENDIX VII — Green's Function - Displacement Discontinuity	

LIST OF FIGURES

		page
Figure 2-1	Isotropic, linear elastic, homogeneous region v with an enclosed surface s.	2-3
Figure 2-2	Discretized body.	2-9
Figure 2-3	Failure envelope.	2-21
Figure 3-1	Triangular Elements.	3-2
Figure 3-2	Corners.	3-4
Figure 3-3	Corner Singularity.	3-5
Figure 3-4	Singular and Linear Force Distributions.	3-5
Figure 3-5	Total Applied Surface Forces.	3-7
Figure 3-6	Elasto-Plastic Behaviour.	3-9
Figure 3-7	Mining With Backfill - Excavate Block 1.	3-11
Figure 3-8	Mining With Backfill - Excavate Block 2.	3-11
Figure 3-9	Mining With Backfill - Backfill Block 1.	3-12
Figure 3-10	Elasto-Visco-Plastic Element.	3-14
Figure 3-11	Convergence To Static Equilibrium.	3-18
Figure 3-12	Isotropic, linear elastic, homogeneous region v with an enclosed excavation surface s and interface surface s'.	3-19
Figure 3-13	Failure envelope.	3-22
Figure 3-14	A general mining example.	3-30
Figure 3-15	The boundary of the elastic host material.	3-32
Figure 3-16	Square-shaped Drift.	3-38
Figure 3-17a	Principal Stresses on the x_1 Axis for a Square-shaped Drift.	3-38
Figure 3-17b	Plastic Strain on the x_1 Axis for a Square-shaped Drift.	3-38
Figure 3-18	Two Rectangular Drifts with a Wide Pillar, Height:Width = 0.5.	3-39

LIST OF FIGURES (continued)

		page
Figure 3-19	Two Rectangular Drifts with a Square Pillar, Height:Width = 1	3-40
Figure 3-20	Two Rectangular Drifts with a Narrow Pillar. Height:Width = 2.	3-40
Figure 3-21a	Principal Stresses at Mid-Height of a Wide Pillar, Height:Width = 0.5.	3-41
Figure 3-21b	Plastic Strain at Mid-Height of a Wide Pillar, Height:Width = 0.5.	3-41
Figure 3-22a	Principal Stresses at Mid-Height of a Square Pillar, Height:Width = 1.	3-42
Figure 3-22b	Plastic Strain at Mid-Height of a Square Pillar, Height:Width = 1.	3-42
Figure 3-23a	Principal Stresses at Mid-Height of a Narrow Pillar, Height:Width = 2.	3-43
Figure 3-23b	Plastic Strain at Mid-Height of a Narrow Pillar, Height:Width = 2.	3-43
Figure 3-24	Major Principal Stress at Mid-Height of a Square Pillar, Height:Width = 1.	3-45
Figure 3-25	Major Principal Stress at the Centre of a Square Pillar, Height:Width = 1.	3-46
Figure 3-26	Circular tunnel discretization.	3-52
Figure 3-27	Principal stresses around a circular tunnel.	3-53
Figure 3-28	Plastic strains around a circular tunnel.	3-55
Figure 3-29	Displacements around a circular tunnel.	3-55
Figure 4-1	Elastic Medium, D, with Local Plastic Regions, V, and Excavations Bounded by S.	4-2
Figure 4-2	Parallelepiped Grid.	4-4
Figure 4-3	Coefficient Matrix Size versus Number of Boundary Element Nodes.	4-9
Figure 4-4	Loading History for an Elastic Spring and Elastoplastic Rod.	4-18
Figure 4-5	Mining Configuration and Notations in the Reference State.	4-21

LIST OF FIGURES (continued)

		page
Figure 4-6	Boundary Description for Case In Which Yielding Material Can Occur.	4-24
Figure 4-7	Internal Discretized Region Loaded at Boundary by Elastic Host Rock.	4-26
Figure 4-8	Mining Configuration and Notations in the Reference State.	4-26
Figure 4-9	Illustration of Work Done on Compression of Backfill.	4-28
Figure 4-10	MINE3D Models for Square-Shaped Drift.	4-31
Figure 4-11	Tangential Boundary Stress Around Tunnel.	4-33
Figure 4-12	FLAC Model of Square Drift.	3-34
Figure 4-13	Stresses Along A - A′.	4-35
Figure 4-14	Stresses Along C - C′.	4-36
Figure 4-15	Y-Displacements Along B - B′.	4-36
Figure 4-16	X-Displacements Along B - B′.	4-37
Figure 4-17	Displacements Along C - C′.	4-37
Figure 4-18	Stresses Along A - A′.	4-38
Figure 4-19	Stresses Along C - C′.	4-39
Figure 4-20	Y-Displacements Along B - B′.	4-40
Figure 4-21	X-Displacements Along B - B′.	4-41
Figure 4-22	Displacements Along C - C′.	4-42
Figure 4-23	Pillar Between Two Stopes.	4-44
Figure 4-24	FLAC Model of Rectangular Drifts Separated by a Weak Pillar.	4-45
Figure 4-25	Stresses Along O - O′.	4-47
Figure 4-26	Displacements Along B - B′ and C - C′.	4-48
Figure 4-27	Displacements Along A - A′.	4-49
Figure 4-28	Stresses Along O′- O" for Two Mining Steps.	4-50

LIST OF FIGURES (continued)

		page
Figure 4-29	Displacements Along B - B′ and C - C′ for Two Mining Steps.	4-50
Figure 4-30	Displacements Along A - A′ for Two Mining Steps.	4-51
Figure 4-31	Stresses Along B - B′ and C - C′ in Stopes 1 & 2.	4-53
Figure 4-32	Displacements Along A - A′ in Stope 1.	4-54
Figure 4-33	Volume Nodes Where Failure Limit Has Been Reached.	4-55
Figure 4-34	Total Displacement Vectors at End of Each Mining Step.	4-56
Figure 4-35	MINE3D Model of Destress Slot in Large Crown Pillar.	4-58
Figure 4-36	3DEC Model of Destress Slot in Large Crown Pillar.	4-59
Figure 4-37	Displacement Vectors on Horizontal Plane through Destress Slot.	4-61
Figure 4-38	Displacement Vectors on Vertical Plane through Destress Slot.	4-62
Figure 4-39	Principal Stresses on Horizontal Plane through Destress Slot.	4-63
Figure 4-40	Principal Stresses on Vertical Plane through Destress Slot.	4-64
Figure 4-41	Comparison of MINE3D Iteration Rate versus Number of Surface Nodes.	4-68

LIST OF TABLES

		page
Table 3-1	Singularities.	3-6
Table 3-2	Summary of Energy Contributions.	3-31
Table 3-3	Properties used in the Analysis Examples.	3-37
Table 3-4	Properties for the Circular Tunnel Example.	3-53
Table 3-5	Results from MINE2D and from Analytical Calculations.	3-54
Table 4-1	Influence of Corner Offset Factor.	4-12
Table 4-2	Properties Used in MINE3D Analysis Examples.	4-30

1.0 INTRODUCTION

Numerical modelling is the process of simulating rock mass behaviour with mathematical equations. It permits the prediction of displacements, strains, stresses and failure zones at any location. The stabilizing effect of various backfill options can be compared. It does not specify how to design, but it does provide the ability to compare the stability and safety of proposed alternative mining layouts. Potential problems may be identified in advance of mining for safer and more cost effective layouts. It provides the ability to apply rock mechanics design principles quantitatively. The problem is to correctly predict the behaviour of the rock in response to mining.

Bulk mining in massive ore bodies creates stopes, pillars and mine workings which form a complex arrangement of three-dimensional excavations. In deep mining, pillar failures and failure zones around openings are a fact of life. If the numerical modelling is to be effective, it must be able to deal with failure in a realistic manner. It must identify areas where failure should occur, then reduce the strength of the failed areas and transfer the excess stress to intact areas. The results of this modelling will depend on how well failure is simulated.

Pillar strength is heavily dependant on the degree of confinement provided by the fill. This is particularly evident in post failure states where even modest confining pressures can limit the dilation necessary for pillar yielding. Experience has clearly indicated that fill confinement can also influence the nature of pillar failures by reducing or eliminating violent failures.

Failure zones are not confined to pillars and abutments but have also been observed at large distances away from mine openings. This type of failure is often observed as a series of localized shear bands spanning the limits of mining.

To properly simulate the behaviour of bulk mining at depth, it is therefore necessary to use three-dimensional modelling. The actual physical shapes of the openings must be accounted for to properly model their interaction. In addition, the non-elastic behaviour of the rock, ore and backfill must be incorporated if realistic results are to be obtained.

The development of the boundary element modelling method to include the simulation of the failed zones around mined openings is discussed in this report. This development gives the model the ability to accommodate multiple stope layouts, with openings of regular shape. Pillar failures, as well as the interaction of yielding pillars with backfill, will be accommodated. For example, the areas around the openings, including the pillars, could fail plastically. By modelling the backfill with elasto-plasticity as

well, the interaction of the pillar failure and the response of the backfill would be accommodated.

This development is embodied in the three-dimensional code MINF3D. This code has two distinguishing features: (1) the ability to simulate localized regions of plastic yield within an elastic continuum; and (2) the capability to model interacting regions of different material types, thus allowing the simulation of backfill emplacement. The theoretical basis for this development and the capabilities and limitations of MINE3D are discussed in this report.

2.0 GENERAL THEORETICAL BASIS

The individual topics pertaining to boundary element modelling and material plasticity are described in this section. These topics cover the general research areas for the theoretical development of plasticity in the boundary element method.

2.1 Initial Stresses - Strain Suppression

'Plastic' behaviour of solids is characterized by a non-unique stress-strain relationship. Complex constitutive relations supersede the simple linear elasticity assumptions normally associated with the boundary element method. To incorporate the general case of plasticity requires that the body be deformed according to prescribed constitutive relations which may be a function of the current stress or strain state. This can be accommodated by superposing initial stresses, due to permanent plastic deformations, on the body. The method of strain suppression can be utilized to determine the body and surface forces necessary to induce the permanent set. The following discussion follows that given by Timoshenko and Goodier (1970).

Consider a body subdivided into small elements and suppose that each of these elements undergoes a certain plastic deformation or change in shape produced by inelastic deformation. Let this plastic deformation be defined by the strain components

$$\epsilon^{\circ}_{ij} \qquad (2.1\text{-}1)$$

where these are obtained from the displacement components u_k by the following strain-displacement relations assuming infinitesimal strain

$$\epsilon_{kl}=(u_{k,l}+u_{l,k})/2 \qquad (2.1\text{-}2)$$

Here, and in the discussion which follows, indicial notation will be used (see Appendix VI). The indices vary from 1 to 2 for two-dimensional problems, and from 1 to 3 for three-dimensional problems. Assume that these strain components (Eq. (2.1-1)) are small and are represented by continuous functions of the coordinates. If they also satisfy the compatibility conditions, the elements into which the body is subdivided fit each other after permanent set, Eq. (2.1-1) and there will be no initial stresses produced. Observation of the compatibility equations (Eq. (2.1-3)) illustrates that any continuous, constant or linear distribution satisfies these conditions, and hence will not produce initial stresses.

$$2\epsilon_{ij,ji}=\epsilon_{ii,jj}+\epsilon_{jj,ii}$$

$$\epsilon_{ii,jk} = -\epsilon_{jk,ii}+\epsilon_{ik,ij}+\epsilon_{ij,ij} \qquad (2.1\text{-}3)$$

Consider now a general case when the strain components (Eq. (2.1-1)) do not satisfy the compatibility conditions so that the elements into which the body is subdivided do not fit each other after permanent set (Eq. (2.1-1)), and forces must be applied to the surface of these elements in order to make them satisfy the compatibility equations. Assuming Hooke's law,

$$\sigma_{ij} = \sigma^{\circ}_{ij} + D_{ijkl}(\epsilon_{kl}-\epsilon^{\circ}_{kl}) \qquad (2.1\text{-}4)$$

we find that the permanent set can be eliminated by applying to each element the initial stresses

$$\sigma^{\circ}_{ij} = -D_{ijkl}\epsilon^{\circ}_{kl} \qquad (2.1\text{-}5)$$

These initial stresses can be induced by applying certain body and surface forces to the body formed by the small elements. These forces must satisfy the equations of equilibrium

$$\sigma_{ij,j} + \psi_i = 0 \qquad (2.1\text{-}6)$$

and the boundary conditions

$$\phi_i = n_j\sigma_{ij} \qquad (2.1\text{-}7)$$

where n_j represents the direction cosines of the outward normal to the boundary. Substituting the stress components in these equations, we find that the necessary body forces are

$$\psi_i = \sigma^{\circ}_{ij,j} \qquad (2.1\text{-}8)$$

and the surface forces are

$$\phi_i = -n_j\sigma^{\circ}_{ij} \qquad (2.1\text{-}9)$$

By applying the body forces (Eq. (2.1-8)) and surface forces (Eq. (2.1-9)), we remove the initial permanent set so that the elements fit one another and form a continuous body. Assume now that the elements into which the body was subdivided are joined together and remove these forces. Then evidently the stresses in the body are

obtained by superposing on the stresses (Eq. (2.1-5)) the stresses that are produced in the elastic body by the body forces

$$\psi_i = -\sigma^{\circ}_{ij,j} \tag{2.1-10}$$

and the surface forces

$$\phi_i = n_j \sigma^{\circ}_{ij} \tag{2.1-11}$$

Thus the problem of determining the initial stresses is reduced to the usual system of equations of the theory of elasticity in which the magnitudes of the fictitious body and surface forces are completely determined if the permanent set (Eq. (2.1-1)) is given.

2.2 Indirect Boundary Element Method

Consider an isotropic, linear elastic, homogeneous region v with an enclosed surface s, as shown in Figure 2-1.

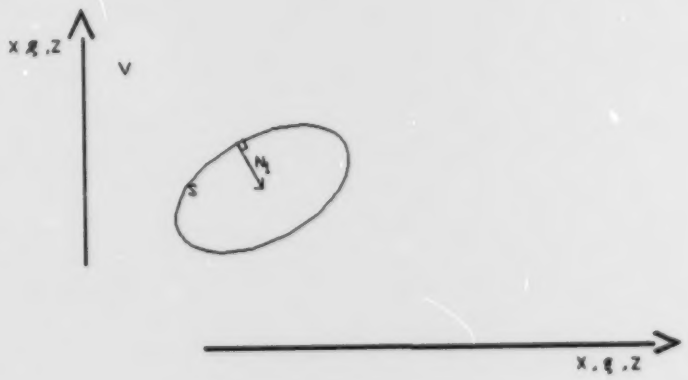

Figure 2-1 Isotropic, linear elastic, homogeneous region v with an enclosed surface s.

Stresses and displacements at any point in the body can be determined by superposing the effects of surface tractions $\phi_j(\xi)$, distributed over s, and body forces $\psi_j(x)$, distributed over v.

In the indirect boundary element method (BEM), this is expressed entirely in terms of integral equations of a unit singular solution (Green's function) of the original differential equations (Eqs. (2.1-2), (2.1-3), (2.1-4) and (2.1-6)) and distributed at specified intensities over the region of interest. These integrals are given

by Banerjee and Butterfield (1981)

$$u_k(x) = X_k$$

$$+\int_s g_{km}(x,\xi)\,\phi_m(\xi)\,ds(\xi) + \int_v g_{km}(x,z)\,\psi_m(z)\,dv(z)$$

$$\sigma_{ij}(x) = \int_{sc_{ijm}}(x,\xi)\,\varphi_m(\xi) + \int_{vc_{ijm}}(x,z)\,\psi_m(z)\,dv(z) \qquad (2.2\text{-}1)$$

where $ds(\xi)$ and $dv(z)$ indicate that the variables of integration are ξ and z_i respectively. The X_k are unknown rigid-body displacements while $g_{km}(x,\xi)$) and $c_{ijm}(x,\xi 2)$ represent respectively the fundamental singular solution for displacements and stresses induced by the application of a unit point force. These integrals are to be evaluated as Cauchy principal values. At points where the integrand is singular, additional terms must be added in to obtain correct results. These are discussed below in section 6. The function $c_{ijm}(x,\xi)$ can be determined by insertion of $g_{km}(x,\xi)$ into the strain-displacement relations (Eq. (2.1-2)) assuming infinitesimal strain giving

$$b_{klm}(x,\xi) = [g_{km,l}(x,\xi) + g_{lm,k}(x,\xi)]/2$$

then substitution into Hooke's law (Eq (2.1-4)) to yield

$$c_{ijm}(x,\xi) = D_{ijkl}[g_{km,l}(x,\xi) + g_{lm,k}(x,\xi)]/2$$

Definitions of $c_{ijm}(x,\xi)$ are given in Appendix I.

As discussed above, the stressed induced by the application of the permanent set (Eq. (2.1-1)) can be obtained by superposing on the stresses Eq. (2.1-5), the stresses that are produced in the elastic body by the body forces Eq. (2.1-10) and the surface forces Eq. (2.1-11). This is done by including contributions from the strain suppression calculations into both the surface tractions $\varphi_j(\xi)$, and body forces $\psi_j(z)$. The stresses (Eq. (2.2-2)) are therefore modified to include the initial stresses (Eq. (2.1-5)) as shown,

$$\sigma_{ij}(x) = \sigma^{\circ}_{ij}(x) + \sigma^{T}_{ij}(x)$$

$$+\int_{sc_{ijm}}(x,\xi)\,\varphi_m(\xi)\,ds(\xi) + \int_{vc_{ijm}}(x,z)\,\psi_m(z)\,dv(z) \qquad (2.2\text{-}2)$$

The term $\sigma^T_{ij}(x)$ has also been added to represent a continuous initial stress with constant or linear distribution.

Until this point all statements have been exact formulations of the solution to the problem. Any errors in the final result will be due solely from discretization of the integrals and the subsequent numerical solution of the algebraic equations.

2.2.1 Constant Strength Surface Elements - Field Stresses

As an illustrative example of the application of the boundary element method, consider only the surface integrals, discretized into into finite size, planar elements over which the intensities of surface tractions are constant. The initial stresses $\sigma^o_{ij}(x)$ are set to zero. For this case the stresses (Eq. (2.2-2)) at any point in the body can be determined from

$$\sigma_{ij}(x) = \sigma^T_{ij}(x) + \sum_{q=1}^{N} Cs^q_{ijm}(x)\,\varphi^q_m \qquad (2.2\text{-}3)$$

where $Cs^q_{ijm}(x)$ represents the effect on the stresses at the point x_i, of the surface tractions φ^q_m for element q. There are a total of N elements. The initial stresses $\sigma^T_{ij}(x)$ represent pre-existing field stresses which may vary linearly over the body.

The coefficients $Cs^q_{ijm}(x)$ are determined from the first of the integrals in expression (2.2-2), and have the form

$$Cs'^q_{ijm}(x) = \int_q C_{ijm}(x,\xi)\,ds(\xi) \qquad (2.2\text{-}4)$$

where the integrals are evaluated over the element q. Definitions of $Cs'^q_{ijm}(x)$ are given in Appendix II and the relationship between $Cs'^q_{ijm}(x)$ and $Cs^q_{ijm}(x)$ is discussed below.

In the evaluation of the integrals for this case it is convenient to conduct the surface boundary integrations in the local coordinates of the boundary element q, and therefore express φ^q_m in terms of these. This will require transformation of the point of interest x_i' to the local coordinate system x_i as follows

$$x'_i = A^q_{ij}(x_j - x^q_j) \qquad (2.2\text{-}5)$$

where A^q_{ij} represents the coordinate transformation matrix from global to local coordinates (see Appendix III) such that the normal is taken outward from the boundary (i.e. into the excavation) and x^q_j represents the centre point of the element q taken as the mean of the coordinates.

The integrals (Eq.2.2-4)) are evaluated in terms of local coordinates and therefore give a contribution to the stresses (Eq. (2.2-3)) in terms of local coordinates

(2.2-6)

$$\Delta\sigma'_{ij}(x) = Cs'^{q}_{ijm}(x)\,\varphi^{q}_{m}$$

They must be transformed to the global coordinate system (see Appendix III) giving a contribution to the stresses (Eq. (2.2-3)) as follows where

(2.2-7)

$$\Delta\sigma_{ij}(x) = Cs^{q}_{ijm}(x)\,\varphi^{q}_{m}$$

(2.2-8)

$$Cs^{q}_{ijm}(x) = A^{q}_{kj}A_{li}\,Cs'^{q}_{klm}(x)$$

The surface forces φ^{q}_{m} are commonly called "fictitious forces", and are the unknowns for these elements. These are parallel to the axis of the local coordinate system described by A^{q}_{ij} . In two dimensions, there are two components to φ^{q}_{m} , one shear component and one normal component. In three dimensions, there are three components to φ^{q}_{m} , two shear components and one normal component.

Expression (2.2-7) can be used to determine the stresses at any point in the solid medium by superposing the effects of all elements as in Eq. (2.2-3).

(2.2-9)

$$\sigma_{ij}(x) = \sigma^{T}_{ij}(x) + \sum_{q=1}^{N} Cs^{q}_{ijm}(x)\,\varphi^{q}_{m}$$

This expression is used to evaluate the stress distributions throughout in body. This can only be accomplished if the surface forces φ^{q}_{l} used in Eq. (2.2-9) are known. Determination of these is the objective of the boundary element analysis.

2.2.2 Constant Strength Surface Elements - Boundary Stresses

Consider the assembly of expressions (2.2-9) into a form suitable for solution. This requires that the stresses $\sigma_{ij}(x)$ at the centre point x^{p}_{l} of each element p be determined. The contribution of all

elements q at point p is given by

$$\sigma_{ij}^{p} = \sigma_{ij}^{Tp} + \sum_{q=1}^{N} Cs_{ijm}^{qp} \varphi_m^q \qquad (2.2\text{-}10)$$

where

$$\sigma_{ij}^{Tp} = \sigma_{ij}^{T}(x^p) \qquad (2.2\text{-}11)$$

$$Cs_{ijm}^{qp} = Cs_{ijm}^{q}(x^p)$$

The application of these equations for a point on an element located at the surface of an excavation requires additional specialization for the orientation of this element so that the boundary conditions (normal and shear stresses) at this surface can be determined. This is accommodated by transformation of the the stresses (Eqs. (2.2-10) and (2.2-11) as follows (see Appendix III)

$$\sigma'_{ij} = A_{jk}^{p} A_{il}^{p} \sigma_{kl}$$

giving

$$\sigma'^{p}_{ij} = \sigma'^{Tp}_{ij} + \sum_{q=1}^{N} Cs'^{qp}_{ijm} \varphi_m^q \qquad (2.2\text{-}12)$$

where

$$\sigma'^{Tp}_{ij} = A_{jk}^{p} A_{il}^{p} \sigma_{kl}^{Tp}$$

$$Cs'^{qp}_{ijm} = A_{jk}^{p} A_{il}^{p} Cs_{klm}^{qp}$$

The boundary conditions for element p are expressed by

$$t_i^p = n_j \sigma'^{p}_{ij} \qquad (2.2\text{-}13)$$

The values of t_i^p are the known stress conditions (normal and shear) at the excavation surfaces. For this case the normal is oriented the same way as the local coordinate system and therefore the outward normal n_j ceases to have any tangential components.

Substitution of the stresses (Eq. (2.2-12)) into Eq. (2.2-13) gives

$$t_i^p = n_j \sigma_{ij}^{Tp} + \sum_{q=1}^{N} n_j Cs_{ijm}^{qp} \varphi_m^q \qquad (2.2\text{-}14)$$

Expression (2.2-14) can be evaluated to give the boundary stresses t_i^p at the centre of element p. The coefficients Cs_{ijm}^{qp} represent the contribution by element q, to the stresses at element p, and constitute a statement of the principle of superposition of elastic stresses.

In two dimensions there are two unknown φ_m^q and two known t_i^p for each element and the expression (2.2-14) generates two equations for each element. In three dimensions there are three unknown φ_m^q and three known t_i^p for each element and the expression (2.2-14) generates three equations for each element. Therefore all unknowns can be solved for, and the stresses (Eq. (2.2-9)) at any point in the body can be determined.

2.3 Discretization of Integrals for Discontinuous, Constant Strength, Initial Stresses

2.3.1 Constant Strength Interior Elements - Field Stresses

As a first approximation, consider discretization of the body into finite size, planar elements over which the intensities of surface tractions and initial stresses (Eq. (2.1-5)) are constant. Figure 2-2 depicts such a discretization. The body forces (Eq. (2.1-10)) generated by constant initial stresses are found to be zero for this case. The stresses (Eq. (2.2-2)) at any point in the body are therefore determined from the application of surface tractions only and are given as above by

$$\sigma_{ij}(x) = \sigma_{ij}^{o}(x) + \sigma_{ij}^{T}(x) + \sum_{q=1}^{N} Cs_{ijm}^{q}(x)\,\varphi)_m^q \qquad (2.3\text{-}1)$$

The application for the case of elements representing an excavated surface is described above. To apply expression (2.3-1) to the case of internal elements, these elements can be thought of as similar to the small elements used in the discussion of strain suppression. Surface forces must be applied to the surfaces of each element to simulate the application of permanent set. The coefficients for the case of an internal element q are evaluated by accumulating the effects of the surface integrations for each face of the element.

It is convenient to conduct these surface boundary integrations in the local coordinates of the particular element face under consideration as described for the surface boundary elements. The

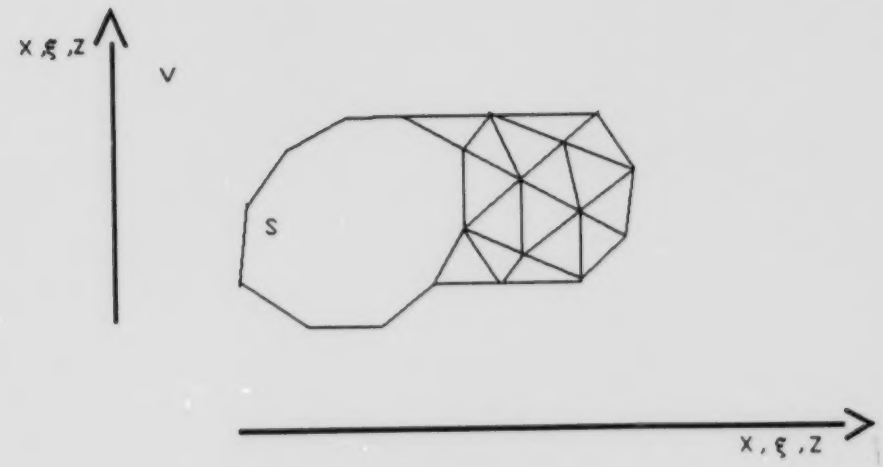

Figure 2-2 Discretized body.

normal for these faces is oriented outward from the element in agreement with the convention used by Timoshenko and Goodier (1970) in the evaluation of the boundary conditions (Eq. (2.1-7)). To evaluate the correct contribution to the surface forces (Eq. (2.1-11)) from the initial stresses (Eq. (2.1-5)), these are first transformed to the local coordinates of the element face under consideration where A_{ij}^{qp} represents the

$$\sigma_{ij}^{\circ\,\prime p} = A_{jk}^{qp} A_{il}^{qp} \sigma_{kl}^{\circ q} \tag{2.3-2}$$

coordinate transformation matrix from global to local coordinates for face p of element q, and $\sigma_{kl}^{\circ q}$ represents the initial stresses at x_i^q, the centre of element q. The surface forces (Eq. (2.1-11)) for face p are therefore given by

$$\varphi_i^{qp} = n_j \sigma_{ij}^{\circ\,\prime q}$$

For this case the normal is oriented the same way as the local coordinate system and therefore the outward normal n_j ceases to have any tangential components. Substituting for the initial stresses (Eq. (2.3-2)), the surface forces become

$$\varphi_i^{qp} = n_j A_{jk}^{qp} A_{il}^{qp} \sigma_m^{qp} \tag{2.3-3}$$

The integrals (Eq. (2.2-4)) are evaluated as discussed above for surface elements giving the following contribution to the stresses (Eq. (2.3-1)) for each face p of element q, in terms of local

coordinates

$$\Delta\sigma'_{ij}(x) = Cs'^{qp}_{ijm}(x)\,\varphi^{qp}_{m}$$

They must be transformed to the global coordinate system giving a contribution to the stresses (Eq. (2.3-1)) as follows

$$\Delta\sigma_{ij}(x) = Cs^{qp}_{ijm}(x)\,\varphi^{qp}_{m}$$

where

$$Cs^{qp}_{ijm}(x) = A^{qp}_{kj}A^{qp}_{ll}Cs'^{qp}_{klm}(x)$$

By substituting for the surface forces (Eq (2.3-3)) and accumulating for all faces, it can be found that the contribution to the stresses (Eq. 2.3-1)) for element q is given by

$$\Delta\sigma_{ij}(x) = Cv^{q}_{ijkl}(x)\,\sigma^{oq}_{kl} \qquad (2.3\text{-}4)$$

where

$$Cv^{q}_{ijkl}(x) = \sum_{p=1}^{M} Cs^{qp}_{ijm}(x)\,n_{p}A^{qp}_{nk}A^{qp}_{ml} \qquad (2.3\text{-}5)$$

M represents the number of faces for element q.

The initial stresses σ^{oq}_{kl} can be considered as the unknowns for these elements. These are oriented in the global coordinate system and can be related to the plastic strains (Eq. (2.1-1)) as in expression (Eq. (2.1-5)). Because

$$\sigma_{ij} = \sigma_{ji}$$

there are three independent components to σ^{oq}_{kl} in two dimensions and six independent components in three dimensions.

Expressions (2.2-7) and (2.3-4) can be used to determine the stresses at any point in the solid medium by superposing the effects of all elements as in Eq. (2.3-1) giving

$$\sigma_{ij}(x) = \sigma^{o}_{ij}(x) + \sigma^{T}_{ij}(x)$$

$$+ \sum_{q=1}^{N}\left[Cs^{q}_{ijm}(x)\,\varphi^{q}_{m} + Cv^{q}_{ijmn}(x)\,\sigma^{oq}_{mn}\right] \qquad (2.3\text{-}6)$$

where $Cs^{q}_{ijm}(x)$ is used determine the effect of surface elements, and $Cv^{q}_{ijmn}(x)$ is used determine the effect of interior elements. This expression is used to evaluate the stress distribution throughout

in body. This can only be accomplished if the surface forces φ_m^q and initial stresses σ_{mn}^{oq} used in Eq. (2.3-6) are known. Determination of these is the objective of the boundary element analysis.

2.3.2 Constant Strength Interior Elements - Boundary Stresses

Consider the assembly of expressions (2.3-6) into a form suitable for solution. This requires that the stresses $\sigma_{ij}(x)$ at the centre point x^p of each element p be determined. The stresses can be evaluated directly from expression (2.3-6) for the case of internal elements by adopting global coordinates for these giving

$$\sigma_{ij}^p = \sigma_{ij}^{Tp} + \sum_{q=1}^{N} \left[Cs_{ijm}^{qp} \varphi_m^q + Cv_{ijmn}^{qp} \sigma_{mn}^{oq} \right] \tag{2.3-7}$$

where

$$\sigma_{ij}^{Tp} = \sigma_{ij}^{T}(x^p)$$

$$Cs_{ijm}^{qp} = Cs_{ijm}^{q}(x^p)$$

$$Cv_{ijmn}^{qp} = Cv_{ijmn}^{q}(x^p) + \delta^{qp}\delta_{im}\delta_{jn} \tag{2.3-8}$$

and δ_{ij} represents the Kronecker delta and δ^{qp} represents a substitution tensor similar to the Kronecker delta with the property that it equals one when p and q are equal. The application of these in the last term of expression (2.3-8) has pulled σ_{ij}^{op} into the coefficient expression Cv_{ijmn}^{qp} .

Expression (2.3-7) can be evaluated to give the stresses at the centre of the internal element p. The coefficients Cs_{ijm}^{qp} and Cv_{ijmn}^{qp} represent the contribution by element q, to the stresses at element p, and constitute a statement of the principle of superposition of elastic stresses.

The application of these equations for a point on an element located at the surface of an excavation requires additional specialization for the orientation of this element so that the boundary conditions (normal and shear stresses) at this surface can be determined. This is accommodated by transformation of the

stresses (2.3-7) as discussed above

$$\sigma'_{ij} = A^p_{jk} A^p_{il} \sigma_{kl} \tag{2.3-9}$$

giving

$$\sigma'^p_{ij} = + \sigma^{Tp}_{ij} + \sum_{q=1}^{N} \left[Cs'^{qp}_{ijm} \varphi^q_m + Cv'^{pq}_{ijmn} \sigma^{\circ q}_{mn} \right] \tag{2.3-10}$$

where

$$\sigma^{Tp}_{ij} = A^p_{jk} A^p_{il} \sigma^{Tp}_{kl} \tag{2.3-11}$$

$$Cs'^{qp}_{ijm} = A^p_{jk} A^p_{il} Cs^{qp}_{kl} \tag{2.3-12}$$

$$Cv'^{qp}_{ijmn} = A^p_{jk} A^p_{il} Cv^{qp}_{klmn} \tag{2.3-13}$$

The boundary conditions for element p are expressed by

$$t^p_i = n_j \sigma'^p_{ij} \tag{2.3-14}$$

The values of t^p_i are the known stress conditions (normal and shear) at the excavation surfaces. For this case the normal is oriented the same way as the local coordinate system and therefore the outward normal n_j ceases to have any tangential components. Substitution of the stresses (Eq. (2.3-10)) into this gives

$$t^p_i = n_j \sigma'^p_{ij} + \sum_{q=1}^{N} \left[n_j Cs'^{pq}_{ijm} \varphi^q_m + n_j Cv'^{pq}_{ijmn} \sigma^{\circ q}_{mn} \right] \tag{2.3-15}$$

Expression (2.3-15) can be evaluated to give the boundary stresses at the centre point of the surface element p.

In two dimensions there are two unknown φ^q_m and two known t^p_i for each surface element and the expression (2.3-15) generates two equations for each of these. There are three unknown σ'^p_{ij} and three unknown $\sigma^{\circ q}_{ij}$ for each internal element and expression (2.3-10) generates three equations for each of these. In three dimensions there are three unknown φ^q_m and three known t^p_i for each surface element and the expression (2.3-15) generates three equations for each of these.

There are six unknown σ_{ij}^{β} and six unknown σ_{ij}^{α} for each internal element and expression (2.3-10) generates six equations for each of these. Therefore, to generate a solution, three additional equations are required in two dimensions, and six additional equations are required in three dimensions, for each internal element. These equations are provided by the theory of plasticity as discussed in Sections 2.6 and 2.7.

2.3.3 Suitability of Constant Strength Interior Elements

Before leaving this section, consider the implications of discretization of integrals for constant strength initial stresses. This discretization scheme results in the division of the body into internal elements, each of which has a different constant initial stress, and hence different constant permanent set applied to it. These initial stresses are imposed by applying surface forces (Eq. (2.3-3)) to the faces of these elements. Although this results in continuous stresses at the edges of the elements, and equilibrium and compatibility are satisfied, there are stress singularities at the corners of these elements. These arise, even though the applied surface forces on any element are in equilibrium. The stress singularities are not important when the discontinuity of initial stress between elements is small compared to the stress state at the element. However, when the discontinuity gets large, for example during advanced stages of plastic deformation, the stress singularities dominate the solution and invalidate the results.

The matrix resulting from the assembly of the coefficients given in expressions (2.3-7) and (2.3-15) is poorly conditioned. The reason for this can be easily understood by considering two adjacent internal elements of equal size. The surface forces (Eq. (2.3-3)) applied to the common side have an equally large effect on the centre points of both elements, and hence lead to coefficients (Eq. (2.3-5)) of equal magnitude both on and off the matrix diagonal. This can be physically interpreted as meaning that the initial stresses in an element have an equally large effect on its own centre point as well as the centre points of all adjacent elements. This problem arises because the stresses (Eq. (2.3-7)) are not evaluated at the same point as the (Green's function) surface tractions are applied. This will necessarily make solutions slow to converge, unless special steps are taken during the solution process to take these element interactions into account.

2.4 Discretization of Integrals for Continuous, Piecewise Linear Strength, Initial Stresses

Although the constant strength initial stress discretization scheme can be applied to a limited range of problems, it is more desirable to choose an alternative scheme which eliminates the corner

singularities and moves the stress point (Eq. (2.3-7)) to the same location where the Green's function is applied. This will make the solution applicable to problems with larger plastic deformations, and will improve the matrix conditioning.

2.4.1 Linear Strength Interior Elements - Field Stresses

A continuous, piecewise linear strength, initial stress distribution can satisfy both of these requirements. As a refinement of the first trial discretization, consider discretization of the body into finite size, planar elements over which the intensities of surface tractions and initial stresses (Eq. (2.1-5)) are continuous, and piecewise linear

$$\sigma_{ij}^{oq}(\xi) = \sum_{p=1}^{M} \delta^{qp}(N^{oqp} + N_k^{1qp}\xi_k)\,\sigma_{ij}^{op} \qquad (2.4\text{-}1)$$

where the coefficients N^{oqp} and N_k^{1qp} represent respectively the constant and linear variation of initial stress $\sigma_{ij}^{oq}(\xi)$ distributed over element q, σ_{ij}^{op} represents the initial stresses at the nodal point p, and δ^{qp} represents a substitution tensor similar to the Kronecker delta with the property that it equals one when nodal point p is coincident with element q, and zero otherwise (see Appendix IV). There are a total of M nodal points. Figure 2-2 depicts such a discretization.

The surface tractions for elements representing the surfaces of excavations need not be linear nor continuous, however they will be assumed so here. The surface forces (Eq. (2.1-11)) need only be applied at the edges of zones where the initial stresses are not continuous. The body forces (Eq. (2.1-10)) generated by linear initial stresses are found to be constant for this case. The stresses (Eq. 2.2-2)) at any point in the body are therefore determined from the application of linear surface tractions and constant body forces and are given by

$$\sigma_{ij}(x) = \sigma_{ij}^{o}(x) + \sigma_{ij}^{T}(x) + \sum_{q=1}^{N}\left\{\sum_{p=1}^{M}\left[\delta^{qp} Cs_{ijm}^{qp}(x)\,\varphi_m^p\right] + Cb_{ijm}^{q}(x)\,\psi_m^q\right\} \qquad (2.4\text{-}2)$$

where $Cs_{ijm}^{qp}(x)$ and $Cb_{ijm}^{q}(x)$ represent respectively, the effect on the stresses at the point x_i, of the surface tractions φ_m^p at nodal point p, and body forces ψ_m^q at element q. There are a total of N elements and M nodal points. The initial stresses $\sigma_{ij}^{T}(x)$ represent pre-existing field stresses which may vary linearly over the body. The coefficients $Cs_{ijm}^{qp}(x)$ are determined from the first of the integrals in expression (2.2-2). These contain contributions from elements q which are coincident with nodal point p, and have the form

$$Cs'^{\Phi\Phi}_{ijm}(x) = N^{o\Phi}\int_q C_{ijm}(x,\xi)\,ds(\xi)$$

$$+N^{1\Phi}\int_q C_{ijm}(x,\xi)\,\xi_k\,ds(\xi) \qquad (2.4\text{-}3)$$

where

$$\varphi^q_m(\xi) = \sum_{p=1}^{M} \delta^{\Phi}\,(N^{o\Phi}+N^{1\Phi}_k\xi_k)\,\varphi^p_m$$

and the integrals are evaluated over the element q, and $N^{o\Phi}$ and $N^{1\Phi}_k$ are defined as in expression (2.4-1). $Cs'^{\Phi\Phi}_{ijm}(x)$ are given in Appendix II.

The coefficients $Cb^q_{ijm}(x)$ representing the effect of the body force Φ^q_m at element q, are determined from the second of the integrals in expression (2.2-2)

$$Cb^q_{ijm}(x) = \int_q C_{ijm}(x,z)\,dv(z)$$

where the integrals are evaluated over element q. Definitions of $Cb^q_{ijm}(x)$ are given in Appendix II.

The relationship between $Cs'^{\Phi\Phi}_{ijm}(x)$ and $Cs^{\Phi\Phi}_{ijm}(x)$ is as discussed above for elements representing surface excavations. Applying the stress transformations described in expressions (2.2-5) through (2.2-8), the following relationship can be derived

$$Cs^{\Phi\Phi}_{ijm}(x) = A^p_{kj}A^p_{li}Cs'^{\Phi\Phi}_{klm}(x) \qquad (2.4\text{-}4)$$

where A^p_{ij} represents the coordinate transformation matrix from global to local coordinates such that the normal is taken outward from the boundary (i.e. into the excavation) at the nodal point p. Here it has been assumed that the boundary surface is planar and hence at the point p, the surface is continuous in position and slope. If the boundary surface has a corner at point p, the surface forces φ^p_m will be set to zero. Therefore, in this present derivation, corners are not accommodated. It is suggested that in future, corners can be included by rounding them to a smooth surface, or by developing coefficients which properly represent the influence of the surface forces at these corners.

By accumulating the coefficients for those surface elements which are coincident on nodal point p, the contribution to the stresses (Eq. (2.4-2)) by the surface forces at point p can be expressed as where

To apply expression (2.4-2) to the case of internal elements, surface forces (Eq. (2.1-11)) need only be applied at the edges of

$$\Delta\sigma_{ij}(x) = Cs^{p}_{ijm}(x)\,\varphi^{p}_{m} \qquad (2.4\text{-}5)$$

$$Cs^{p}_{ijm}(x) = \sum_{q=1}^{N} \delta^{qp} Cs^{qp}_{ijm}(x)$$

zones where the initial stresses are not continuous. This includes the surfaces of excavations. Stress transformations similar to those described in expressions (2.3-2) through (2.3-6) must be applied. To evaluate the correct contribution to the surface forces (Eq. (2.1-11)) from the initial stresses (Eq. (2.1-5)), these are first transformed to the local coordinates of the nodal point p

$$\sigma^{o}_{ij}{}'^{p} = A^{p}_{jk}A^{p}_{il}\sigma^{op}_{kl}$$

where A^{p}_{ij} has already been used in expression (2.4-4). For this case the normal is oriented the same way as the local coordinate system and therefore the outward normal n_j ceases to have any tangential components. The surface forces (Eq. (2.1-11)) for the point p are therefore given by

$$\varphi^{p}_{i} = n_j A^{p}_{jk}A^{p}_{il}\sigma^{op}_{kl} \qquad (2.4\text{-}6)$$

The integrals (Eq. (2.4-3)) are evaluated as discussed above for surface elements giving the following contribution to the stresses (Eq. (2.4-2)) for each element q which is coincident with nodal point p, in terms of local coordinates

$$\Delta\sigma'_{ij}(x) = Cs'^{qp}_{ijm}(x)\,\varphi^{p}_{m}$$

They must be transformed to the global coordinate system giving a contribution to the stresses (Eq. (2.4-2)) as follows

$$\Delta\sigma_{ij}(x) = Cs^{qp}_{ijm}(x)\,\varphi^{p}_{m}$$

where

$$Cs^{qp}_{ijm}(x) = A^{p}_{kj}A^{p}_{il}Cs'^{qp}_{klm}(x)$$

The contribution to the body forces (Eq. (2.1-10)) on element q by the value of initial stress at nodal point p can be obtained by substitution of the initial stresses (Eq. (2.4-1)), into Eq. (2.1-10) giving

$$\psi^{q}_{i} = -\delta^{qp}N^{1qp}_{j}\sigma^{op}_{ij} \qquad (2.4\text{-}7)$$

By substituting for the surface forces (Eq. (2.4-6)), body forces (Eq. (2.4-7)) and accumulating the coefficients for those internal

elements which are coincident on nodal point p, the contribution to the stresses (Eq. (2.4-2)) by the initial stresses (Eq. (2.1-5)) at point p can be expressed as

$$\Delta\sigma_{ij}(x) = Cv^{p}_{ijkl}(x)\,\sigma^{\circ p}_{kl} \qquad (2.4\text{-}8)$$

where

$$Cv^{p}_{ijkl}(x) = \sum_{q=1}^{N} \delta^{qp}\left[Cs^{qp}_{ijm}(x)\,n_m A^{p}_{nk} A^{p}_{nl} - Cb^{q}_{ijk}(x)\,N^{1qp}_{l}\right]$$

The initial stresses $\sigma^{\circ p}_{kl}$ can be considered as the unknowns for these elements. These are oriented in the global coordinate system and can be related to the plastic strains (Eq. (2.1-1)) as in expression (2.1-5). There are three independent components to $\sigma^{\circ p}_{kl}$ in two dimensions and six independent components in three dimensions.

Expressions (2.4-4) and (2.4-8) can be used to determine the stresses at any point in the solid medium by superposing the effects of all nodal points giving

$$\sigma_{ij}(x) = \sigma^{\circ}_{ij}(x) + \sigma^{T}_{ij}(x)$$

$$+\sum_{q=1}^{N}\left[Cs^{q}_{ijm}(x)\,\varphi^{q}_{m} + Cv^{q}_{ijmn}(x)\,\sigma^{\circ q}_{mn}\right] \qquad (2.4\text{-}9)$$

where $Cs^{q}_{ijm}(x)$ is used determine the effect of surface elements, and $Cv^{q}_{ijmn}(x)$ is used determine the effect of interior elements. p and q have been interchanged here for consistency with the development of expressions (2.2-9) and (2.3-6). This expression is used to evaluate the stress distribution throughout in body. This can only be accomplished if the surface forces φ^{q}_{m} and initial stresses $\sigma^{\circ q}_{mn}$ used in (2.4-9) are known. Determination of these is the objective of the boundary element analysis.

2.4.2 Linear Strength Interior Elements - Boundary Stresses

The assembly of expressions (2.4-9) into a form suitable for solution can be conducted following the same procedure as followed for the development of expressions (2.3-7) through (2.3-15) to give the stresses at an interior nodal point p

$$\sigma^{p}_{ij} = \sigma^{Tp}_{ij} + \sum_{q=1}^{N}\left[Cs^{qp}_{ijm}\varphi^{q}_{m} + Cv^{qp}_{ijmn}\sigma^{\circ q}_{mn}\right] \qquad (2.4\text{-}10)$$

and to give the boundary conditions for a nodal point p located at the surface of an excavation

$$t_i^p = n_j \sigma_{ij}^{rp} + \sum_{q=1}^{M} \left[n_j C s_{ijm}^{'qp} \sigma_{mn}^{\circ q} \right]$$

$$t^p = n_j \sigma^{rp} + \sum \left[n_j C s^{'qp} \varphi^q + n_j C v_n^{'qp} \sigma^{\circ q} \right] \qquad (2.4\text{-}11)$$

In two dimensions there are two unknown φ_m^q and two known t_i^p for each surface nodal point and the expression (2.4-11) generates two equations for each of these. There are three unknown σ_{ij}^p and three unknown $\sigma_{ij}^{\circ q}$ for each nodal point coincident with an internal element and expression (2.4-10) generates three equations for each of these. In three dimensions there are three unknown and three known φ_m^q for each surface nodal point and the expression (2.4-11) generates three equations for each of these. There are six unknown σ_{ij}^p and six unknown $\sigma_{ij}^{\circ q}$ for each nodal point coincident with an internal element and expression (2.4-10) generates six equations for each of these. Therefore, to generate a solution, three additional equations are required in two dimensions, and six additional equations are required in three dimensions, for each internal element. These equations are provided by the theory of plasticity as discussed in Sections 2.6 and 2.7.

2.4.3 Suitability of Linear Strength Interior Elements

Before leaving this section, consider the implications of discretization of integrals for continuous, piecewise linear strength, initial stresses. This discretization scheme results in the division of the body into internal elements, each of which has a linear initial stress (Eq. (2.4-1)), and hence linear permanent set applied to it. These initial stresses are imposed by applying surface forces and body forces to these elements. This results in continuous stresses at the edges and corners of the elements, and equilibrium and compatibility are satisfied. There are no stress singularities at the corners of these internal elements because the initial stress distribution is continuous. This is true for nodal points at planar surfaces as well. At surface corners the surface forces are set to zero to eliminate the singularity.

Due to the assumption of continuous, piecewise linear varying initial stresses, the distribution of initial stresses and hence permanent set will be restricted to some degree as with any low order polynomial discretization. The effects of this can be minimized by using large numbers of elements.

The matrix resulting from the assembly of the coefficients given in expressions (2.4-10) and (2.4-11) is well conditioned because the stress point (2.4-10) is at the same location as where the Green's function is applied. There will be duplicated coefficients for

nodal points at the surface where the stresses (Eqs. (2.4-10) and (2.4-11)) are evaluated for both internal elements and surface elements.

2.5 Evaluation of Integrals for Singular Points

The first of the integrals (Eq. (2.2-1)) is a real improper integral at the surface of excavations because the integrand is singular at these points. Throughout the discussion above, all integrals were evaluated as Cauchy principal values, therefore additional terms must be added to obtain correct results.

For a planar boundary, the integral can be written in the local coordinates ξ_i of the boundary such that the normal is taken outwards from the boundary (i.e. into the excavation). The Green's function $c_{ijm}(x,\xi)$ is to be evaluated at the singular point x_i which equals zero such that the boundary is approached from the solid part of the body (negative x_2 and x_3 respectively in two and three dimensions) towards the excavation surface giving in two dimensions

$$x_1 = 0$$
$$x_2 \to 0^-$$
$$\xi_2 = 0$$

With these conditions, the singular integral can be written

$$\lim_{\xi_1 \to 0} \int_{-\xi_1}^{+\xi_1} c_{ijm}(x,\xi)\, d\xi_1 = C^-_{ijm}$$

and evaluated by substitution for $c_{ijm}(x,\xi)$ giving

$$C^-_{121} = C^-_{211} = C^-_{222} = 1/2$$

$$C^-_{112} = \nu/[2(1-\nu)]$$

where the remaining terms are zero and ϵ represents Poisson's ratio for the host material.

In three dimensions, the integral is evaluated such that

$$x_1 = 0$$
$$x_2 = 0$$
$$x_3 \to 0^-$$
$$\xi_3 = 0$$

The singular integral is given by

and evaluated by substitution for $c_{ijm}(x,\xi)$ giving
where the remaining terms are zero.

$$\lim_{\substack{\xi_1 \to 0 \\ \xi_2 \to 0}} \int_{+\xi_1}^{+\ell^2} \int_{-\xi_2}^{+\xi_2} C_{ijm}(x,\xi)\, d\xi_2 d\xi_1 = C^-_{ijm}$$

$$C^-_{131} = C^-_{311} = C^-_{232} = C^-_{322} = C^-_{333} = 1/2$$

$$C^-_{113} = C^-_{223} = \nu/[2(1-\nu)]$$

In the discussion of the application of the method of strain suppression, Timoshenko and Goodier (1970) chose to adopt the convention that the normal for the faces of the internal elements is oriented away from the element, and hence for this case the boundary must be approached from the outside of the internal elements (positive x_2 and x_3 respectively in two and three dimensions). This has the effect of changing the sign of C^-_{ijm} .

2.6 The Theory of Incremental Plasticity

The only difference in the behaviour of an elastically deformed versus an inelastically deformed elemental volume of material is the stress-strain relation for the material. 'Plastic' behaviour of solids is characterized by a non-unique stress-strain relationship where complex constitutive relations supersede the simple linear elasticity assumptions.

In the derivations above it was found that to generate a solution, additional expressions are required to relate the initial stresses (plastic strains) and the stresses for each point considered. Three additional equations are required in two dimensions, and six additional equations are required in three dimensions. These equations are provided by the theory of plasticity as discussed below.

2.6.1 Strength of Material - Failure Criterion

The first of these equations is the failure criterion for the material. A failure envelope must be specified for the material as shown in Figure 2-3. While any relationship can be used, the Mohr-Coulomb criterion as discussed by Jaeger and Cook (1976) has been found

$$\sigma_1 = C_o + q\sigma_3 \qquad (2.6\text{-}1)$$

In the derivations above it was found that to generate a solution, additional expressions are required to relate the initial stresses (plastic strains) and the stresses for each point considered. Three additional equations are required in two dimensions, and six additional equations are required in three dimensions. These equations are provided by the theory of plasticity as discussed below.

2.6.1 Strength of Material - Failure Criterion

The first of these equations is the failure criterion for the material. A failure envelope must be specified for the material as shown in Figure 2-3. While any relationship can be used, the Mohr-Coulomb criterion as discussed by Jaeger and Cook (1976) has been found

$$\sigma_1 = C_0 + q\sigma_3 \qquad (2.6\text{-}1)$$

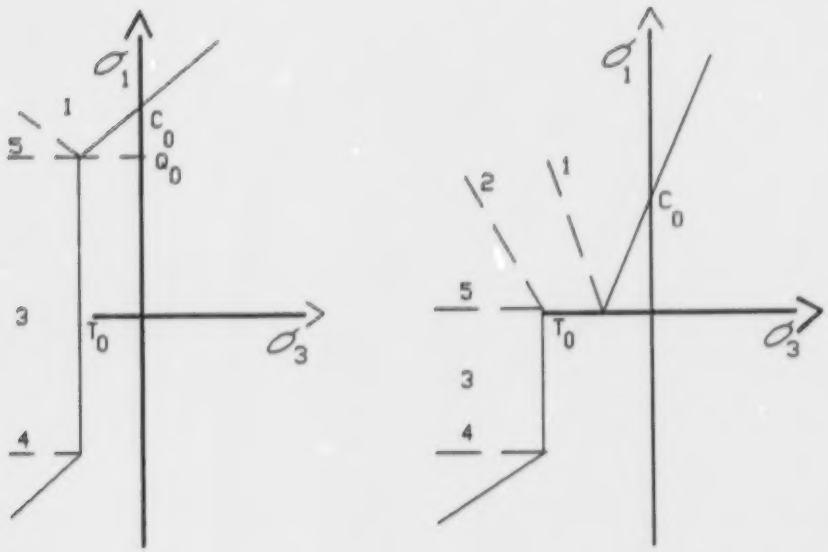

Figure 2-3 Failure envelope.

to be applicable for rocks and soils, and the Hoek-Brown criterion is recommended by Hoek and Brown[5]

$$\sigma_1 = \sigma_3 + \sqrt{mC_0\sigma_3 + sC_0^2} \qquad (2.6\text{-}2)$$

A second relation can be obtained by consideration of the dilation of the material with plastic deformation. Dilation is an effect similar to that of Poisson's ratio in elasticity theory. It is well known that upon yield, cohesive materials under low confinement (less than there compressive strength) tend to dilate initially and then achieve a relatively constant volume with continued plastic deformation. Under higher confinement (greater than there compressive strength), compaction may be observed initially.

For the case of uniaxial compressions, the dilation rate is defined by

$$\beta = -d\epsilon_3^\circ / -d\epsilon_1^\circ = -d\epsilon_2^\circ / d\epsilon_1^\circ$$

where ϵ_1°, ϵ_2°, ϵ_3° represent respectively the major, intermediate and minor principal plastic strains, and $d\epsilon_1^\circ$, $d\epsilon_2^\circ$, $d\epsilon_3^\circ$ represent the variations of these, called plastic strain increments. This provides one additional expression in two dimensions and two additional expressions in three dimensions. The details of the three dimensional case are discussed below. For total strain plasticity this expression is approximated by

$$\beta = -\epsilon_3^\circ / \epsilon_1^\circ = -\epsilon_2^\circ / \epsilon_1^\circ$$

If it is assumed that normality of stresses and plastic strains or plastic strain increments applies, the dilation rate is determined by the negative reciprocal of the slope of the failure envelope in the appropriate zone (as depicted in Figure 2-3) giving

$$\beta = -d\sigma_3 / d\sigma_1$$

Since the constants in expressions (2.6-1), (2.6-2) and (2.6-3) may be functions of the stress or strain, the dilation will also be dependant on these.

Additional expressions can be obtained by requiring that the principal plastic strains (for total strain plasticity)

$$\sigma_1, \sigma_2, \sigma_3 \mid \epsilon_1^\circ, \epsilon_2^\circ, \epsilon_3^\circ$$

or incremental plastic strains (for incremental plasticity)

$$\sigma_1, \sigma_2, \sigma_3 \mid d\epsilon_1^\circ, d\epsilon_2^\circ, d\epsilon_3^\circ$$

be parallel to the principal stresses. This provides the one additional expression required in two dimensions and the three additional expressions in three dimensions.

These relationships can be more rigorously derived from plastic potential theory as described by Johnson and Mellor (1973) and Zienkiewicz (1977). The failure criterion is called a yield

surface when it is extended to accommodate post-peak deformations. As above, this provides one equation. An expression called a plastic potential function is used to determine the relationship between the stresses and plastic strain increments by differentiation

$$d\epsilon^{\circ}_{ij} = \lambda \frac{\partial Q}{\partial \sigma_{ij}} \qquad (2.6\text{-}4)$$

where Q is the plastic potential function, and λ is a proportionality constant which contributes one additional unknown to the problem. This expression provides three independent equations in two dimensions and six independent equations in three dimensions thereby making solution possible.

If the yield surface and the potential function are specified as distinct expressions the approach is known as non-associated plasticity. If they are identical, they are called the flow rule and the approach is called associated plasticity.

Throughout most of the following discussion, incremental plasticity theory will only be considered. Total strain plasticity theory can be implemented by using the same relations and substituting ϵ°_{ij} for $d\epsilon^{\circ}_{ij}$.

2.6.3 Details of Plastic Behaviour

Consider the failure envelope illustrated in Figure 2-3. There are five possible stress zones which must be considered. As discussed above, for solution, the potential function (or dilation rate) must be specified. Assuming normality of stresses and plastic strain increments applies, the plastic strain increments can be determined from the failure envelope illustrated in Figure 2-3 using expression (2.6-4). It is assumed that there is no dependance of this failure envelope on the intermediate principal stress σ_2, except for the limits imposed by cases where the intermediate principal stress is equal to the major or minor principal stress. The following three cases must be considered

$$\sigma_1 > \sigma_2 > \sigma_3 \qquad (2.6\text{-}5)$$

$$\sigma_1 = \sigma_2 \qquad (2.6\text{-}6)$$

$$\sigma_2 = \sigma_3 \qquad (2.6\text{-}7)$$

The first condition (2.6-5) will be assumed to apply in two

dimensions. The last two conditions (2.6-6) and (2.6-7) represent edges of the applicable region for the failure envelope and are known as Koiter's corners (1953) and must be considered in three dimensions.

During the solution process described below, the stresses are first estimated by elasticity theory and hence are permitted to exceed the strength envelope by a small amount. It will be assumed that the closest point on the failure surface is representative of the actual desired stress state. In order to eliminate ambiguity at edges (2.6-6) and (2.6-7) and other points where the normal to the failure envelope is not unique, the strain increments will be defined by the direction of the line joining the actual with the desired stress state. This process is equivalent to rounding all edges and corners with an infinitesimally small radius. This assumption does not alter the results of the determination of the plastic strain increments (Eq. (2.6-4)) when the failure surface is well defined.

It will be assumed that normality applies for all zones except zone one. Zone one represents the case where yielding is induced by compressive or shear stresses, and the yield strength is specified be either of Eqs. (2.6-1) or (2.6-2). The potential function for this zone is specified by expression (2.6-1) with q determining the dilation rate.

The plastic strain increments can be determined from Eq. (2.6-4) for cases where σ_2 is greater than σ_3, but and less than the strength giving

$$d\epsilon_1^\circ = \lambda,\ d\epsilon_2^\circ = 0,\ d\epsilon_3^\circ = -q\lambda \tag{2.6-8}$$

If σ_2 exceeds the strength then the desired stress state must be determined. For the Mohr-Coulomb criterion (Eq. (2.6-1)) the stress point of interest lies on the line defined by

$$\sigma_1 = \sigma_2 = C_o + q\sigma_3 \tag{2.6-9}$$

and the plastic strain increments can be determined for the normal to this point (see Appendix V)

$$\begin{aligned} d\epsilon_1^\circ &= (\sigma_1 - dC_o)\lambda \\ d\epsilon_2^\circ &= (\sigma_2 - dC_o)\lambda \\ d\epsilon_3^\circ &= [\sigma_3 - (d-1)C_o/q]\lambda \end{aligned} \tag{2.6-10}$$

where
If σ_2 equals σ_3 then the stress point of interest lies on the line defined by

$$d = C_o[\ \sigma_1 + \sigma_2 + (\sigma_3 + C_o/q\ )/q\ ] \qquad (2.6\text{-}11)$$

$$\sigma_1 = C_o + q\sigma_2 = C_o + q\sigma_3 \qquad (2.6\text{-}11)$$

and the plastic strain increments can be determined for the normal to this point (see Appendix V)

$$\begin{aligned} d\epsilon_1^\circ &= (\sigma_1 - dC_o)\lambda \\ d\epsilon_2^\circ &= [\sigma_2 - (d-1)C_o/q]\lambda \\ d\epsilon_3^\circ &= [\sigma_3 - (d-1)C_o/q]\lambda \end{aligned} \qquad (2.6\text{-}12)$$

where

$$d = C_o[\ \sigma_1 + (\ \sigma_2 + \sigma_3 + 2C_o/q)/q\ ] \qquad (2.6\text{-}13)$$

If q is set equal to q" and the Mohr-Coulomb strength criterion is used, then normality applies for zone one as well. An additional restriction is that $d\epsilon_1^\circ$ be positive, and hence truly parallel to σ_1. Failure of this condition indicates that yielding should not occur.

Zone two is characterised by compressive yielding which is not dependant on the minor principal stress. If σ_2 is less than the strength then all plastic deformation is in the direction of σ_1

$$\begin{aligned} d\epsilon_1^\circ &= \lambda \\ d\epsilon_2^\circ &= d\epsilon_3^\circ = 0 \end{aligned} \qquad (2.6\text{-}14)$$

If σ_2 exceeds the strength then the stress point of interest lies on the line defined by

$$\sigma_1 = \sigma_2 = 0 \qquad (2.6\text{-}15)$$

and the plastic strain increments can be determined for the normal to this point (see Appendix V)

$$\begin{aligned} d\epsilon_1^\circ &= \sigma_1\lambda \\ d\epsilon_2^\circ &= \sigma_2\lambda \\ d\epsilon_3^\circ &= 0 \end{aligned} \qquad (2.6\text{-}16)$$

As for zone one, it is required that $d\epsilon_1^\circ$ be positive. Failure of this condition indicates that yielding should not occur.

Zone three is characterised by tensile yielding which is not dependant on the major principal stress. If σ_2 is inside the failure envelope then all plastic deformation is in the direction of σ_3.

$$d\epsilon_1^\circ = d\epsilon_2^\circ = 0 \qquad (2.6\text{-}17)$$
$$d\epsilon_3^\circ = \lambda$$

If σ_2 falls outside the failure envelope then the stress point of interest lies on the line defined by

$$\sigma_2 = \sigma_3 \qquad (2.6\text{-}18)$$

and the plastic strain increments can be determined for the normal to this point (see Appendix V)

$$d\epsilon_1^\circ = 0 \qquad (2.6\text{-}19)$$
$$d\epsilon_2^\circ = d\epsilon_3^\circ = \lambda$$

An additional restriction is that $d\epsilon_3^\circ$ be negative. Failure of this condition indicates that yielding should not occur.

Zone four is characterised by pure tensile yielding. The stress point of interest is defined by

$$\sigma_1 = \sigma_2 = \sigma_3 = T_o \qquad (2.6\text{-}20)$$

and the plastic strain increments can be determined for the normal to this point (see Appendix V)

$$d\epsilon_1^\circ = (\sigma_1 - T_o)\lambda$$
$$d\epsilon_2^\circ = (\sigma_2 - T_o)\lambda \qquad (2.6\text{-}21)$$
$$d\epsilon_3^\circ = (\sigma_3 - T_o)\lambda$$

An additional restriction is that $d\epsilon_1^\circ$ and hence also $d\epsilon_3^\circ$ be negative. If the first condition fails it is possible that zone three should be used. If the second condition fails yielding should not occur.

Zone five is characterised by combined tensile and compressive yielding. If σ_2 is inside the failure envelope then the stress point of interest is defined by

$$\sigma_1 = Q_o \qquad (2.6\text{-}22)$$
$$\sigma_3 = T_o$$

and the plastic strain increments can be determined for the normal to this point (see Appendix V)
If σ_2 exceeds Q_o then the stress point of interest is defined by

$$d\epsilon_1^\circ = (\sigma_1 - Q_\circ)\lambda$$
$$d\epsilon_2^\circ = 0 \qquad (2.6\text{-}23)$$
$$d\epsilon_3^\circ = (\sigma_3 - T_\circ)\lambda$$

$$\sigma_1 = \sigma_2 = Q_\circ$$
$$\sigma_3 = T_\circ$$

and the plastic strain increments can be determined for the normal to this point (see Appendix V)

$$d\epsilon_1^\circ = (\sigma_1 - Q_\circ)\lambda$$
$$d\epsilon_1^\circ = (\sigma_2 - Q_\circ)\lambda \qquad (2.6\text{-}24)$$
$$d\epsilon_3^\circ = (\sigma_3 - T_\circ)\lambda$$

If σ_2 is less than $T_\circ$ then the stress point of interest is defined by

$$\sigma_1 = Q_\circ \qquad (2.6\text{-}25)$$
$$\sigma_2 = \sigma_3 = T_\circ$$

and the plastic strain increments can be determined for the normal to this point (see Appendix V)

$$d\epsilon_1^\circ = (\sigma_1 - Q_\circ)\lambda$$
$$d\epsilon_2^\circ = (\sigma_2 - T_\circ)\lambda \qquad (2.6\text{-}26)$$
$$d\epsilon_3^\circ = (\sigma_3 - T_\circ)\lambda$$

An additional restriction is that $d\epsilon_1^\circ$ be positive and $d\epsilon_3^\circ$ be negative. If the first condition fails it is possible that zone three should have been considered. If the second condition fails it is possible that zone two should have been considered.

2.7 Plasticity in the Boundary Element Method

2.7.1 Stress-Strain Characteristics of Internal Elements

To make use of the equations developed in Section 7, in the solution of plasticity problems, the additional relationships between stress and plastic strains (Eq. (2.3-7)) or (2.4-10)) are required. These can be put into a form suitable for solution by differentiation

$$\partial\sigma_{ij}^p / \partial\sigma_{kl}^{\circ p} = Cv_{ijkl}^{pp}$$

Since Cv_{ijkl}^{pp} are constants, this partial differential can be written in terms of ordinary differentials giving

$$d\sigma^{p}_{ij} = Cv^{pp}_{ijkl} d\sigma^{\circ p}_{kl}$$

Substituting for the plastic strains (Eq. (2.1-5)) it can be found that

$$d\sigma^{p}_{ij} = -M_{ijkl} d\epsilon^{\circ}_{kl}$$

where

$$M_{ijkl} = Cv^{pp}_{ijmn} D_{mnkl}$$

This expression can be specialized for the orientation of the principal stresses giving

$$d\sigma'^{p}_{ij} = -M'_{ijkl} d\epsilon^{\circ p}_{kl}$$

where σ'^{p}_{ij} are the principal stresses and

$$M'_{ijkl} = A_{jm} A_{in} M_{mnkl}$$

where A_{ij} represents the coordinate transformation matrix from global to local coordinates such that the local coordinate system is chosen at the orientation of the principal stresses (see Appendix III). This expression can be further specialized for the orientation of the principal plastic strains which is required to be the same as that of the principal stresses, giving

$$d\sigma'^{p}_{ij} = -M^{\circ}_{ijkl} d\epsilon^{\circ\prime p}_{kl} \qquad (2.7\text{-}1)$$

where $\epsilon^{\circ\prime p}_{ij}$ are the plastic strain components in the orientation of the principal stresses, and

$$M^{\circ}_{ijkl} = M'_{ijmn} A_{km} A_{ln}$$

Expression (2.7-1) taken together with the failure envelope shown in Figure 2-3, and the plastic strain increments (Eq. (2.6-4)) as described in expressions (2.6-8) through (2.6-27) provide all the information required to solve plasticity problems.

2.7.2 Plastic Solution Technique

Deformations must be driven in a controlled manner by load stepping or by time stepping and assuming some time dependant strength relationship. The former case will be considered here and each load increment will be assumed to generate one increment in plastic strain. In the solution process three vectors must be considered:

1) the current best guess for the stress state,
2) the current best guess for the strain increment,

3) the accumulated total plastic strain state.

The guesses will be updated by iteratively calculating new guesses until all equations are satisfied to within an allowable stress error. Different stages of mining can be simulated by altering the boundary conditions of selected elements to enable or disable there influence. One possible solution process for incremental strain plasticity proceeds as follows:

1) Set the total plastic strain state to zero. Initialize the current strain increment to zero. Initialize the current stress state to the preexisting field stresses. This represents the stress state prior to excavation.

2) Assign the boundary conditions to simulate the mining step. Initialize the load step parameter δ to zero. The surface boundary conditions used in Eqs. (2.3-15) and (2.4-11) can be incremented by linear load stepping as follows

$$t_i^p = n_j \sigma_{ij}^{T'p} + \kappa (T_i^p - n_j \sigma_{ij}^{T'p})$$

where T_i^p represent the required surface boundary conditions and δ represents the loading factor varying from zero to one.

3) Apply a load step by incrementing the load step factor δ.

4) Calculate a guess at the stress state which from expressions (2.3-7) or (2.4-10). The stress state is calculated by one Gauss-Seidel iteration.

5) If the stress state at any point (centre of internal elements for discontinuous, constant initial stress distribution, or nodal points for continuous, piecewise linear initial stress distribution) exceeds the strength envelope as depicted in Figure 2-3, calculate the plastic strain increments required to bring the stresses back onto the strength envelope and update the current strain increment.

6) Repeat steps 4 and 5 until all equations are satisfied to within an allowable stress error. Then update the total plastic strain.

7) Repeat step 3 through 6 until a load factor of one is achieved. At this point a complete solution is available and field stress distributions may be calculated from expression (2.3-6) or expression (2.4-9).

8) Altering the boundary conditions of selected elements to simulate further excavation then repeat steps 2 through 7 until all excavations are complete.

3.0 TWO-DIMENSIONAL FORMULATION (Program MINE2D)

3.1 Introduction

The concepts discussed in Section 2 were first implemented in a two-dimensional version of the model MINE2D. This section discusses the development of MINE2D and the capabilities of this code. Verification test results are also presented.

3.2 Quadrilateral Elements

Until now, all code development and testing has been conducted with triangular elements due to the simplicity of their formulation. These elements use a linear interpolation for initial stress

$$\sigma^{\circ}_{ij} = A_{ij} + B_{ijk} X_k \qquad (3.2\text{-}1)$$

where A_{ij} and B_{ijk} are constants and X_k are cartesian coordinates. The constants A_{ij} and are determined by interpolating between the corner points of the element. Recall from the Section 2 that the required surface and body forces can be determined by substitution into the equations of equilibrium

$$\sigma_{ij,j} + \Psi_i = 0 \qquad (3.2\text{-}2)$$

giving

$$\Phi_i = n_j \cdot \sigma^{\circ}_{ij} = n_j \cdot (A_{ij} + B_{ijk} \cdot X_k) \qquad (3.2\text{-}3)$$

for the surface forces. The body force terms are given by the differentiation of the initial stresses

$$\Psi_i = -\sigma^{\circ}_{ij,j} = -B_{ijj} \qquad (3.2\text{-}4)$$

giving constant terms for the body forces. In these expressions n_j represents the direction cosines of the outward normal to the boundary of the volume element, and indicial notation has been used (see Appendix VI). As expected, these elements induced anisotropic response of the continuum and had to be doubled up and averaged (as shown in the diagram below) to eliminate this effect.

Although this averaging technique was successful, it required four element evaluations for each quadrilateral cell and hence unnecessarily large computer time. As an alternative to triangular elements, quadrilateral elements can be developed. First, assume that the surface force distribution is linear along the element edges. This is easily accommodated by linear interpolation between element corner points. This ensures that there will not be any mismatch in the applied forces from one element to the next.

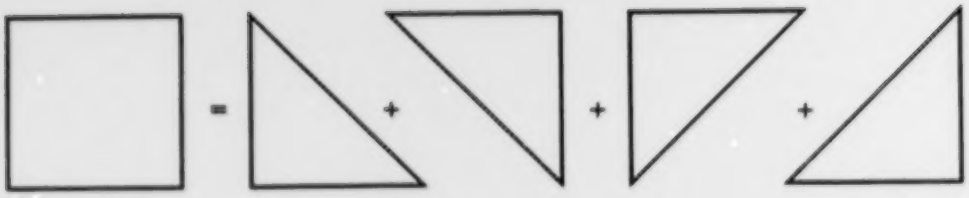

Figure 3-1 Triangular Elements

In order to determine the required body force distribution as in Eq. (3.2-4), a general expansion for the initial stress distribution for a quadrilateral with linear variation along its edges is required. Any such expression will involve complicated terms which would prove difficult to integrate, therefore as an alternative it is assumed that the initial stress distribution is given by Eq. (3.2-1) with one additional term C_{ij}

$$\sigma^{\circ}_{ij} = A_{ij} + B_{ijk} \cdot X_k + (1-\delta_{kl}) \cdot C_{ij} \cdot X_k \cdot X_l \qquad (3.2\text{-}5)$$

where A_{ij}, B_{ijk}, C_{ij} are determined by interpolating between the corner points of the element, and δ_{kl} represents the Kronecker delta (see Appendix I). As in Eq. (3.2-3), the body force terms are given by differentiation of the initial stresses

$$\Psi_i = -\sigma^{\circ}_{ij,j} = -B_{ijj} - (1-\delta_{jk}) \cdot C_{ij} \cdot X_k \qquad (3.2\text{-}6)$$

giving body force terms which are constant plus linear in X_k .

The constants B_{ijj} or C_{ij} must now be modified in order to ensure that equilibrium of forces is maintained within each element. In Eq. (3.2-6) it can be observed that C_{ij} represents the variation of the body force across the quadrilateral and dictates the moment which will be applied to the quadrilateral by the body forces. The magnitude of the body force term is represented by B_{ijj} and it is this coefficient which should be adjusted to maintain equilibrium. Integrating the equations of equilibrium (Eq. (3.2-2))

$$\iint \Psi_i \cdot dA = -\iint \sigma^{\circ}_{ij,j} \cdot dA \qquad (3.2\text{-}7)$$

where A indicates the surface area of the quadrilateral

$$A = \iint dA$$

Substituting for the body forces (Eq. (3.2-6)) in the left hand side of (Eq. (3.2-7)) it can be found that

$$-\iint \Psi_i \cdot dA - A \cdot [\, B_{iij} + (1-\delta_{jk}) \cdot C_{ij} \cdot \overline{x}_k \,] \qquad (3.2\text{-}8)$$

where $\overline{x}_k$ represents the moment arm of the centre of gravity of the quadrilateral

$$\overline{x}_k = \iint x_k \cdot dA \qquad (3.2\text{-}9)$$

The right hand side of Eq. (3.2-7) can be transformed into a path integral by use of Green's theorem (Kreyszig, 1972), giving

$$\iint \sigma^{\circ}_{ij,j} \cdot dA = e_{jk} \cdot \int \sigma^{\circ}_{ij} \cdot dx_k \qquad (3.2\text{-}10)$$

where e_{ij} represents the permutation symbol (see Appendix I). The right hand side of this equation is easily evaluated from the interpolated linear edge distribution of the initial stresses.

Solving for B_{iij} from Eqs. (3.2-7), (3.2-8) and (3.2-10) it can be found that the value required to maintain equilibrium is given by

$$B_{iij} = e_{jk} \cdot \int \sigma^{\circ}_{ij} \cdot dx_k / A - (1-\delta_{jk}) \cdot C_{ij} \cdot \overline{x}_k / A$$

For the special case of a rectangular element it can be found that this is in fact the same value as was obtained from interpolation of Eq. (3.2-5) and therefore for this case no modification would result.

These quadrilateral elements perform almost identically to the superimposed triangles illustrated in Figure 3-1. However, only a single element evaluation is required in place of four triangles and these quadrilateral elements do not exhibit geometric bias. Also, only half as many elements are used to describe the geometry. Although doubling up and averaging is not required for these elements, due to the higher order polynomial expansion used, a certain number of higher order integrals must be evaluated to obtain the influence coefficients.

3.3 Corners

In the first pass at code development, corners were ignored by simply setting all values (surface forces and initial stresses) to zero. While this enabled testing and verification of the numerical approach, it created a notable loss of accuracy particularly when using small numbers of elements. In order to improve the accuracy

for this case and thus permit better economy in analysis, corners have been studied in greater detail.

There are several situations which must be considered for a generalized mining geometry. These are illustrated in Figure 3-2. In this figure, only some of the corners are illustrated, however,

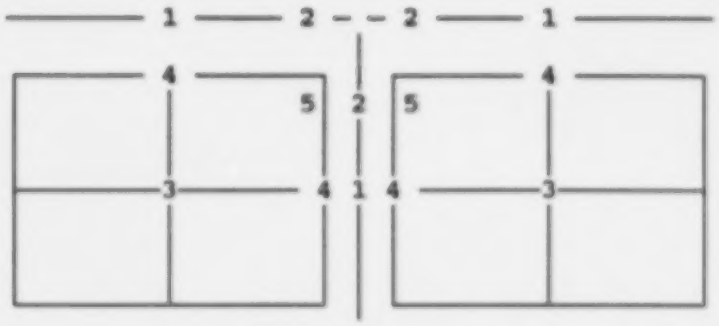

Figure 3-2 Corners

all required combinations of corners are considered. The corners labelled '1' are located on surface elements which are along straight boundaries and hence there is no singularity in stress. This condition was discussed thoroughly in Section 2 and the required contribution to the coefficient matrix is given by

$$\begin{matrix} 1 \\ - \\ 2 \end{matrix}\begin{bmatrix} 0 & \nu/(1-\nu) & 0 \\ 0 & 1 & 0 \\ 0 & 0 & 1 \end{bmatrix}$$

The corners labelled '2' are located at the ends of surface elements which may not necessarily be along straight boundaries and hence there is a singularity in stress at these points. In order to avoid this singularity it has been suggested by many authors (Banerjee and Butterfield, 1981) to create a double point at such locations by moving the point at which the integrals are evaluated in a small distance from the actual corner. For this case the required contribution to the coefficient matrix is the same as for case '1'. The exact distance at which the point should be inset from the element end can be determined by considering the nature of the singularity in stress at the corner. Timoshenko and Goodier (1970) provide the details of this singularity as

$$r^{\lambda-1} \qquad (3.3\text{-}1)$$

where r is the distance from the corner, and λ represents a parameter determined from the following relation

$$\lambda \cdot \sin(\theta) + \sin(\lambda\theta) = 0 \qquad (3.3\text{-}2)$$

and θ is the angle of solid material enclosed by the surfaces creating the corner as shown in Figure 3-3.

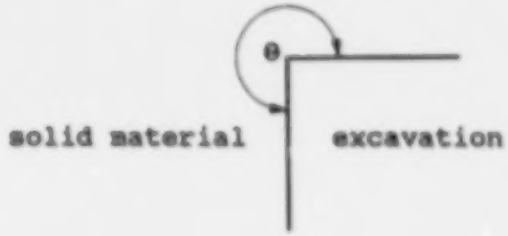

Figure 3-3 Corner Singularity

Consider the distribution of force applied to an element such that the force is singular at a corner according to the Eq. (3.3-1). Since in the boundary element model only linear variation of force have been permitted, we must calculate what assumed linear distribution is equivalent to the actual singular distribution. This can be determined by integrating the two force distributions and adjusting the inset distance of the corner point so that the total applied force is the same for both distributions. This arrangement is illustrated in Figure 3-4.

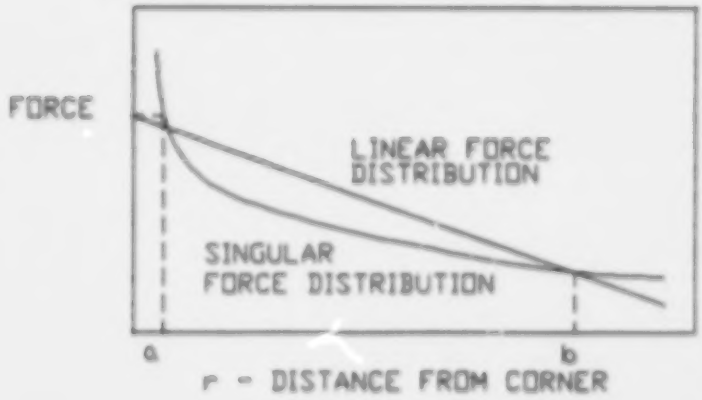

Figure 3-4 Singular and Linear Force Distributions

The integral of the linear term is given simply by

$$(b^{\lambda-1} + a^{\lambda-1}) \cdot b/2 \qquad (3.3\text{-}3)$$

where a is the location of the inset corner point, and b is the length of the element. The integral of the singular term is given by

$$\int_0^b r^{\lambda-1} dr = b^\lambda/\lambda \qquad (3.3\text{-}4)$$

Equating the two integrals (Eqs. (3.3-3 and 3.3-4) and reorganizing the equation gives the following result

$$\frac{a}{b} = \left[\frac{2-\lambda}{\lambda}\right]^{1/(\lambda-1)} \qquad (3.3\text{-}5)$$

Some values for this inset distance ratio are tabulated in Table 3-1. The following table illustrates a few values for the parameter λ as determined from Eq. (3.3-2), and the inset distance ratio determined from Eq. (3.3-5), given θ in degrees.

θ	$\pm\lambda$	a/b
180	1.0000	0.13534
210	0.7519	0.12969
260	0.5628	0.11714
270	0.5445	0.11549
280	0.5303	0.11415
360	0.500	0.11111

Table 3-1 Singularities

In general of most interest are corners of excavations with values of θ near 270°. It can be observed in Table 3-1 that the inset distance ratio is not very sensitive to θ.

In application it is found that smaller inset distances result in larger values of applied boundary force. Also, when using a small number of elements, smaller inset distances tend to result in excess applied surface forces compared to the same problem analysed using a large number of elements. This is illustrated in Figure 3-4 where the integral of the applied surface force is plotted as a function of the inset distance ratio (a/b) . These results have been generated by considering a square shaped excavation in an elastic medium analysed with several different discretizations. In Figure 3-5, n indicates the number of elements used to discretize each side of the excavation.

It can be observed in this figure that the best choice for the inset distance ratio is approximately 0.134 for the surface normal forces, and 0.130 for the surface shear forces. These values can be compared to the value 0.146, which is obtained by Chebyshev interpolation (Hornbeck, 1975). Also, Banerjee and Butterfield

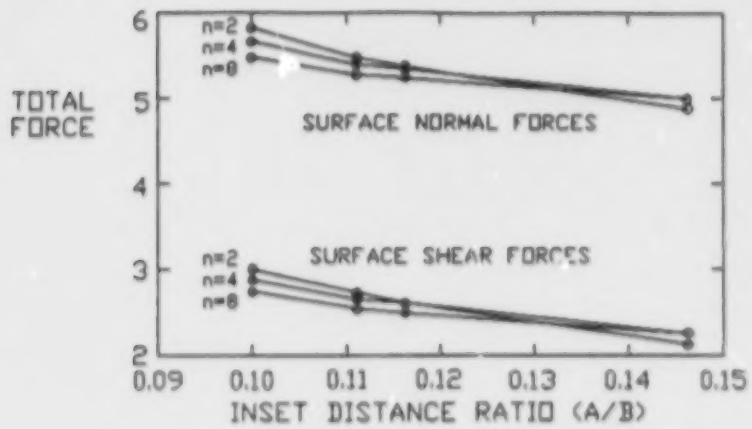

Figure 3-5 Total Applied Surface Forces

(1981) recommend that this is a potential source of instability unless the inset distance ratio is sufficiently large, therefore ensuring that the double nodes (corners labelled '2') are truly independent. Although, the number of Gauss-Seidel iterations (Section 3.7, "Solution Process") required to solve problems has been observed to increase for smaller values of the inset distance ratio, numerical instability has not been a problem.

It can be concluded that the larger values are most desirable to maintain good numerical stability, where as smaller values are desirable to ensure adequate accommodation of the corner effects. Several geometries would have to be studied in order to make the optimum choice, however, it can also be observed in Figure 3-5 that the results are not very sensitive to the choice of this value for the case considered here, and the inset distance ratio corresponding to a 270° angle is a good choice.

Referring again to Figure 3-2, it can be observed that the corners labelled '3' are completely surrounded by volume elements. Because the initial stress distribution has been chosen as piecewise linear, and there are no discontinuities at these points, there is no contribution to the coefficient matrix to be made here.

The corners labelled '4' are on the edge of volume elements which are along straight boundaries and hence there is no singularity in stress. The required contribution to the coefficient matrix is almost the same as for the surface element corner labelled '1' and is given by

$$-\frac{1}{2}\begin{bmatrix} 0 & \nu/(1-\nu) & 0 \\ 0 & 1 & 0 \\ 0 & 0 & 1 \end{bmatrix}$$

The negative sign arises due to the fact that the boundary of the volume element must be approached from the outside. This condition was discussed thoroughly in Section 2.

The corners labelled '5' are located at the corners of volume elements which may not necessarily be along straight boundaries and hence there is a singularity in stress at these points. In order to avoid this singularity, a "double point" is created at such locations by moving the point at which the integrals are evaluated in a small distance from the actual corner towards the centre of the element. For this case there is no required contribution to the coefficient matrix just as for case '3' since the point is completely surrounded. The inset distance used has been chosen as the same one used for the surface inset distance so that these points will lie directly under the surface points '2'. This choice should assist in improving the stability of the solution.

3.4 Multiple Materials

Mining problems typically involve several materials including the host rocks, dykes, ore and backfill. In order to simulate such a system with the application of the boundary element method described here, one starts with an elastic, host material extending to infinity, and volume elements must be placed at all locations where there are non-host materials or stress states. As the stresses change in these areas due to excavation or equilibration, intial stresses are applied to these volume elements to force behaviour to correspond to alternate constitutive relations. While the underlying host material continues to deform elastically, the superimposed material may behave as a visco-plastic material with different modulii from the host.

To demonstrate this behaviour consider the stress-strain relationships illustrated in Figure 3-6. The host material can be observed to behave linearly elastic, while the ore material behaves elasto-plastic with different elastic modulii than the host material. The following relationships describe the stress-strain behaviour as well as stating the effect of the surface forces ϕ , and initial stresses σ° , on the stress state of both the host and ore materials

$$\sigma = \begin{cases} = \sigma_{Host} + C_S\phi + C_V\sigma^{\circ} \\ = \sigma_{host} + \sigma^{\circ} + D_{Host}\varepsilon \\ = \sigma_{Ore} + D_{Ore}\cdot(\varepsilon-\varepsilon^{\circ}) \end{cases} \qquad (3.4\text{-}1)$$

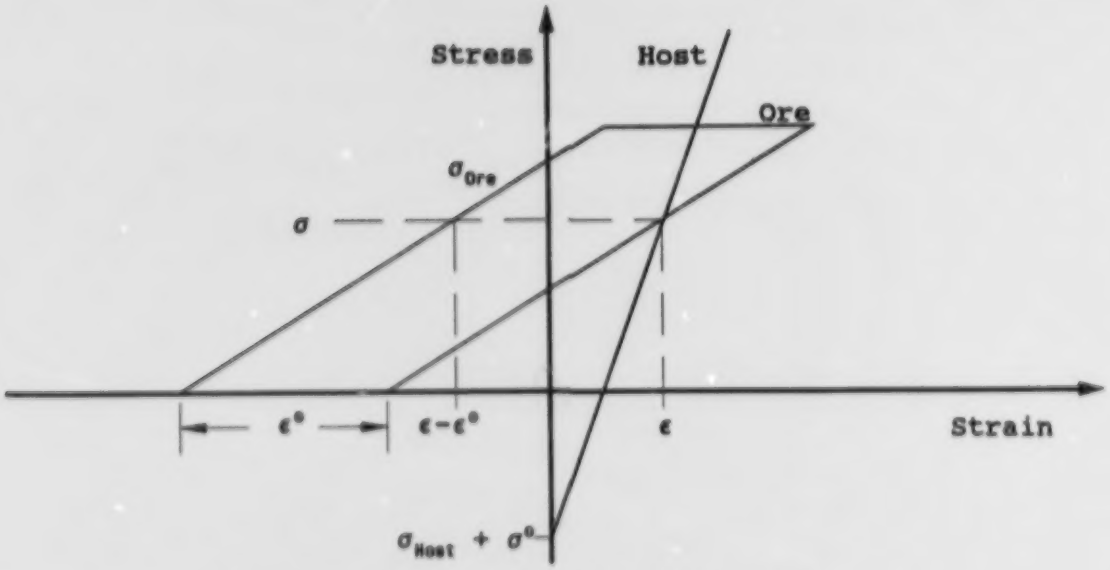

Figure 3-6 Elasto-Plastic Behaviour

Here, σ and ϵ represent respectively the stress and total strain common to both materials, ϵ° represents initial (plastic) strain in the ore, Cs and Cv represent respectively the coefficient matrices relating surface forces and initial stresses to induced stresses, σ_{Host} and D_{Host} represent respectively the field stresses and elastic stress-strain relations for the host material, and σ_{Ore} and D_{Ore} represent respectively the field stresses and elastic stress-strain relations for the ore.

What is implied in these relationships is that the stress and the total strain must be equal in both the host and ore materials, while all non-linear straining in the ore is accommodated by elastically deforming the host with initial stresses. Although this discussion has referred only to host and ore materials, the same relationships apply to any elasto-plastic material which is in place at the beginning of the analysis. The placement of materials during subsequent mining steps requires special considerations which are discussed later (Section 3.5, "Backfill Placement - Mining Steps").

Equations (3.4-1), can be used to determine the increments in stress $d\sigma$ initial stress $d\sigma^\circ$ and initial strain required to go from the current equilibrium state given by σ, σ° and ϵ°, to a new equilibrium stress state given by

$$\begin{aligned} \sigma &\rightarrow \sigma + d\sigma \\ \sigma^\circ &\rightarrow \sigma^\circ + d\sigma^\circ \\ \epsilon^\circ &\rightarrow \epsilon^\circ + d\epsilon^\circ \end{aligned} \qquad (3.4\text{-}2)$$

First solving for the total strain from the second and third of Eq. (3.4-1) it can be found that

$$\varepsilon = D_{Host}^{-1}\cdot(\sigma \sigma_{Host} - \sigma^{\circ}) - D_{Ore}^{-1}\cdot(\sigma - \sigma_{Ore}) + \varepsilon^{\circ}$$

and noting that for the isotropic materials considered here

$$D_{Host}\cdot D_{Ore} = D_{Ore}\cdot D_{Host} \qquad (3.4\text{-}3)$$

this equation can be rewritten as

$$D_{Ore}\cdot(\sigma - \sigma_{Host} - \sigma^{\circ}) = D_{Host}\cdot(\sigma - \sigma_{Ore}) + D_{Host}\cdot D_{Ore}\cdot\varepsilon^{\circ} \qquad (3.4\text{-}4)$$

Assuming that the surface forces do not change, a first guess for the increment in intial stress can be found by differentiation of the first of equations (3.4-1) giving

$$d\sigma = Cv\cdot d\sigma^{\circ} \qquad (3.4\text{-}5)$$

As the solution procedure progresses, the surface forces settle on specific values and the assumption that they do not change becomes progressively more valid.

Substituting Eqs. (3.4-2 and (3.4-5) into Eq. (3.4-4), it can be found that

$$[D_{Host} \cdot Cv + D_{ore} - D_{ore} \cdot Cv] \cdot d\sigma^{\circ} = D_{ore}\cdot(\sigma-\sigma_{Host}-\sigma^{\circ}) - D_{Host}\cdot(\sigma-\sigma_{ore}-D_{Host}\cdot D_{ore}\cdot(\varepsilon^{\circ} + d\varepsilon^{\circ}) \qquad (3.4\text{-}6)$$

This relation can now be used to estimate the initial stress required to satisfy all three of equations (3.4-1), thereby superimposing the elasto-plastic behaviour of the ore material on the elastic, initially stressed host material.

3.5 Backfill Placement - Mining Steps

In the process of mining, excavations are made and then backfilled. In order simulate this process using the boundary element method, it is necessary to first bring the stresses at the surfaces of excavations down to zero from their initial field stress values, and then to place new material within these excavations at some initially pre-stressed value. In this application of the boundary element method, one starts with an elastic, host material extending to infinity, and all excavations or non-host materials must be superimposed. The following discussion is presented in order to avoid confusion as to the actual stress state in the interior of excavations where backfill is placed. To demonstrate this process,

consider the hypothetical example illustrated in Figure 3-7. In this figure, the volume elements are labelled block 1 and block 2, and the surface elements are labelled 3 through 9. To accomplish

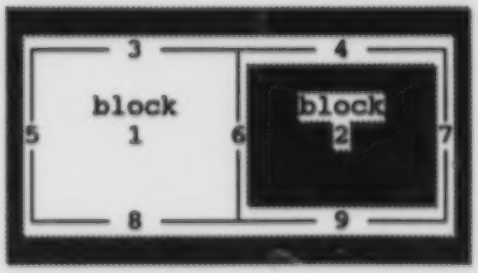

Figure 3-7 Mining With Backfill - Excavate Block 1

the excavation of block 1, the influence of volume elements within block 1 must be nulled, and the surface elements surrounding it (elements 3, 5, 6 and 8) must be activated. The volume elements within block 2 will only be active if the material properties and stress state assigned to this block are different from the host material (linear elastic host material). Surface elements 4, 7 and 9 are not activated at this mining step. The problem can now be analysed by the method discussed in Section 3.7 ("Solution Process"). The stresses within block 1 are calculated for use in subsequent mining steps, however, their values have no bearing on the current results.

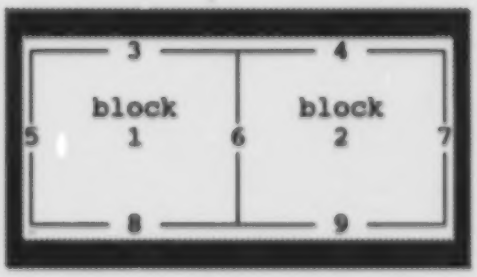

Figure 3-8 Mining With Backfill - Excavate Block 2

Next, consider the excavation of block 2 (Figure 3-8). All volume elements within blocks 1 and 2 are deactivated, and all surface elements except 6 are activated. Surface element 6 must be nulled. The problem can now be solved.

Consider the backfilling of block 1 (as illustrated in Figure 3-9). If the backfill is to be placed at a known stress state

$\sigma_{Placement}$

an intermediate step is required to bring the surface stresses acting on block 1 to the required values by assigning the desired surface stresses to elements 3, 5 and 8. In this example, element 6 cannot be activated and hence the backfill will not be placed in any equilibrium stress state except zero horizontal initial stress. If the entire excavation were to be backfilled at this mining step, the desired placement stress would be assigned to elements 3, 4, 5, 7, 8 and 9, and hence the backfill could be placed at any equilibrium stress state of known value.

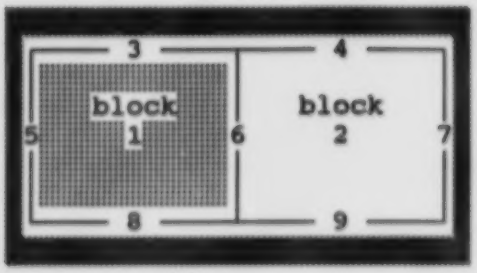

Figure 3-9 Mining With Backfill - Backfill Block 1

Whether or not the previous equilibrating step is conducted, the backfill can be placed at any desired initial stress state ($\sigma_{Backfill}$) and the model will equilibrate the stresses. Now consider the backfilling of block 1. All volume elements within block 1 are activated and assigned backfill properties. The current stress state

$$\sigma^p = \sigma_{Host} + Cs \cdot \phi + Cv \cdot \sigma^o \qquad (3.5\text{-}1)$$

in these elements must be recorded so that it can be subtracted from the calculated stress state during the solution procedure. In this equation, σ_{Host} represents the initial field stress state in the host material, Cs and Cv represent respectively the coefficient matrices relating the surface forces ϕ, and initial stresses σ^o, to the induced stresses. It is the variation in stress from this current stress state which is of interest, as it is this variation in stress which represents the true stress in the backfill.

Surface elements 4, 7 and 9 continue to be active, and element 6 must also be activated to bring the surface stresses along its boundary to the desired value (normally zero). As with the volume elements within block 1, it is the variation in stress from the current stress state which represents the true stress at this surface. Surface elements 3, 5 and 8 are not activated, however, there current influence must be maintained in order to preserve the stress state associated with the previous mining step.

The following relationships describe the stress-strain behaviour as well as stating the effect of the surface forces ϕ , and initial stresses σ^o, on the stress state of both the host and backfill

materials

$$\begin{aligned}\sigma &= \sigma_{Host} + CS \cdot \phi + Cv \cdot \sigma^{\circ} - \sigma^{P} + \sigma_{Placement} \\ &= \sigma_{Placement} + \sigma^{\circ} + D_{Host}\varepsilon \\ &= \sigma_{Backfill} + D_{Backfill} \cdot (\varepsilon - \varepsilon^{\circ})\end{aligned} \qquad (3.5\text{-}2)$$

where σ and ϵ represent respectively the stress and total strain common to both materials, ϵ° represents initial (plastic) strain in the backfill, σ_{Host} and D_{Host} represent respectively the field stresses and elastic stress-strain relations for the host material, and $\sigma_{Backfill}$ and $D_{Backfill}$ represent respectively the field stresses and elastic stress-strain relations for the backfill. Observation of these relations reveals that if the backfill is placed in equilibrium, the stress state will be exactly equal to the placement stress. This will be the case until there is some change in the surface forces, initial stresses, initial strains or total strain, induced by some change in the geometry.

Just as for the case of multiple materials (see Section 3.4, "Multiple Materials"), it is implied in these relationships that the stress and the total strain must be equal in both the host and backfill materials, while all non-linear straining in the backfill is accommodated by elastically deforming the host with initial stresses.

3.6 Elasto-Visco-Plastic Behaviour

In Section 2 the theory of incremental plasticity and the plastic solution technique were discussed in detail. Early in the project, experience with that approach was not entirely satisfactory. It was found that convergence rates were less than optimum because the load stepping algorithm is insensitive to the magnitudes of plastic strain. Ideally, small load steps are desirable during periods of large plastic straining, and large load steps speed convergence during periods of little or no plastic straining.

3.6.1 Elasto-Visco-Plastic Theory

The theory of visco-plasticity (Zienkiewicz, 1977) does just what is required by controlling the rate of plastic deformations. In Figure 3-10 an elasto-visco-plastic element is illustrated. In this figure, σ' and σ° represent respectively the stresses induced by the elasto-plastic, and the viscous behaviour of the material, and ϵ and ϵ° represent respectively the elastic and visco-plastic components of the total strain ϵ.

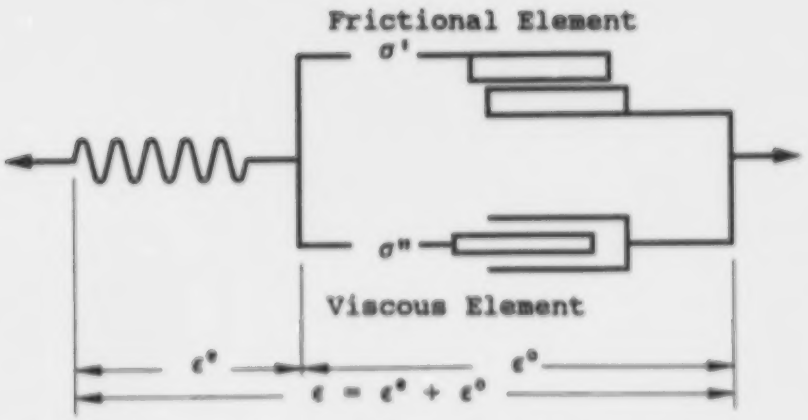

Figure 3-10 Elasto-Visco-Plastic Element

In the theory of visco-plastic behaviour, additional stress components are introduced, the magnitudes of which are proportional to the magnitude of the plastic strain rate as follows

$$\sigma^{\circ} = C_1 \cdot \varepsilon^{\circ} + C_2 \cdot |\varepsilon^{\circ}| \cdot \varepsilon^{\circ} \qquad (3.6\text{-}1)$$

where $\varepsilon_{\circ}$ represents the plastic strain rate with time, and C_1 and C_2 represent respectively modulii describing the stress-strain rate relations. The second term on the right hand side is a modified form of viscous behaviour where the induced stress depends on the square of the plastic strain rate. This has been introduced because it has the desirable property of decaying very quickly as the magnitude of the strain increment approaches zero.

The stress increment induced by a plastic strain increment is found by differentiation of this expression giving

$$d\sigma^{\circ} = \gamma \cdot d\varepsilon^{\circ} \qquad (3.6\text{-}2)$$

where γ represents a viscous parameter defined by

$$\begin{aligned} \gamma &= \gamma_1 + \gamma_2 \cdot |d\varepsilon^{\circ}| \\ \gamma_1 &= C_1/\Delta t \\ \gamma_2 &= C_2/\Delta t^2 \end{aligned} \qquad (3.6\text{-}3)$$

and Δt represents the increment of time over which the increment of plastic strain occurs.

To obtain a first best guess of the plastic strain increment, it can be assumed that during the plastic strain increment, the total strain will remain constant. As the solution procedure progresses, the stress and strain state settle on specific values and the assumption that they do not change becomes progressively more accurate. Then from Eq. (3.4-1) or (3.5-2), the incremental

stress-strain relations are easily obtained by differentiation giving

$$d\sigma = -D \cdot d\varepsilon^{*} = d\sigma' + d\sigma^{*}$$

Here, D can represent either D_{Ore} or $D_{Backfill}$ depending on which material was under consideration. By substituting Eq. (3.6-2) the components of stress induced by the viscous element are incorporated to give

$$d\sigma' = -D \cdot d\varepsilon^{*} - \gamma \cdot d\varepsilon^{*}$$

which can be rewritten as

$$d\sigma' = -D' \cdot d\varepsilon^{*} \qquad (3.6\text{-}3)$$

where

$$D' = D + I \cdot \gamma$$

and I represents an identity matrix.

3.6.2 Elasto-Visco-Plastic Examples

In Section 2 it was demonstrated that the stresses could be related to the plastic strain increment with the following three assumptions:

i) stresses are limited by a strength criterion;
ii) strain increments are interrelated depending on the stress conditions;
iii) strain increments are parallel to the stresses

To demonstrate the application of this theory, consider a Mohr-Coulomb plastic failure condition

$$\begin{aligned} \sigma_1' &= C_o + q \cdot \sigma_3' \\ d\varepsilon^{*}_3 &= -\beta \cdot d\varepsilon^{*}_1 \end{aligned} \qquad (3.6\text{-}4)$$

where σ_1' and σ_3' represent respectively the major and minor principal stress components, $d\varepsilon^{*}_1$ and $d\varepsilon^{*3}$ represent respectively the major and minor principal plastic strain increments, and C_o, q and ß represent respectively the unconfined compressive strength, the friction coefficient and the dilation rate. Alternatively, the Hoek-Brown failure criterion (Hoek and Brown, 1980) could be considered

$$\sigma_1 = \sigma_3 + \sqrt{m \cdot \sigma_c \cdot \sigma_3 + s \cdot \sigma_c^2} \qquad (3.6\text{-}5)$$

where m and s represent strength parameters, and σ_c represents the small scale unconfined compressive strength. This is accommodated by taking the tangent to this curve at the current stress state and substituting for

$$C_o = (m\sigma_c \cdot \sigma_3 + 2 \cdot s \cdot \sigma_3^2) / [2\sqrt{2 \cdot m \cdot \sigma_c \cdot \sigma_3 + s \cdot \sigma_c^2}]$$
$$q = 1 + m\sigma_c / [2\sqrt{m\sigma_c \cdot \sigma_3 + s \cdot \sigma_c^2}]$$

Selection of an appropriate failure zone depending on the current stress state was discussed in detail in Section 2.6.1. The condition considered here corresponds to zone 1.

Given that the strength criterion is exceeded, the required stress state can be determined as

$$\sigma_1' + d\sigma_1' = C_o + q(\sigma_3' + d\sigma_3')$$

substituting for $d\sigma'$ from Eq. (3.6-3) and reordering gives

$$\sigma_1' - C_o - q \cdot \sigma_3' = -d\sigma_1' + q \cdot d\sigma_3'$$
$$= [D_{11}' \cdot d\varepsilon^{e1} + D_{12}' d\varepsilon^{e3}] - q \cdot [D_{21}' \cdot d\varepsilon^{e1} + D_{22}' \cdot d\varepsilon^{e3}]$$

and finally substituting Eq. (3.6-4) and reordering again gives

$$\sigma_1' - C_o - q\sigma_3' = \{D_{11}' - \beta \cdot D_{12}' - q[D_{21}' - \beta \cdot D_{22}']\} \cdot d\varepsilon_1^e$$

from which $d\varepsilon^{e1}$ can easily be obtained.

As another example, consider the the application of this theory to a material in which the tensile strength, T_o has been exceeded.

The condition considered here corresponds to zone 3 (Section 2.6.1). The required stress and strain increment relations are given by

$$\begin{aligned} \sigma_3' &= T_o \\ d\varepsilon_1^e &= 0 \\ \sigma_3' &= T_o \\ d\varepsilon_1^e &= 0 \end{aligned} \qquad (3.6\text{-}6)$$

The required stress state can be determined as

$$\sigma_3' + d\sigma_3' = T_o$$

substituting for $d\sigma'$ from Eq. (3.6-3) and reordering gives

$$\sigma_3' - T_* = -d\sigma_3' - D_{22}' \cdot d\epsilon_3^e$$

from which $d\epsilon^{e1}$ can easily be obtained.

In both of these examples it can be noted that we are dealing with the plastic (frictional) components of stress, σ', however, the viscous component can easily be determined from Eq. (3.6-1) or (3.6-2) if desired. Since as part of the solution, the viscous stress component and the plastic strain increment are known, the current time increment can also be determined from Eqs. (3.6-2) and (3.6-3) if desired.

Since solutions are obtained by elasto-visco-plastic time stepping, unstable problems can be successfully analysed. These include problems such as hangingwall sloughing, where no static equilibrium state is possible.

Use of the C_1 term only (i.e. set C_2 equal to zero) presents a problem if the solution of interest corresponds to the case when static equilibrium is achieved (i.e. when viscous components are zero). It is apparent that the viscous stress components will not equal zero until the strain increment is zero theoretically requiring an infinite number of time steps. Although in practice, the solution process would be stopped when the viscous stress increment reached some small limiting value, it often takes an excessively large number of plastic strain increments (or time steps) to reach this point. The only solution in this case is to increase the time step size (i.e. reduce the magnitude of γ_1) as plastic flow progresses. It is highly desirable to avoid manual intervention in the solution process, and therefore this is not a viable alternative to consider.

Use of C_2 term only (i.e. set C_1 equal to zero) in Eq. (3.6-1) provides a solution to this problem. It can be observed in this equation that the viscous stress component varies as the square of the plastic strain increment, and approaches zero very quickly as the plastic strain increment approaches zero. In fact, for this case, the magnitude of γ in Eq. (3.6-2) can be observed to depend linearly on the magnitude of the plastic strain increment. This has the desirable effect of progressively reducing the viscous effect as the magnitude of the plastic strain increment reduces, thereby accelerating convergence to a static equilibrium solution.

In Figure 3-11, the magnitude of the viscous stress in the viscous element is plotted for two alternatives. For this example, the magnitudes of γ_1 and γ_2 have been chosen so that the plastic strain increments are approximately equivalent in magnitude during the first few time steps. It can be observed that although both cases approach static equilibrium asymptotically, the case where γ_1 is

used (γ_2 set equal to zero, shown by a dashed line) is much slower to converge, requiring a total of 60 iterations compared to only 18 iterations for the case where γ_2 is used (γ_1 set equal to zero, shown by a solid line).

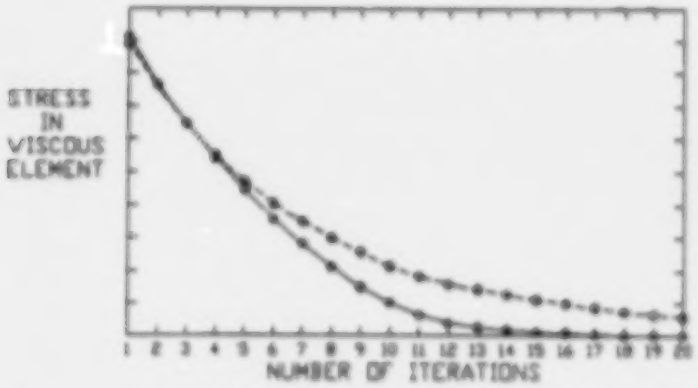

Figure 3-11 Convergence To Static Equilibrium

3.7 Fault Slip - Seam Mining Simulation

In this section the incorporation of fault slip simulation into the indirect boundary element method (BEM) is discussed. This is accomplished by superposing displacement discontinuities with the surface and body forces which are already used to simulate excavations and nonhomogeneous zones. A procedure similar to that developed by Crouch (1976) has been used here which enables fault slip and seam mining to be approximated.

3.7.1 Displacement Discontinuities

Consider an isotropic, linear elastic, homogeneous region v with an enclosed excavation surface s, and interface surface s', as shown in Figure 3-12.

The stresses and displacements at any point in the body can be determined by superposing the effects of surface tractions $\phi_j(\xi)$, distributed over s, and body forces $\Psi_j(x)$ distributed overv, and discontinuities in displacement $\Gamma_j(\xi)$, distributed over s'.

Using the indirect boundary element method (BEM), as in Section 2, the required integrals for the displacements $u_s(x)$ and stresses

$\sigma_{ij}(x)$ are given by

$$u_k(x) = X_k + \int_s g_{km}(x,\xi)\phi_m(\xi)\,ds(\xi) + \int_v g_{km}(x,z)\phi_m(z)\,dv(z) + \int_{s'} g'_{km}(x,\xi)\Gamma_m(\xi)\,ds'(\xi) \quad (3.7\text{-}1)$$

$$\sigma_{ij}(x) = \sigma^{o}_{ij}(x) + \sigma^{r}_{ij}(x) + \int_s c_{ijm}(x,\xi)\phi_m(\xi)\,ds(\xi)$$

$$+ \int_v c_{ijm}(x,\xi)\phi_m(z)\,dv(z) + \int c'_{ijm}(x,\xi)\Gamma_m(\xi)\,ds'(\xi) \quad (3.7\text{-}2)$$

Figure 3-12 Isotropic, linear elastic, homogeneous region v with an enclosed excavation surface s and interface surface s'

where $ds(\xi)$, $dv(z)$ and $ds'(\xi)$ indicate that the variables of integration are ξ_i, z_i, ξ_i respectively. The X_k are unknown rigid-body displacements. Where $g_{km}(x,\xi)$ and $c_{ijm}(x,\xi)$ represent respectively the fundamental singular solution for displacements and stresses induced by the application of a unit point force, and $g'_{km}(x,\xi)$ and $c'_{ijm}(x,\xi)$ represent respectively the Green's function for a unit singular solution for stresses and displacements induced by a discontinuity in displacement (Wiles and Curran, 1982). Parameters $\sigma^{o}_{ij}(x)$ and $\sigma^{r}_{ij}(x)$ represent respectively initial stresses required to suppress the permanent set, and the pre-existing field stresses. In these expressions n_i represents the direction cosines of the outward normal to the surface s or s', and indicial notation has been used (see Appendix VI). Definitions of these parameters are given in Appendix I and VII.

All of the formulations discussed in Sections 2.3, 2.4 and 2.5 can be taken again to develop expressions suitable for solving problems. The stresses at any point in the solid medium can be obtained as before with the addition of terms representing the

effect of a discontinuity in displacement occurring on the surfaces s'

$$\sigma_{ij}(x) = \sigma^{o}_{ij}(x) + \sigma^{T}_{ij}(x)$$

$$+ \sum_{q=1}^{N} \left[Cs^{q}_{ijn}(x) \Phi^{q}_{n} + CV^{q}_{ijmn} + Cd^{q}_{ijn}(x) \Gamma^{q}_{n} \right] \qquad (3.7\text{-}3)$$

where $Cs^{q}_{ijn}(x)$, $CV^{q}_{ijmn}(x)$, $Cd^{q}_{ijn}(x)$ represent respectively the effect of the surface forces Φ^{q}_{n}, initial stresses σ^{oq}_{mn} and displacement discontinuities Γ^{q}_{n}, at nodal point q, on the stress at position x. There are a total of N nodal points. This expression can be used to evaluate the stress distribution throughout the body, however, this can only be accomplished if the surface forces, initial stresses and displacement discontinuities are known. Determination of these is the objective of the boundary element analysis.

The assembly of expressions in Eq. (3.7-3) into a form suitable for solution can be conducted following the same procedure used in Section 2 to give the stresses at an interior nodal point p

$$\sigma^{p}_{ij} = \sigma^{Tp}_{ij} + \sum_{q=1}^{N} \left[Cs^{qp}_{ijn} \Phi^{q}_{n} + CV^{qp}_{ijmn} \sigma^{oq}_{mn} + Cd^{qp}_{ijn} \Gamma^{q}_{n} \right]$$

where

$$\begin{aligned} \sigma^{Tp}_{ij} &= \sigma^{T}_{ij}(X^{p}) \\ Cs^{qp}_{ijn} &= Cs^{q}_{ijn}(X^{p}) \\ CV^{qp}_{ijmn} &= CV^{q}_{ijmn}(Xp) + \delta^{qp}\delta_{im}\delta jn \\ Cd^{qp}_{ijn} &= Cd^{q}_{ijn}(X^{p}) \end{aligned} \qquad (3.7\text{-}4)$$

and δ_{ij} represents the Kronecker delta and δ^{qp} represents a substitution tensor similar to the Kronecker delta with the property that it equals one only when p and q are coincident.

The boundary tractions for a nodal point p located at the surface of an excavation or the surface of a displacement discontinuity can be found from this expression by effecting stress transformations to the local coordinates (denoted by the primes) of the surface node giving

$$t'^{p} = n_{j}\sigma^{Tp}_{ij} + \sum_{q=1}^{N} \left[n_{j} Cs'^{qp}_{ijn} \Phi^{q}_{n} + n_{j} CV'^{qp}_{ijmn} \sigma^{oq}_{mn} + n_{j} Cd'^{qp}_{ijn} \Gamma^{q}_{n} \right] \qquad (3.7\text{-}5)$$

Details of this stress transformation are given in Section 2.

In two dimensions there are two unknown surface forces Φ_s^q and two known surface tractions t_i^p for each nodal point p on the surface s, and Eq. (3.7-5) generates two equations. There are three unknown stresses σ_{ij}^p and three unknown initial stresses σ_{ij}^{oq} for each interior nodal point p, and Eq. (3.7-4) generates three equations. There are two unknown displacement discontinuities Γ_s^q and two unknown surface tractions t_i^p for each nodal point p on the surface s', and Eq. (3.7-5) generates two equations. In order to solve for all unknowns, three additional equations are required for each internal point, and two additional equations are required for each interface point. For interior points, these are provided by the theory of plasticity as discussed in detail Section 2. For the interface points, additional considerations are required as discussed below.

In three dimensions there are three unknown surface forces Φ_s^q and three known surface tractions t_i^p each nodal point p on the surface s, and Eq. (3.7-5) generates three equations. There are six unknown stresses σ_{ij}^p and six unknown initial stresses σ_{ij}^{oq} for each interior nodal point p, and Eq. (3.7-4) generates six equations. There are three unknown displacement discontinuities Γ_s^q and three unknown surface tractions t_i^p for each nodal point p on the surface s', and Eq. (3.7-5) generates three equations. In order to solve for all unknowns, six additional equations are required for each internal point, and three additional equations are required for each interface point. For interior points, these are provided by the theory of plasticity as discussed in detail in Section 2. For the interface points, additional considerations are required as discussed below.

3.7.2 Strength of Material - Failure Criterion

As discussed above, additional equations are required for each interface point. The first of these equations is the failure criterion for the fault. A failure envelope must be specified for the material as shown in Figure 3-13. While any relationship can be used, the Mohr-Coulomb criterion as discussed by Jaeger and Cook (1979)

$$|\sigma_s| = S_o + \sigma_n \tan\Phi \qquad (3.7\text{-}6)$$

has been used here, where S_o and Φ are commonly referred to respectively as the cohesion and friction angle. Parameters σ_s and σ_n represent respectively the shear and normal stresses acting on the interface surface, and can be exchanged for σ_2 and σ_1 respectively in indicial notation. In the case of three-dimensional analysis there are two orthogonal components to the shear stress σ_2 and σ_3 . These must be resolved by vector addition into one maximum component given by

$$\sigma_s = \sqrt{\sigma_1^2 + \sigma_3^2}$$

Also, a tension cut-off given by

$$\sigma_n = T_o \qquad (3.7\text{-}7)$$

has been incorporated to permit opening of the fault under tensile loading conditions. A compression limit given by

$$\sigma_n = C_o \qquad (3.7\text{-}8)$$

has also been incorporated to limit compressive stresses when simulating pillar yielding. The material properties are given by S_o, ϕ, T_o, C_o . To extend these failure criterion to apply for post-peak deformations, the constants in the expressions can be made any general function of stress or strain and will probably be related to the amount of damage incurred by the material with continued plastic deformation.

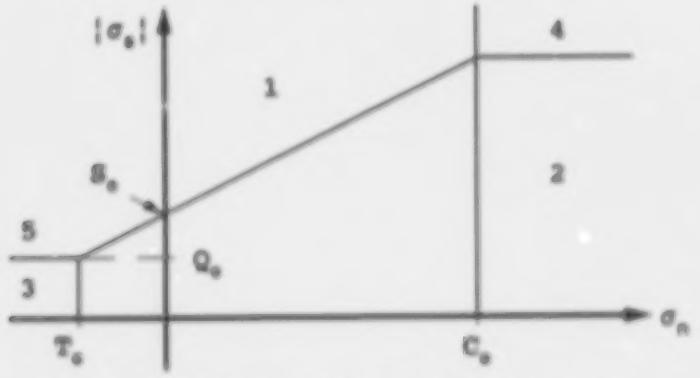

Figure 3-13 Failure Envelope

As a first approximation, it is assumed that the material behaves elastically until the stresses reach the peak strength defined by the strength criterion Eqs. (3.7-6), (3.7-7) and (3.7-8) described by the following constants S_o', ϕ', T_o', C_o' . Plastic deformations occur beyond this point according to material properties representative of the residual strength of the material and described by the following constants S^r_o, ϕ^r, $T^r o$, $C^r o$.

A second relation can be obtained by consideration of the dilation of the material with plastic shear deformation. This is simply defined by

$$\beta = -d\varepsilon^p_n / d\varepsilon^p_s$$

where ε^p_n and ε^p_s represent respectively the normal and shear plastic strains, and $d\varepsilon^p_n$ and $d\varepsilon^p_s$ represent the variations of these called plastic strain increments. For total strain plasticity theory this expression is approximated by

$$\beta = -\varepsilon^p_n/\varepsilon^p_s$$

If it is assumed that normality of stresses and plastic strains or strain increments applies, the dilation rate is determined by the negative reciprocal of the slope of the failure envelope in the appropriate zone (as depicted in Figure 3-13) giving

$$\beta = |d\sigma_s/d\sigma_n$$

Since the constants in Eqs. (3.7-6), (3.7-7) and (3.7-8) may be functions of stress or strain, the dilation will also be dependant on these.

This provides the one additional expression required in two-dimensional analysis. For the three-dimensional case an additional expression is obtained by requiring that the plastic strain increments are parallel to the stresses

$$\sigma_1, \sigma_2, \sigma_3 \mid d\varepsilon^p_1, d\varepsilon^p_2, d\varepsilon^p_3$$

Just as for the stresses, the maximum plastic shear strain is defined as the vector sum of the two shear components.

These relationships can be more rigorously derived from plastic potential theory as described by Johnson and Mellor (1973) and Zienkiewicz (1977). The failure criterion is called a yield surface when it is extended to accommodate post-peak deformations. As above, this provides one equation. An expression called a plastic potential function is used to determine the relationship between the stresses and plastic strain increments by differentiation

$$d\varepsilon^p_i = \lambda \frac{\partial Q}{\partial \sigma_i} \qquad (3.7\text{-}9)$$

where Q is the plastic potential function, and λ is a proportionality constant which contributes one additional unknown to the problem. This expression provides two independent equations in two dimensions and three independent equations in three dimensions thereby making solution possible.

If the yield surface and the potential function are specified as distinct expressions the approach is known as non-associated plasticity. If they are identical, they are called the flow rule and the approach is called associated plasticity.

Throughout most of the following discussion, incremental plasticity theory will only be considered. Total strain plasticity theory can be implemented by using the same relations and substituting ε^p_i for $d\varepsilon^p_i$.

3.7.3 Details of Plastic Behaviour

Consider the failure envelope illustrated in Figure 3-13. There are five possible stress zones which must be considered. As discussed above, for solution, the dilation rate must be specified. Assuming normality of stresses and plastic strain increments applies, the plastic strain increments can be determined from the failure envelope illustrated in Figure 3-13.

During the solution process described in Section 2, the stresses are first estimated by elasticity theory and hence are permitted to exceed the strength envelope by a small amount. It will be assumed that the closest point on the failure surface is representative of the actual desired stress state. In order to eliminate ambiguity at the edges where the normal to the failure envelope is not unique, the strain increments will be defined by the direction of the line joining the actual with the desired stress state. This process is equivalent to rounding all edges and corners with an infinitesimally small radius. This assumption does not alter the results of the determination of the plastic strain increments when the failure surface is well defined.

It will be assumed that normality applies for all zones except zone one. Zone one represents the case where yielding is induced by shear stresses, and the yield strength is specified by Eq. (3.7-6). The potential function for this zone is also specified by Eq. (3.7-6) with $\tan\phi$ determining the dilation rate. The plastic strain increments can be determined from Eq. (3.7-9) giving

$$d\varepsilon^p_s = \lambda, \quad d\varepsilon^p_n = -|\lambda| \tan\phi$$

Note that ϕ may or may not be equal to ϕ' or ϕ^r , as desired by the user.

Zone two is characterized by compressive yielding which is not dependant on the shear stress, and hence all plastic deformation is in the direction of σ_n

$$d\varepsilon^p_n = \lambda, \quad d\varepsilon^p_s = 0$$

Where $d\varepsilon_n^p$ is positive (compressive).

Zone three is characterized by tensile yielding which is not dependant on the shear stress, and hence all plastic deformation is in the direction of σ_n

$$d\varepsilon_n^p = \lambda, \quad d\varepsilon_s^p = 0$$

and it is necessary that $d\varepsilon_n^p$ be negative (tensile).

Zone four is characterized by combined compressive yielding accompanied by shearing. The desired stress state is given by

$$\sigma_n = C_o, \quad \sigma_s = S_o + C_o\tan\phi$$

The plastic strain increments can be determined for the normal to this point as

$$d\varepsilon_n^p = (\sigma_n - C_o)\lambda, \quad d\varepsilon_s^p = (|\sigma_s| - S_o - C_o\tan\phi)\lambda \qquad (3.7\text{-}10)$$

and it is also necessary that σ_n be positive (compressive).

Zone five is characterized by combined tensile yielding accompanied by shearing. The desired stress state is given by

$$\sigma_n = T_o, \quad \sigma_s = Q_o$$

The plastic strain increments can be determined for the normal to this point as

$$d\varepsilon_n^p = (\sigma_n - T_o)\lambda, \quad d\varepsilon_s^p = (|\sigma_s| - Q_o)\lambda$$

It is also necessary that σ_n be negative (tensile).

3.7.4 Gouge or Seam Material

Mining problems typically involve several materials including the host rocks, dykes, ore and backfill. In order to simulate such a system with the seam elements described here, the relationship between the surface stresses and displacement discontinuities are adjusted to force behaviour corresponding to a fictitious gouge or seam material present in the interface. While the host material continues to deform elastically, the interface material may behave as a visco-plastic material with different modulii from the host.

The following relationships describe the stress-strain behaviour as well as stating the effect of the surface forces ϕ , and initial

stresses σ^* , and displacement discontinuities Γ , on the stress state

$$\begin{aligned}\sigma &= \sigma_{Host} + Cs\Phi + Cv\sigma^* + Cd\Gamma \\ &= \sigma_{Interface} + D_{Interface}(\varepsilon-\varepsilon^*)\end{aligned} \qquad (3.7\text{-}11)$$

Here, σ and ε represent respectively the stress and total strain in the interface material, ε^* represents initial (plastic) strain in the interface, *Cs*, *Cv*, *Cd* represent respectively the coefficient matrices relating surface forces, initial stresses and displacement discontinuities to induced stresses, and $\sigma_{Interface}$ and $D_{Interface}$ represent respectively the field stresses and elastic stress-strain relations for the interface. It is worth noting that, although it is not necessary, normally this stress-strain matrix is assumed to only have diagonal coefficients representing the independent normal and shear stiffness of the interface material.

The strain is related to the actual displacement discontinuity by the simple relationship

$$\varepsilon_i = \Gamma_i / T \qquad (3.7\text{-}12)$$

where *T* represents the thickness of the fictitious interface material. Although this discussion has referred only to host and interface materials, the same relationships apply to any elasto-plastic material which is in place either at the beginning of the analysis, or as in the case of backfill, place at a later stage in the analysis.

The relations in Eq. (3.7-10), can be used to determine the increments in stress *De* and displacement discontinuity $d\Gamma$ required to go from the current equilibrium state given by σ and Γ , to a new equilibrium stress stage given by

$$\begin{aligned}\sigma &= \sigma + d\sigma \\ \Gamma &= \Gamma + d\Gamma\end{aligned}$$

Assuming that the surface forces and initial stresses do not change, a first guess for the increment in displacement discontinuity can be found by differentiation of the first of Eq. (3.7-10) giving

$$d\sigma = Cd \cdot d\Gamma$$

As the solution procedure progresses, the surface forces and initial stresses settle on specific values and the assumption that they do not change becomes progressively more valid.

Substituting Eqs. (3.7-12), (3.7-13) and (3.7-14) into the second of Eq. (3.7-11), it can be found that

$$(D_{Interface}/T - Cd)\cdot d\Gamma = \sigma - \sigma_{Interface} - D_{Interface}(\Gamma/T - \varepsilon^{o})$$

This relation can now be used to estimate the increment in displacement discontinuity required to satisfy the two equations Eq. (3.7-11), thereby coupling the elasto-plastic behaviour of the interface material with the host response. This formulation is extended to the elasto-visco-plastic case in exactly the same way as described in Section 3.6.

3.8 Displacements

In Section 2 the details of the formulation of the boundary element method for stress calculations was discussed. That discussion is now extended to include the calculation of displacements. Expression (3.7-1) is a statement of the integrals which have to be evaluated for this calculation. As in Section 2, the surface forces and displacement discontinuities are assumed to vary linearly with position over the surface of element n as follows

$$\phi_i^n(\xi) = \sum_{q=1}^{M} \delta^{nq}(N^{nq} + N_k^{inq}\xi_k)\phi_i^q \qquad (3.8\text{-}1)$$

$$\Gamma_i^n(\xi) = \sum_{q=1}^{M} \delta^{nq}(N^{nq} + N_k^{inq}\xi_k)\Gamma_i^q \qquad (3.8\text{-}2)$$

In Section 2, the development of quadrilateral elements required interpolation of second order for the initial stresses

$$\sigma_{ij}^{o}(x) = \sum_{q=1}^{M} \delta^{nq}(N^{nq} + N_k^{inq}Z_k + N_{km}^{inq}Z_kZ_m)\sigma_{ij}^{oq}$$

where the coefficients N^{nq}, N_k^{inq}, N_{km}^{inq} represent respectively the constant, linear and quadratic variation on element n and δ^{nq} represents a substitution tensor similar to the Kronecker delta with the property that it equals one only when nodal point q is coincident with element n. There are a total M nodal points. The

body forces can be determined from this expression by differentiation as follows

$$\Phi_i^q(x) = -\sigma_{ij,j}^{qq}(x) = \sum_{p=1}^{M} -\delta^{pq}(N_j^{1pq} + 2N_{jk}^{1pq}x_k)\sigma_{ij}^{q} \qquad (3.8\text{-}3)$$

The integrals in expression (3.7-1) can now be developed on an element by element basis by substitution of Eqs. (3.8-1), (3.8-2) and (3.8-3), giving

$$Gs'^{pq}_{kl}(x) = N^{pq}\int_{s^p} g_{kl}(x,\xi)\,ds(\xi) + n_j^{1pq}\int_{s^p} g_{kl}(x,\xi)\,\xi_j\,ds(\xi)$$

$$Gb'^{pq}_{kl}(x) = N_j^{1pq}\int_{v^p} g_{kl}(x,z)\,dv(z) + 2N_{jm}^{1pq}\int_{v^p} g_{kl}(x,z)\,z_m\,dv(z)$$

$$Gd'^{pq}_{kl}(x) = N^{pq}\int_{s^p} g_{kl}(x,\xi)\,ds(\xi) + n_j^{1pq}\int_{s^p} g'_{kl}(x,\xi)\,\xi_j\,ds(\xi)$$

The displacement at a point x can now be determined by rotating these displacement components to the global coordinate system

$$Gs^{pq}_{kl}(x) = A^q_{jl}Gs'^{pq}_{jl}(x)$$

$$Gb^{pq}_{kl}(x) = A^q_{jl}Gb'^{pq}_{jl}(x)$$

$$Gd^{pq}_{kl}(x) = A^q_{jl}Gd'^{pq}_{jl}(x)$$

where A^q_{jl} represents the coordinate transformation matrix from global to local coordinates such that the normal is taken outward from the boundary (i.e. into the excavation) at the point q.

By accumulating the coefficients for those surface elements which are coincident on nodal point q, the contribution to the displacements by the surface forces and displacement discontinuities are given respectively by

$$Gs^q_{kl}(x)\Phi^q_l \qquad (3.8\text{-}4)$$

$$Gd^q_{kl}(x)\Gamma^q_l \qquad (3.8\text{-}5)$$

where

$$Gs^{q}_{ai}(x) = \sum_{\beta=1}^{n} \delta^{\alpha\beta} Gs^{\beta\gamma}_{ki}(x)$$

$$Gd^{q}_{ai}(x) = \sum_{\beta=1}^{n} \delta^{\alpha\beta} Gd^{\beta\gamma}_{ki}(x)$$

The contribution of the initial stresses can also be determined by subtracting the effects of the surface forces and body forces required to suppress these initial stresses. As in Section 2, the required surface forces can be found as

$$\Phi^{\gamma}_{i} = n_j A^{\gamma}_{j} A^{\gamma}_{i} \sigma^{o\gamma}_{ik}$$

giving the contribution

$$Gs^{\alpha\gamma}_{ki}(x) \Phi^{\gamma}_{i}$$

where

$$Gs^{\alpha\gamma}_{ki}(x) = A^{\alpha}_{j} A^{\gamma}_{i} Gs'^{\alpha\gamma}_{ji}(x) \qquad (3.8\text{-}6)$$

By accumulating the coefficients for those interior elements which are coincident on nodal point q, the contribution to the displacements by the initial stresses are given by

$$Gv^{q}_{aj}(x) \sigma^{o\gamma}_{ij}$$

where

$$Gv^{q}_{aj}(x) = \sum_{\beta=1}^{n} \delta^{\alpha\beta} [\, Gs^{\beta\gamma}_{ki}(x) n_{\alpha\beta} A^{\alpha}_{j} - Gb^{\beta\gamma}_{ij}(x) \,]$$

By superposing the effects of the surface forces (Eq.(3.8-4)), initial stresses (Eq. (3.8-6)) and displacement discontinuities (Eq. (3.8-5)), thereby accumulating all terms contributing to expression (3.7-1), it can be found that

$$u_a(x) = X_a + \sum_{q=1}^{n} [\, Gs^{q}_{ai}(x) \Phi^{\gamma}_{i} + Gv^{q}_{aj}(x) \sigma^{o\gamma}_{ij} + Gd^{q}_{ai}(x) \Gamma^{\gamma}_{i} \,]$$

This expression is easily specialised for a given internal nodal point p giving

$$u^{p}_{a} = X_a + \sum_{q=1}^{n} [\, Gs^{\alpha\gamma}_{ki} \Phi^{\gamma}_{i} + Gv^{\alpha\gamma}_{kij} \sigma^{o\gamma}_{ij} + Gd^{\alpha\gamma}_{ki} \Gamma^{\gamma}_{i} \,]$$

where

$$u_k^p = u_k(x^p)$$
$$Gs_{kl}^{qr} = Gs_{kl}^{q}(x^p)$$
$$Gv_{klj}^{qr} = Gv_{klj}^{q}(x^p)$$
$$Gd_{kl}^{qr} = Gd_{kl}^{q}(x^p)$$

For a surface nodal point one need only rotating from global to local coordinates as follows

$$A_{ik}^{p} u_k^p$$

This completes all of the required formulation to determine the displacements. These values will now be used to determine the energy transferred during excavation and deformation of the body.

3.9 Energy Release

The calculation of the energy released due to mining can be determined from the stresses, strains and displacements. Since in this model, there may be numerous zones of material with properties, and behaviour different than the host, several methods of calculation will have to be incorporated to determine all of the contributing terms. Consider the most general case where we have an elastic host material with excavated zones which may have internal support pressure applied to their surfaces, backfilled zones, and zones of inelastic behaviour with properties different from the host material. These zones may be represented by either volume elements or displacement discontinuities.

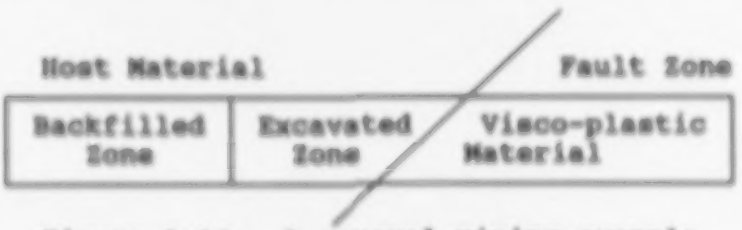

Figure 3-14 A general mining example

As mining excavations are made, energy is exchanged from place to place through the movement of forces through displacements at all of the boundaries depicted in Figure 3-14. Elastic strain energy is stored and released from various locations W_e . Some energy may be expended in the plastic deformation of material W_p and shearing of faults W_f . This may be accompanied by work done in viscous deformation W_v . Energy may be used in the deformation of backfill W_b and supports W_s . A certain amount of energy U_s is removed with the excavation of material of volume V_s .

Finally, there is a component of energy associated with the change in stress acting on the surface of excavations. The maximum value attainable for this component W_s, is representative of slow controlled unloading of surfaces. However, a more common situation is rapid unloading due to the near instantaneous removal of the pre-existing stress as a result of explosive excavation methods. The stress re-equilibration for this case involves inertial effects which are not accommodated by the simulation method used here. For this case, it is often assumed (Salamon, 1984) that the component W_s zero. The excess energy can be determined by summing all of the contributions as follows

$$W_s - W_s - W_c - W_p - W_f - W_b - W_v$$

where W_s may or may not be included as desired. There may be a viscous component W_v associated with the visco-plastic deformation.

Energy Component	Fictitious Force Element	Displacement Discontinuity Element	Initial Stress Element
W_c	$-\Delta W_d$	$-\Delta W_d$	$+\Delta W_c$
W_b	$+\Delta W_d$	$+\Delta W_d$	
W_v	$-\Delta W_d+\Delta W_v$	$-\Delta W_d+\Delta W_v$	
W_s	$+\Delta W_s$	$-\Delta W_s$	
U_e	$+\Delta U_e$	$+\Delta U_e$	$+\Delta U_e$
W_p			$+\Delta W_p$
W_f		$+\Delta W_f$	
W_v		$+\Delta W_v-\Delta W_f$	$+\Delta W_v-\Delta W_p$

Table 3-2 Summary of Energy Contributions

This component has not been included in this summation since it represents an artificial energy sink imposed only to control the deformation rates.

A summary of all the terms required is given in Table 3-2. Calculation of the energy contributions will be discussed for each possible case in the following subsections.

3.9.1 Work Done on the Surface of The Elastic Host Material

In the boundary element formulation used here, the host material has been assumed to be homogeneous, of infinite extent, and behave in a linear elastic manner. During any stress re-equilibration due to excavation, boundary stress adjustment, fault slip or inelastic material behaviour, there will be some change in the strain energy stored in the elastic host medium. The only mechanism for exchange

of this energy, is the movement of surface forces through displacements at the boundary. For this case, the boundary is defined as the interface between the host material and any excavation surface, volume element, or displacement discontinuity, as shown in Figure 3-15 by the double line.

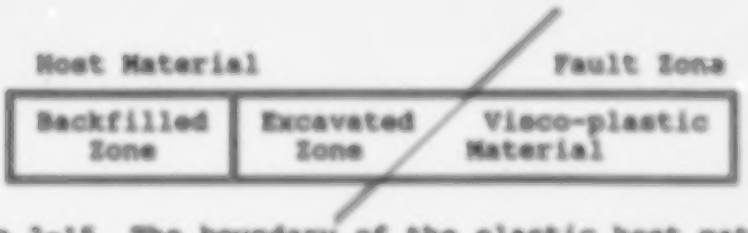

Figure 3-15 The boundary of the elastic host material

The surface displacements and stresses are obtained as part of the analysis procedure. The energy exchange can be determined from the integral of the normal and shear surface force P_i through their corresponding surface displacements u_i

$$\Delta W_s = \int_{u_i^I}^{u_i^{II}} P_i \, du_i = -(u_i^{II} - u_i^I)(\sigma_i^{II} + \sigma_i^I) L/4$$

where the Roman numeral superscripts *I*, *II* represent respectively the force and displacement before and after the re-equilibration. It has been assumed that these values vary from state *I* to state *II* in a linear fashion. For each nodal point, the surface forces are determined as the negative of the product of the surface tractions σ_i with the half length $L/2$, of the element associated with that point. The negative sign is required since by definition, the normal is taken outward from the boundary (i.e. into the excavation), and compressive stresses are positive.

A negative quantity for this component represents work being done on the host rock mass, and therefore the strain energy stored in the host would increase. The more common situation is a positive quantity for this component, indicating a decrease in strain energy stored in the host material, and hence energy is leaving the host material and becoming available to do work. The total stored strain energy W_s is therefore reduced by this quantity. If the boundary represents an interface between the host material and a backfilled zone, this component can be considered as a contribution to the work done on the backfill material W_b . If the boundary represents an excavation surface, this component can be considered as a negative contribution to the surface work done term W_b .

On excavation surfaces, there may also be surface stresses applied to represent some sort of internal support. The work done by these surface stresses can be determined in a similar manner as above with the one difference that these loads are assumed to be applied prior to re-equilibration and held constant during successive

$$\Delta W_s = \int_{u_i^f}^{u_i^{ff}} p_i \, du_i = -(u_i^{ff} - u_i^f)\, \sigma_i^{ff} L/2$$

mining steps. A positive quantity for this component can be considered as a contribution to the work done on supports W_s as well as surface work done term W_s .

In order to determine the energy U_e stored in the material which is to be excavated V_e , two components must be added; a contribution corresponding to the energy stored in V_e prior to any mining, and a contribution corresponding to the work done on the surfaces of V_e since the initial unmined state. The contribution to these two components are determined respectively, by the following integrals

$$U_e = \iiint \Phi(\sigma^f)\, dV + \int_{u_i^f}^{u_i^{ff}} p_i \, du_i$$

where the integrations are taken around the entire boundary. The latter integral can be evaluated as follows

$$\int_{u_i^f}^{u_i^{ff}} p_i \, du_i = -u_i^{ff} (\sigma_i^{ff} + \sigma_i^f) L/4$$

where it is recalled that σ_i^f represents the pre-existing field stresses prior to any mining. The strain energy density Φ can be represented in terms of stresses for the three-dimensional case as (Jaeger and Cook, 1979)

$$\Phi(\sigma^f) = (\sigma_1^{ff} + \sigma_2^{ff} + \sigma_3^{ff} - 2\nu(\sigma_1^f\sigma_2^f + \sigma_2^f\sigma_3^f + \sigma_3^f\sigma_1^f))/(2E) \quad (3.9\text{-}1)$$

By substitution of

$$\sigma_3^f = \nu(\sigma_1^f + \sigma_2^f)$$

the strain energy density for the plane strain case can be found as

$$\Phi(\sigma^f) = [\,(1-\nu^2)(\sigma_1^{ff} + \sigma_2^{ff} - 2\nu(1+\nu)\sigma_1^f\sigma_2^f)/(2E) \quad (3.9\text{-}2)$$

The contribution by these elements to the volume V_e can be determined from the integral

$$\Delta V_e = \iiint dV$$

3.9.2 Work Done on Displacement Discontinuities

The calculations for this case are very similar to those conducted above except there are two sides to a displacement discontinuity and there may be an infilling material with a fictitious thickness T. The stresses on both sides and throughout the infilling material are uniform, and the relative displacement between the two sides is by definition, the value of the displacement discontinuity.

At each nodal point, the work done on the surfaces can be determined from the integral of the normal and shear surface force P_i through their corresponding displacement discontinuity Γ_i.

$$\Delta W_d = \int_{\Gamma_i^I}^{\Gamma_i^{II}} P_i d\Gamma_i = -(\Gamma_i^{II} - \Gamma_i^I)(\sigma_i^{II} + \sigma_i^I) L/4$$

As above, the surface forces are determined as the negative of the product of the surface tractions σ_i with the half length $L/2$, of the element associated with that point.

A positive quantity for this component represents a reduction in strain energy stored in the host material, and hence energy is leaving the host material and becoming available to do work. The total stored strain energy W_s is therefore reduced by this quantity. If the displacement discontinuity represents an excavation, this component can be considered as a negative contribution to the surface work done term W_s.

If the displacement discontinuity represents a backfilled zone, this component can be considered as a contribution to the work done on the backfill material W_b. If the displacement discontinuity represents an unmined seam or fault element, this component can be considered as a direct transfer of energy from the host material to the interface material, and the total stored strain energy is not affected.

If the displacement discontinuity represents an excavation, there may also be surface stresses applied to represent some sort of internal support. The work done by these surface stresses can be determined in a similar manner as above

$$\Delta W_s = \int_{\Gamma_i^I}^{\Gamma_i^{II}} p_i du_i = -(\Gamma_i^{II} - \Gamma_i^I)\sigma_i^{II} L/2$$

with the one difference that these loads are assumed to be applied prior to re-equilibration and held constant during successive mining steps. A positive quantity for this component can be considered as a contribution to the work done on supports W_s , as well as surface work done term W_b .

Since the stresses are uniform throughout the infilling material, the energy U_e stored in the material which is to be excavated V_e , is easily determined as half the product of the stress and elastic strain with the volume of the infilling material for each nodal point

$$U_e = \iiint \sigma_i d\varepsilon^e_i dV = \sigma_i \varepsilon^e_i / 2 = TL\sigma^2_i / (4D_{interface})$$

where the elastic strain is determined from

$$\varepsilon^e_i = \sigma_i / D_{interface}$$

and T and L represent respectively the thickness of the infilling material and the element length. The contribution to the volume mined V_e , for each nodal point is given by

$$\Delta V_e = T(L/2)$$

The plastic work done on the infilling material must also be determined, since this work uses energy. It can be found from the integral of the inelastic component of strain with the stress, integrated over the volume of the infilling material

$$\Delta W_p = \iiint_{\varepsilon^{*,I}_i}^{\varepsilon^{*,II}_i} \int \sigma_i' d\varepsilon^*_i dV = d\varepsilon^*_i (\sigma_i'^{II} + \sigma_i'^{I}) TL/4$$

where the Roman Numeral superscripts *I*, *II* represent respectively the force and displacement before and after the re-equilibration. It has been assumed that these values vary from state to state II in a linear fashion. The increment in plastic strain $d\varepsilon^*_i$ takes place during this same re-equilibration. The stress σ_i' represents the "frictional" components of the stress only. These are separated from the viscous components according to the relations described in Section 3.6. The visco-plastic work done on the infilling material can also be determined, from the above relation by substituting the total stress σ_i for the "frictional" component σ_i' . The viscous work done W_v is given by the difference between the visco-plastic and the plastic component.

3.9.3 Work Done on Volume Element

In the last two sections the energy components for the host material (outside the double line in Figure 3-15) and the displacement discontinuities have been described. In this section,

the energy components associated with the response of the material inside the double line will be determined. The total strain energy stored elastically in these zones can be determined from the stresses by evaluating the following integral for each zone

$$\iiint \Phi(\sigma)\, dV$$

where Φ has been defined above (Eq. (3.9-1)) by substitution of the current stress state σ. Evaluation of this expression is conducted by straight forward application of numerical integration over either a triangular of quadrilateral zone as required (Abramowitz and Stegun, 1970). The difference in the value of this quantity before and after mining takes place represents the contribution to the strain energy U_e stored in the material which is to be excavated

$$V_e = \iiint dV$$

The change in stored strain energy ΔW_e can be determined by the same method by taking the difference of the total stored strain energy before and after the re-equilibration

$$\Delta W_e = \iiint [\Phi(\sigma^{II}) - \Phi(\sigma^{I})]\, dV$$

The plastic work done during the re-equilibration is determined by evaluating the integral of the "frictional" components of the stress with the plastic strains over the volume of the zone

$$\Delta W_p = \iiint \int_{\sigma^{I}_{ij}}^{\sigma^{II}_{ij}} \sigma_{ij}' \, d\varepsilon^{p}_{ij}\, dV = \iiint [d\varepsilon^{p}_{ij}(\sigma_{ij}'^{II} + \sigma_{ij}'^{I})/2]\, dV$$

where the integral on the right hand side is conducted by straight forward application of numerical integration (Abramowitz and Stegun, 1970). As above, the total visco-plastic work can be determined from the above relation by substituting the total stress σ_{ij} for the "frictional" component σ_{ij}'

$$\iiint [d\varepsilon^{p}_{ij}(\sigma^{II}_{ij} + \sigma^{I}_{ij})/2]\, dV$$

The viscous work done W_v is given by the difference between the visco-plastic and the plastic component.

3.10 Verification Analyses

Several analysis examples will now be considered. The properties given in Table 3-3 will be used in all cases. The yield and residual strengths are assumed to be equal, with no reduction in

strength or dilation occurring during yielding. In all cases the surface stresses on the excavations are taken from the equivalent field stress values to zero in one step, and the plastic strain increments are determined as one large strain increment without the use of viscous behaviour. The program iterates until a maximum error in stress (for all degrees of freedom) of 0.1 MPa is achieved.

Young's Modulus	E	=	10^5 MPa
Poisson's Ratio	ν	=	0.2
Unconfined Compressive Strength	C_o	=	100 MPa
Tensile Strength	T_o	=	0 MPa
Friction Angle	ϕ	=	30°(q-3)
Dilation Rate	β	=	1
Viscous parameter 1	γ_1	=	0 MPa
Viscous parameter 2	γ_2	=	0 MPa
Field Stresses	σ_{11}	=	350 MPa
Field Stresses	σ_{22}	=	350 MPa
Field Stresses	σ_{12}	=	0 MPa

Table 3-3 - Properties used in the Analysis Examples

3.10.1 Square-shaped Drift

This first analysis example demonstrates the use of the model for a square-shaped drift with a dimension of 2 metres on each side (Figure 3-16). Since there are two planes of symmetry only the upper right hand quadrant need be considered.

The discretization consisted of dividing the boundary of the excavation into equal length elements, and the solid around the excavation into quadrilaterals. Considering the upper right hand quadrant only, the discretization shown in Figure 3-16 uses two elements per side. Analyses were also conducted with four and eight elements per side. The stress plots in Figure 3-17 are labelled respectively n equals two, four and eight, to denote the corresponding discretization.

The principal stresses and strains along the x_1 axis are plotted in Figure 3-17, for all discretizations. These are superimposed on some analysis results generated using FLAC (Itasca, 1987) using the identical properties as specified in Table 3-3. Although several analyses were conducted, the only results presented for FLAC are those with a discretization of similar density to the finest mesh used with MINE2D (n=8). With coarser discretizations, the accuracy of the results obtained using FLAC seriously deteriorate, just as the results from the boundary element analysis do. In Figure 3-17a, both the major and minor principal stresses are illustrated,

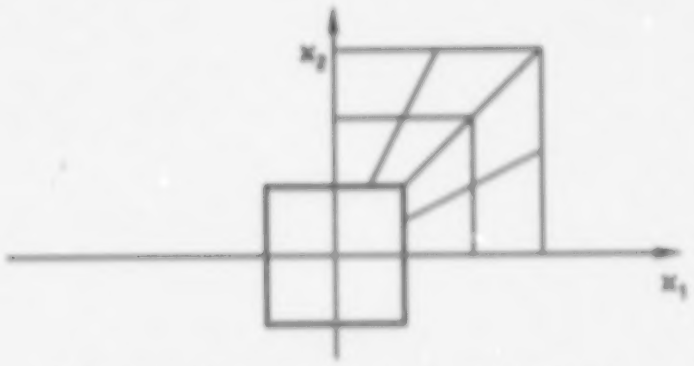

Figure 3-16 Square-shaped Drift

however, only the major principal stresses are labelled corresponding to the discretization used.

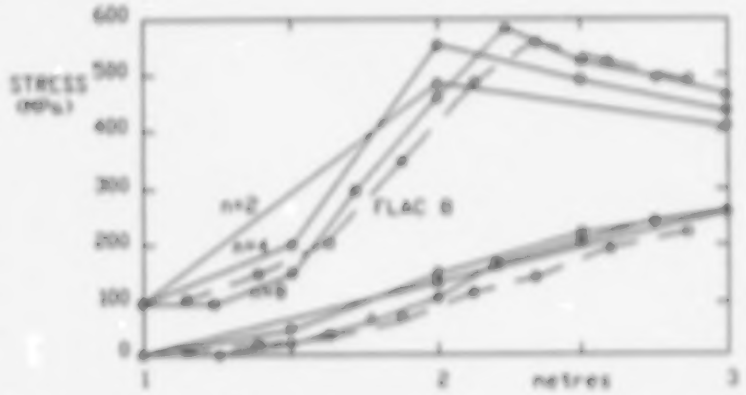

Figure 3-17a Principal Stresses on the x_1 Axis for a Square-shaped Drift

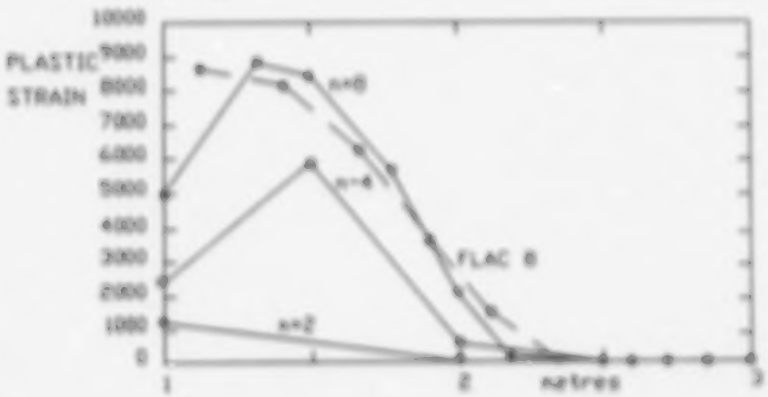

Figure 3-17b Plastic Strain (multiplied by Young's Modulus) on the x_1 Axis for a Square-shaped Drift

These figures demonstrate that both FLAC and MINE2D give almost identical results. Although the discretization used with FLAC does not appear to be fine enough near the boundary to accurately model the plastic deformations, this does not appear to seriously affect the results.

3.10.2 Two Rectangular Drifts with a Weak Pillar

This second analysis example demonstrates the use of the model for two rectangular shaped drifts with a pillar between them. Only the pillar (not the hangingwall and footwall material) will be permitted to yield. The drifts and pillar are 2 m wide in all cases. The drift and pillar height are kept equal in all cases, but have been adjusted such that pillars with height to width ratios of one half, one and two have been generated (Figures 3-18, 3-19 and 3-20). Since there are two planes of symmetry only the upper right hand quadrant need be considered.

For the examples shown in Figures 3-18, 3-19 and 3-20, the discretization consisted of dividing the boundary of the excavation into equal length elements, and the pillar between the excavations into squares. Considering the upper right hand quadrant only, the discretization shown in these figures uses two element across the width. Analyses were also conducted with four and eight elements along the width. The height is discretized into the necessary number of elements to maintain square element shapes.

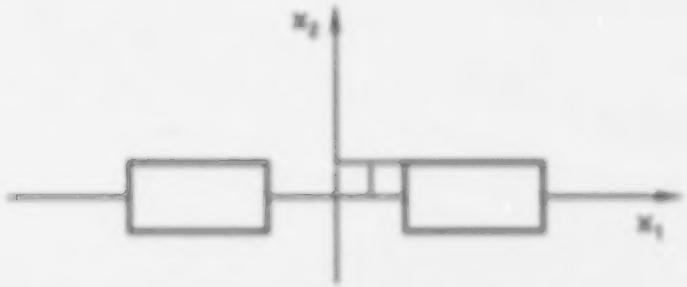

Figure 3-18 Two Rectangular Drifts with a Wide Pillar, Height to Width Ratio of One Half

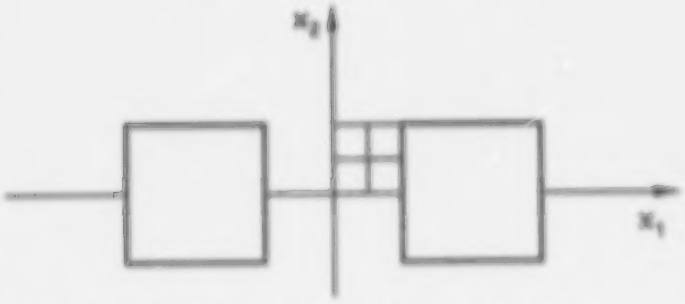

Figure 3-19 Two Rectangular Drifts with a Square Pillar, Height to Width Ratio of One

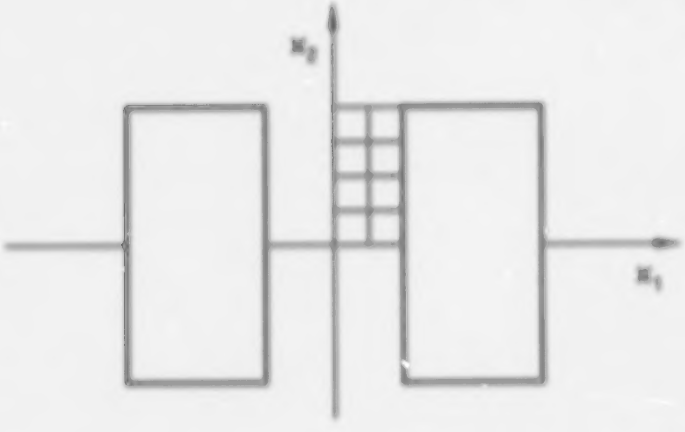

Figure 3-20 Two Rectangular Drifts with a Narrow Pillar, Height to Width Ratio of Two

The principal stresses and strains along the x_1 axis (mid-height of the pillar), are plotted in Figures 3-21, 3-24 and 3-25. These are superimposed on some analysis results generated using FLAC. Although several analyses were conducted, the only results presented for FLAC are those with a discretization of similar density to the finest mesh used with MINE3D (n=0). In Figures 3-21a, 3-22a and 3-23a, both the major and minor principal stresses are illustrated, however, only the major principal stresses are labelled corresponding to the discretization used.

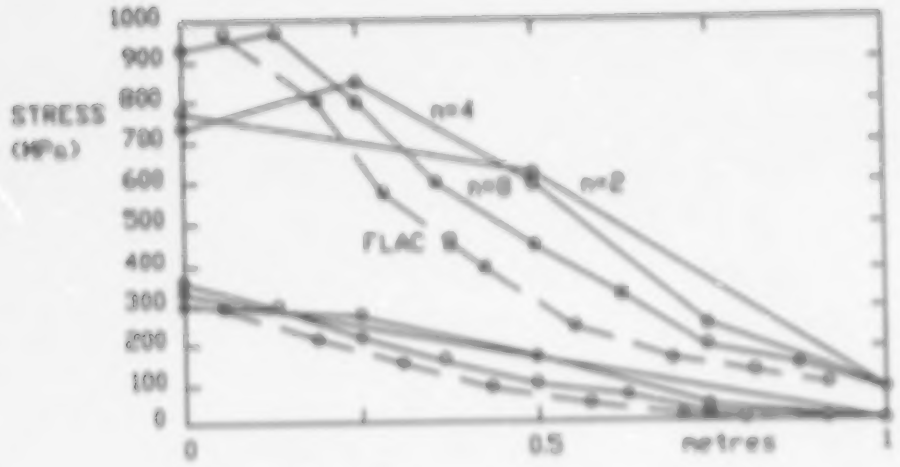

Figure 3-21a Principal Stresses at Mid-Height of a Wide Pillar, Height:Width = 0.5

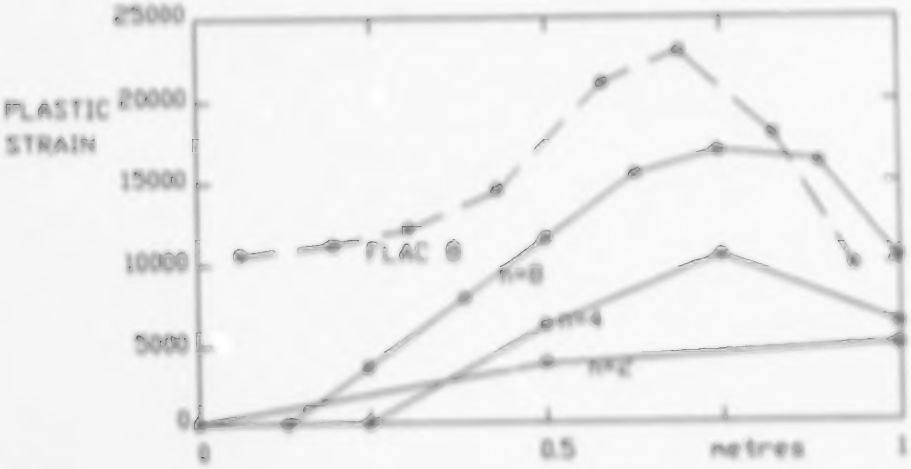

Figure 3-21b Plastic Strain at Mid-Height of a Wide Pillar, Height:Width = 0.5

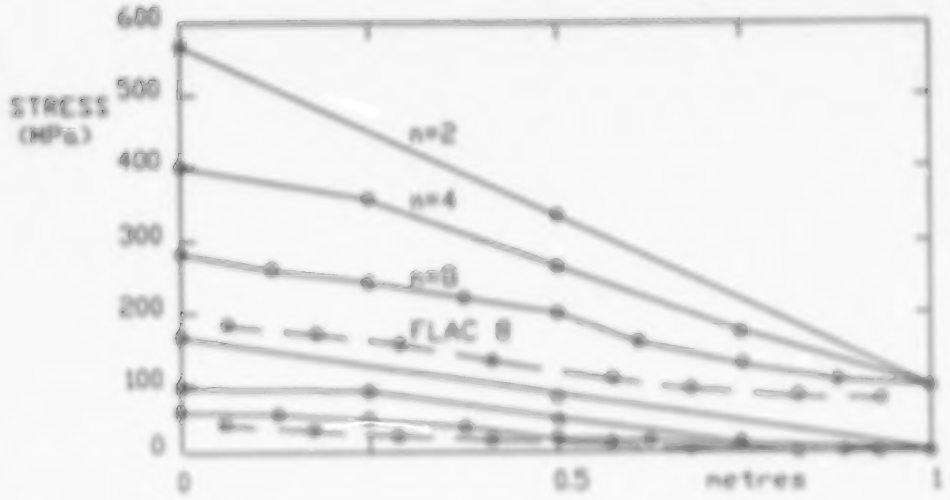

Figure 3-22a Principal Stresses at Mid-Height of a Square Pillar, Height to Width Ratio of One

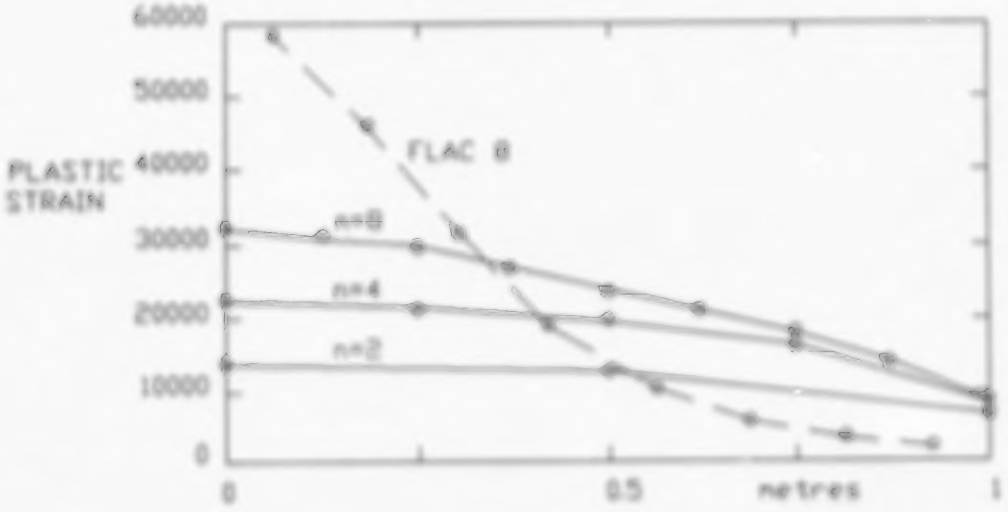

Figure 3-22b Plastic Strain at Mid-Height of a Square Pillar Height to Width Ratio of One

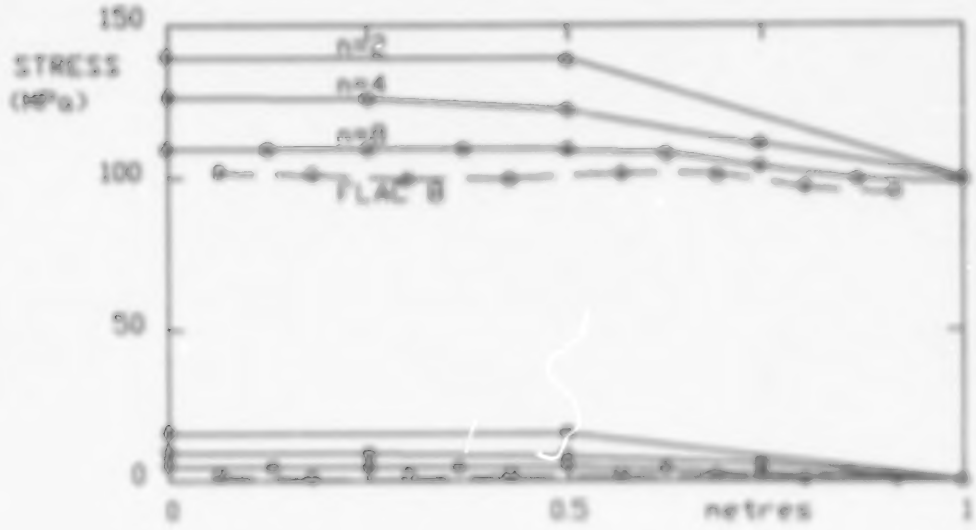

Figure 3-23a Principal Stresses at Mid-Height of a Narrow Pillar, Height to Width Ratio of Two

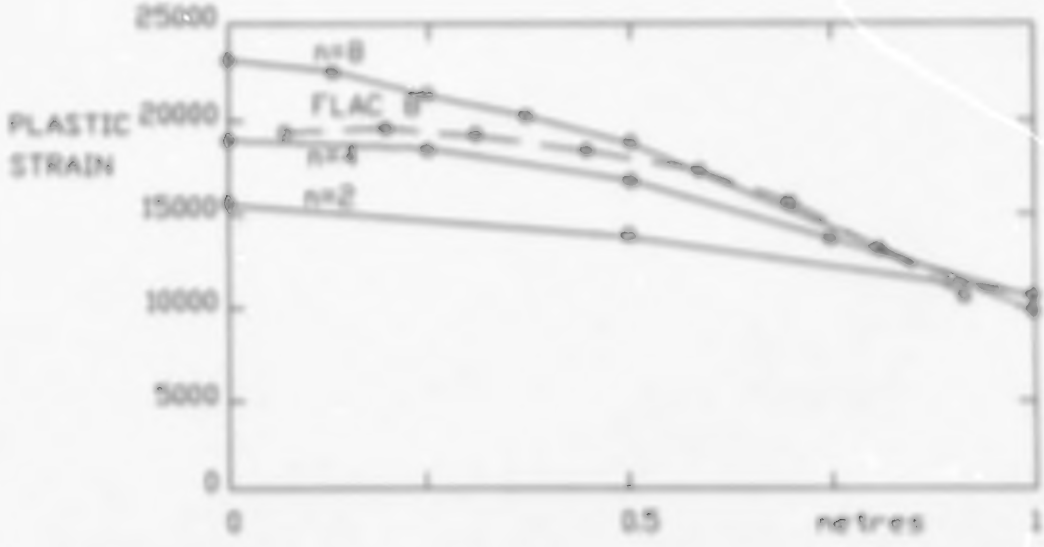

Figure 3-23b Plastic Strain at Mid-Height of a Narrow Pillar, Height to Width Ratio of Two

These figures demonstrate that both FLAC and MINE2D give almost identical results. However, figures 3-21a, 3-22a and 3-23a illustrate that in all cases, FLAC may be underestimating the stress near the boundary, where for continued yielding, the major principal stress must be equal to the unconfined compressive strength (100 MPa) because the minor principal stress is zero (boundary condition). This appears to result in FLAC underestimating the stresses across the entire pillar width. It is also worth noting that the analysis time for MINE2D is less than a third that required for FLAC (for the case of eight elements across the pillar width).

The stresses and plastic strains are essentially the same in all cases except for the square pillar (Figure 3-19). For this case FLAC gives a significantly different distribution of plastic strain, and very much lower values of stress. The reason for this is probably due to the nature of the problem. Comparison of the stress and strain data for the wide (Figure 3-21) versus narrow (Figure 3-23) pillar illustrates that there is a transition in behaviour. The confining stress in the centre of the wide pillar is nearly equal to the pre-existing field stress, where as the confining stress at the centre of the narrow pillar is nearly non-existant.

The square pillar represents an intermediate case, where some, but not all of the confining pressure is released. It is expected that such a case would be very sensitive to the shear resistance of the material. Displacement formulations, such as FLAC, are well known to behave overly stiff and often "lock-up" (Zienkiewicz, 1977) because of the limited deformability of the low order polynomial expansions used for the element shape functions. Special steps are often taken (Marti and Cundall, 1982) to avoid these problems. Although it is not thoroughly discussed in the literature, it appears as though the modification required to "soften up" the behaviour may in fact create a condition where the behaviour is too soft. Such an effect would result in the behaviour observed for the square shaped pillar discussed above. The boundary element method used to develop MINE2D is a stress based formulation, not a displacement formulation, and therefore does not suffer from the stiffness problems discussed above.

It should be noted that FLAC uses the same Mohr-Coulomb failure criterion and non-associated flow rule as MINE2D and is therefore solving the same set of plasticity equations. However, FLAC solves the equations by inertial-viscous time stepping rather than viscous time stepping alone. The inertial effects may be expected to induce larger magnitude plastic deformations.

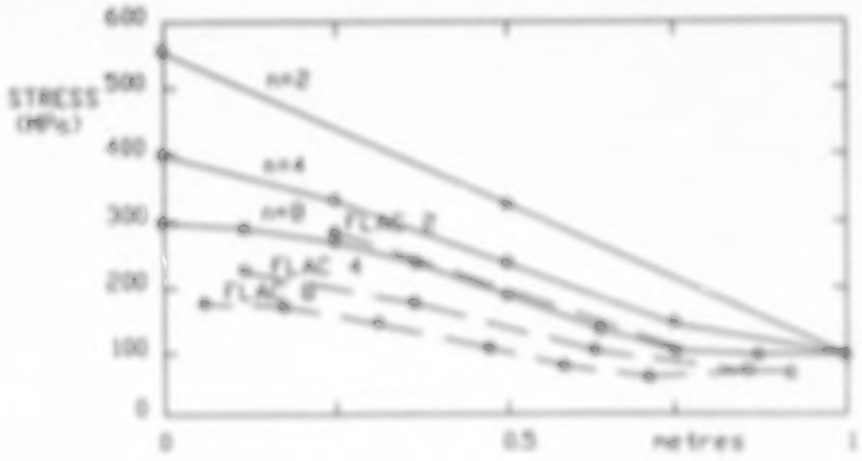

Figure 3-24 Major Principal Stress at Mid-Height of a Square Pillar, Height:Width = 1

To generate the results presented in the above figures, FLAC was run several times with many different meshes, and the discretizations extended for 20 metres on either side of the excavations. By trial and error, it was found that this distance was the minimum required to reduce the far field boundary effects to an acceptably small value.

With coarser discretizations, the accuracy of the results obtained using FLAC seriously deteriorate, just as the results from the boundary element analysis do. This effect is demonstrated in Figure 3-24 where the major principal stresses in a pillar with its height equal to its width, are plotted for several different discretizations.

In Figure 3-25, the major principal stress at the centre of the same pillar are plotted as a function of the number of elements used in the analysis. Since FLAC does not provide stresses exactly at the centre of the pillar, the values nearest the centre, as illustrated in Figure 3-24, have been used. It can be observed that FLAC and MINE2D are asymptotically approaching different values of stress as the number of elements is increased. The asymptotic values, are shown in the figure by the horizontal dashed lines, and have been determined by curve fitting the exponential decay function

$$\sigma_1 = a + be^{-cn}$$

where σ_1 represents the major principal stress nearest the centre of the pillar (vertical axis), a, b and c are constants with a representing the asymptote, n represents the number of elements (horizontal axis), and e represents the exponential function. The

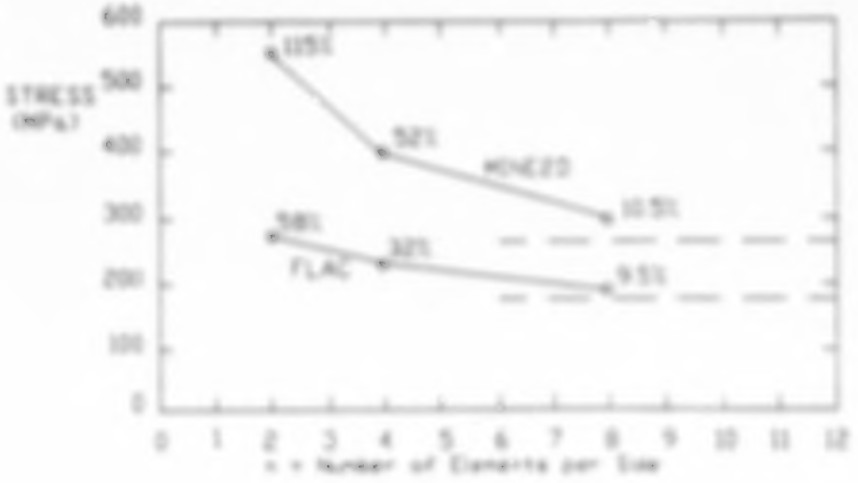

Figure 3-25 Major Principal Stress at the Centre of a Square Pillar, Height:Width = 1

percentage error of the stresses, over the asymptotic values are presented on the figure.

It can be observed in Figure 3-25, that FLAC is giving smaller percentage errors for small numbers of elements. This advantage is offset by the fact that, for the examples analysed here, FLAC requires approximately three times as much computer time as MINE2D (for the same value of n). Also, MINE2D appears to be approaching its asymptote more quickly than FLAC. The analysis time required for both procedures was found to increase approximately as $n^{2.3}$ and the total number of nodes increases approximately as the square of n. More examples will have to be considered before definitive statements concerning the relative economy of the two procedures can be made, however, these examples demonstrate that MINE2D is at least as efficient as FLAC.

The answer to the obvious question concerning which analysis technique is more accurate, cannot be answered by the comparisons presented here. However, this question may not be as important as one might think, since observation of the results illustrates that the analyses are in close enough agreement that similar conclusions would be drawn in either case. Also, of all the example problems discussed, the square pillar (height to width ratio of one) example is the case where the results from MINE2D and FLAC differ the most.

It is apparent that the boundary element formulation MINE2D, offers many advantages over domain methods such as FLAC. In MINE2D, as with any boundary element method, only the surfaces and zones where non-linear deformations are expected to take place need to be discretized. This provides considerable simplification of the data input, and a large savings in the total number of degrees of

freedom which must be considered in an analysis.

In FLAC, as with any domain method, the interior of the rock mass needs to be discretized out to a distance far enough away from the excavations such that the far field boundaries have no significant effect. For problems with zones of non-linear deformations, this distance is increased over what is normally used for elastic cases, due to the disturbance in the stress field at distance from the excavations. For the square-shaped drift problem presented above (Section 3.11.1, "Square-shaped Drift"), a distance of 3? radii was found to be required to reduce the far field boundary effects to an acceptable level. These effects will be even further amplified with the addition of features such as joints and faults which may slip out to considerable distances from the excavations.

3.10.3 Circular Tunnel in a Homogeneous Stress Field

This analysis example demonstrates the comparison of the MINE2D model in with the analytic solution for the case of a circular tunnel under homogeneous stress conditions. In this example, the yield and residual strengths are assumed to be equal, with no reduction in strength or dilation occurring during yielding. In all cases the surface stresses on the excavations are taken from the equivalent field stress values to zero in one step, and the plastic strain increments are determined by letting the program step through viscous behaviour. Before examining the results, consider the analytic solution.

The closed form analytic solution for this problem is well known and has been published by Jaeger and Cook (1979). Their derivation is limited to determination of the extent of the failure zone, and the stress distribution. To complete the comparison between this solution and the MINE2D model it will be necessary to extend the analytic solution to provide plastic strains, displacements and energy components. This work has been completed and documented elsewhere (Wiles, 1989a). The pertinent results are summarized here.

Prior to any failure of material, the stresses are given by the elastic solution

$$\sigma_r = [1-(R/r)^2]p_0 + (R/r)^2 p_i \qquad (3.10\text{-}1)$$

$$\sigma_\theta = [1+(R/r)^2]p_0 - (R/r)^2 p_i \qquad (3.10\text{-}2)$$

$$u = (p_0-p_i)R^2/(2Gr) \qquad (3.10\text{-}3)$$

where G represents the shear modulus of the material.

The strength of the failed material is defined by the Coulomb criterion of failure

$$\sigma_\theta = C_o + q\sigma_r$$
$$C_o = 2S_o\tan(45+\phi/2)$$
$$q = \tan^2(45+\phi/2)$$

where p_o and p_i' represent respectively the far field stress, and the radial stress at the elastic-plastic interface R' .

Letting r represent the radial position, and R represent the inner excavation boundary, the outer radius of the failed annulus is given by

$$R' = R\left\{\frac{[P_i'-C_o/(1-q)]}{[P_i-C_o/(1-q)]}\right\}^{1/(q-1)}$$

$$P_i' = (2p_o-C_o)/(1+q)$$

The radial and circumferential stresses and radial displacements in the elastic zone ($r > R'$) are given by respectively

$$\sigma_r = [1-(R/r)^2]p_o + (R/r)^2p_i$$
$$\sigma_\theta = [1+(R/r)^2]p_o - (R/r)^2p_i$$
$$u = (p_o-p_i)R^2/(2Gr)$$

The stress, plastic strain and displacement in the plastic zone ($r < R'$) are given by

$$\sigma_r = C_o/(1-q) + [p_i-C_o/(1-q)](r/R)^{(q-1)} \qquad (3.10\text{-}4)$$

$$\varepsilon_r^o = \frac{(1-\nu)(q^2-1)}{2G(1+q\beta)}[p_i-C_o/(1-q)](r/R)^{(q-1)}[1-(R'/r)^{(q+1/p)}]$$

$$u = \frac{[p_i'-C_o/(1-q)]r}{2G(1+q\beta)}\left\{\begin{matrix}[(1-2\nu)(1+q\beta)+(1-\nu)(q-1)](r/R')^{(q-1)} \\ +\beta(1-\nu)(q^2-1)(R'/r)^{(1+1/\beta)} \\ -(1-2\nu)(1+q\beta)(1+q)/2\end{matrix}\right\}$$

(3.10-5)

where

$$\varepsilon_\theta^\circ = -\beta\varepsilon_r^\circ$$

Consider the enlargement of the excavation in three stages. At stage 0, the surface stresses p, are equal to the pre-mining value p_o such that no mining has taken place. At stage I, the surface stresses are reduced the final value p_i, while the material is permitted to re-equilibrate elastically only. At stage II, the visco-plastic straining is permitted to occur and further re-equilibration takes place. The surface stress path at radius R, can be summarized as follows

$$\begin{aligned} p^\circ &= p_o \\ p^I &= p_i \\ p^{II} &= p_i \end{aligned}$$

where the superscripts 0, I, II represent respectively the three states discussed above. The surface stress at radius R' can be determined as

$$\begin{aligned} p'^\circ &= p_o \\ p'^{II} &= p_o - (p_o - p_i)(R/R')^2 \\ p'^{II} &= p_i' \end{aligned}$$

where the stresses for state I and state II are determined respectively from expressions (3.10-1) and (3.10-4) by substitution of R' for r. The surface displacements at radius R are given by

$$\begin{aligned} u^\circ &= 0 \\ u^I &= (p_o - p_i)R/(2G) \end{aligned}$$

$$u^{II} = \frac{[p_i' - C_o/(1-q)]R}{2G(1+q\beta)} \left\{ \begin{array}{l} [(1-2\nu)(1+q\beta) + (1-\beta)(1-\nu)(q-1)](r/R')^{(q-1)} \\ + \beta(1-\nu)(q^2-1)(R'/r)^{(1+1/\beta)} \\ - (1-2\nu)(1+q\beta)(1+q)/2 \end{array} \right\}$$

where the displacements for state I and state II are determined respectively from expressions (3.10-3) and (3.10-5) by substitution of R for r. The surface displacements at radius R' can also be determined from these same expressions by substitution of R' for r.

$$\begin{aligned} u'^\circ &= 0 \\ u'^I &= (p_o - p_i)R^2/(2GR') \\ u'^{II} &= (p_o - p_i')R'/(2G) \end{aligned}$$

During the transition from stage 0 to stage I, the stored strain energy change can be determined from the integral of the work done on the inner surface R, for the case where this surface is unloaded in a static-controlled manner

$$W_c^I = -\int\int_{u^o}^{u^I} p\,du\; r\,d\theta = -2\pi R(u^I-u^o)(p^I+p^o)/2 = -\pi R^2(p_o^2-p_i^2)/(2G)$$

where the superscripts ^{0} and ^{I} represent respectively the force and displacement before and after the re-equilibration. During this same transition, the work done by the support pressure p_i can be determined from

$$W_s^I = \int\int_{u^o}^{u_I} p_i\,du\; r\,d\theta = 2\pi R(u^I-u^o)p_i = \pi R^2(p_o-p_i)p_i/G$$

The maximum work done in excess of the support pressure can be determined as

$$W_\theta^I = -\int\int_{u^o}^{u^I}(p-p_i)\,du\,r\,d\theta = -2\pi R(u^I-u^o)(p^I-p_i+p^o-p_i)/2$$
$$= -\pi R(p_o-p_i)^2/(2G)$$

where it has been assumed that the surface is unloaded in a static controlled manner. If the surface is unloaded instantaneously, there is no surface stress in excess of the support pressure, and hence the minimum work done in excess of the support pressure is zero. As discussed above, this case is assumed by Salamon (1984).

The volume excavated is just the volume of the cylinder of radius R

$$V_m = \pi R^2$$

The strain energy stored in the volume V_m is given by

$$U_m = \int\int \Phi(p_o)\,r\,dr\,d\theta = \pi R^2(1-2\nu)p_o^2/(2G)$$

where p_o has been substituted for all of the stress components in Φ (which is given by Eq. (3.9-2))

During the transition from stage I to stage II, the stored strain energy change W_c^{II} can be determined from the integral of the work

done on the surface R'

$$-\iint_{u'_I}^{u'_{II}} p' du' r d\theta = -2\pi R' (u'^{II} - u'^{I}) (p'^{II} + p'^{I})/2$$

$$= -\pi R^2 [(p_o - p'_i)(R'/R)^2 - (p_o - p_i)(R/R')][p_o + p'_i - (p_o - p_i)(R/R')^2]/(2G)$$

plus the strain energy stored within the failed annulus at stage II

$$\iint_R^{R'} \Phi(\sigma^{II}) r dr d\theta = \frac{\pi R^2 (1-2\nu)}{2G} \left\{ \frac{C_o^2}{(1-q)^2} [(R'/R)^2 - 1] \right.$$

$$+ \frac{2C_o}{(1-q)} [p_i - C_o/(1-q)] [(R'/R)^{(q+1)} - 1]$$

$$\left. + \frac{(1-\nu)(1+q^2) - 2\nu q}{2q(1-2\nu)} [p_i - C_o/(1-q)]^2 [(R'/R)^{2(q-1)}] \right\}$$

less the strain energy stored in the elastic annulus at state I

$$\iint_R^{R'} \Phi(\sigma^I) r dr d\theta = \pi (R'^2 - R^2) [(1-2\nu) p_o^2 + (p_o - p_i)^2 (R/R')^2]/(2G)$$

The work done by the support pressure p_i can be determined from

$$W_e^{II} = \iint_{u^I}^{u^{II}} P_i du \cdot r \cdot d\theta = 2\pi R (u^{II} - u^I) p_i$$

During the state 0 to state I transition the surface stresses were reduced to the support pressure p_i . Since there is no surface stress in excess of this value, there is no work done in excess of the support pressure

$$W_\theta^{II} = 0$$

The total plastic work done can now be determined by integrating the stresses through the plastic strain path, and over the annulus of failed material

$$W_p^{II} = \iint \left[\int \sigma_r d\varepsilon_r^p + \int \sigma_\theta d\varepsilon_\theta^p \right] r dr d\theta$$

Substituting for the stresses and strains and evaluating this expression, the following result can be found for the total plastic work done

$$W_p^{II} = \frac{\pi(1-\nu)(q+1)}{G(1+q\beta)} \int_{R'-R}^{R'} \int_{r-R}^{R''}$$

$$\left\{ \begin{array}{c} C_o(1-\beta)\,[p_i'-C_o/(1-q)]\,[(1-q)(r/R'')^q-(1+1/\beta)(R''/r)^{1/\beta}] \\ +\,(1-q)(1-q\beta)\,[p_i'-C_o/(1-q)]^2 \\ [(1-q)(r/R'')^{(2q-1)}-(1+1/\beta)(R''/r)^{(1-q+1/\beta)}] \end{array} \right\} dR''\,dr$$

For the specific case where β is unity and q equals three, the integrals can be evaluated to give

$$W_p^{II} = \pi(1-\nu)R^2[p_i'+C_o/2]^2[8(R'/R)^2+(R/R')^4-12\ln(R'/R)-9]/(3G)$$

This example demonstrates the use of the model for a one metre radius circular tunnel under homogeneous stress conditions. Since there are two planes of symmetry, only the upper right hand quadrant need be considered. The discretizations used for each of the analyses are shown in Figure 3-26.

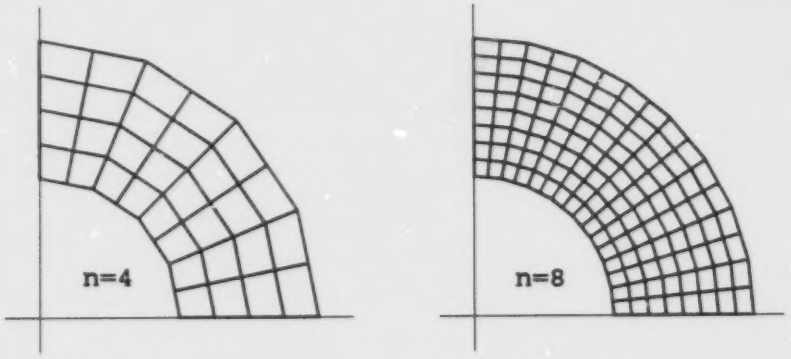

Figure 3-26 Circular tunnel discretization

The properties given in Table 3-4 have been used for this analysis. The program iterates until a maximum error in stress (for all degrees of freedom) of 0.01 MPa is achieved. Some of the results are summarized in Table 3-5 for comparison with analytic calculations.

The values for the MINE2D results are only approximate since the radial symmetry is not perfect. This is because of the approximation of the excavation surface with straight line segments, and approximation of the failed region with straight

sided quadrilateral elements. Since the excavation volume being modelled is slightly smaller, the displacements, plastic strains, and some of the energy components are therefore underestimated.

The principal stresses, plastic strains, and displacements are presented respectively in Figures 3-27, 3-28 and 3-29 along with the distribution determined from the analytic solution. The closed circles represent the results from the MINE2D analysis with n=4, and the open circles represent the results with n equal to eight, as shown in Figure 3-26. These Figures demonstrate that MINE2D gives results which converge on the analytic solution with progressively finer discretizations.

Young's Modulus	E	=	70 GPa
Poisson's Ratio	ν	=	0.2
Unconfined Compressive Strength	C_o	=	26.29 MPa
Tensile Strength	T_o	=	0 MPa
Friction Angle	ϕ	=	30° (q=3)
Dilation Rate	β	=	1
Viscous parameter 1	γ_1	=	2 GPa
Viscous parameter 2	γ_2	=	0 MPa
Field Stresses	p_o	=	100 MPa
Support Pressure	p_i	=	1 MPa

Table 3-4 - Properties for the Circular Tunnel Example

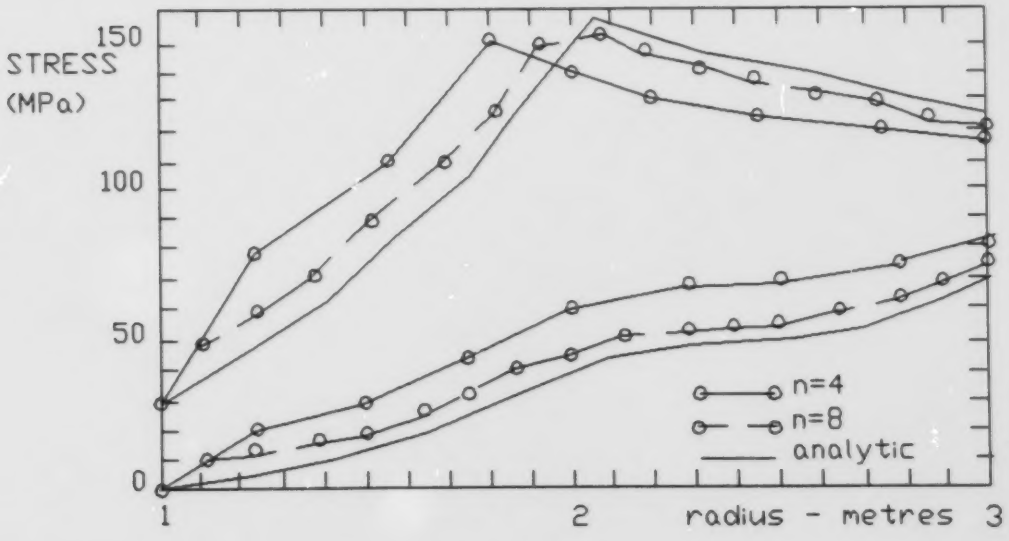

Figure 3-27 Principal stresses around a circular tunnel

Component	Analytical Results	Mine2D Results n=4	n=8
$\sigma_r^I(R)$	1 Mpa	1 Mpa	1 Mpa
$\sigma_\theta^I(R)$	199 Mpa	170 Mpa	185 Mpa
$\varepsilon_r^I(R)$	0	0	0
$\varepsilon_\theta^I(R)$	0	0	0
$u_r^I(R)$	0.001697 m	0.001662 m	0.001688 m
$\sigma_r^I(R')$	75.25 MPa	75.00 MPa	75.20 MPa
$\sigma_\theta^I(R')$	124.75 MPa	125.00 MPa	125.00 MPa
$\varepsilon_r^I(R')$	0	0	0
$\varepsilon_\theta^I(R')$	0	0	0
$u_r^I(R')$	0.000849 m	0.000825 m	0.000841 m
W_c^I	-0.538505 MJ	-0.543143 MJ	-0.539586 MJ
W_s^I	0.010663 MJ	0.010377 MJ	0.010567 MJ
W_e^I	-0.527841 MJ	-0.513664 MJ	-0.523085 MJ
W_p^I	0 MJ	0 MJ	0 MJ
W_v^I	0 MJ	0 MJ	0 MJ
$-(W_c^I+W_s^I+W_p^I)$	0.527841 MJ	0.532766 MJ	0.529019 MJ
$W_e^I-(W_c^I+W_s^I+W_p^I)$	0 MJ	0.019102 MJ	0.005934 MJ
$\sigma_r^{II}(R)$	1 MPa	1 MPa	1 MPa
$\sigma_\theta^{II}(R)$	29.29 MPa	29.30 MPa	29.30 MPa
$\varepsilon_r^{II}(R)$	-0.005819	-0.004420	-0.005020
$\varepsilon_\theta^{II}(R)$	0.005819	0.004420	0.005020
$u_r^{II}(R)$	0.005625 m	0.003632 m	0.004450 m
$\sigma_r^{II}(R')$	43.43 MPa	55.00 MPa	48.45 MPa
$\sigma_\theta^{II}(R')$	156.57 MPa	142.50 MPa	152.00 Mpa
$\varepsilon_r^{II}(R')$	0	0	0
$\varepsilon_\theta^{II}(R')$	0	0	0
$u_r^{II}(R')$	0.001940 m	0.001497 m	0.001748 m
W_c^{II}	-1.573144 MJ	-0.963857 MJ	-1.311814 MJ
W_s^{II}	0.024678 MJ	0.013505 MJ	0.018172 MJ
W_e^{II}	0 MJ	0 MJ	0 MJ
W_p^{II}	1.355386 MJ	0.776395 MJ	1.115260 MJ
W_v^{II}		0.173961 MJ	0.177476 MJ
$-(W_c^{II}+W_s^{II}+W_p^{II})$	0.193079 MJ	0.173961 MJ	0.178382 MJ
$W_e^I-(W_c^{II}+W_s^{II}+W_p^{II})$	0.193079 MJ	0.173961 MJ	0.178382 MJ
R'	2 m	2 m	2 m
U_m	0.323135 MJ	0.314900 MJ	0.321066 MJ
V_m	3.142 m^3	3.062 m^3	3.121 m^3

Table 3-5 Results from MINE2D and Analytical Calculations

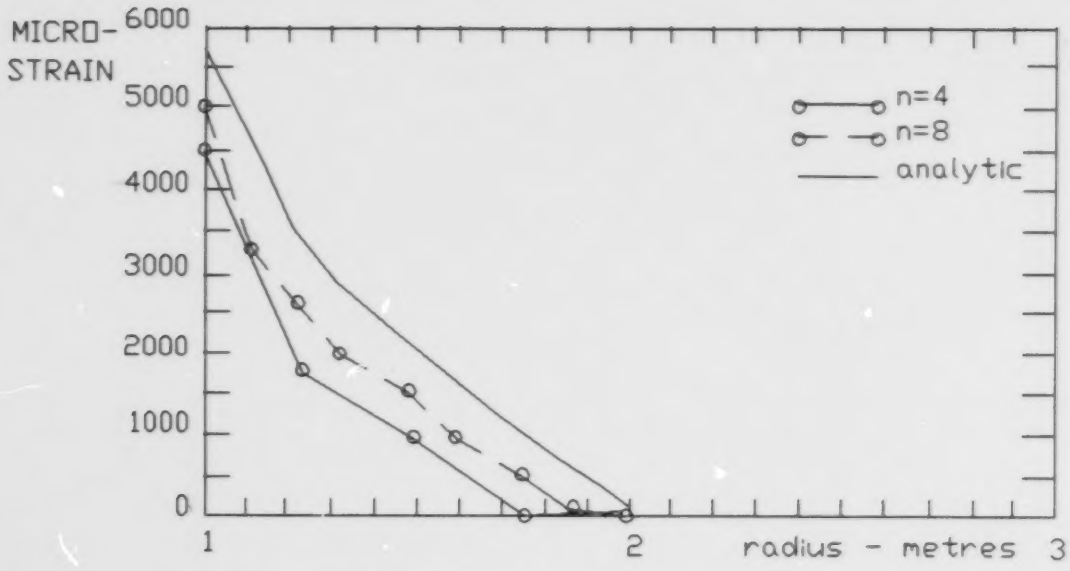

Figure 3-28 Plastic strains around a circular tunnel

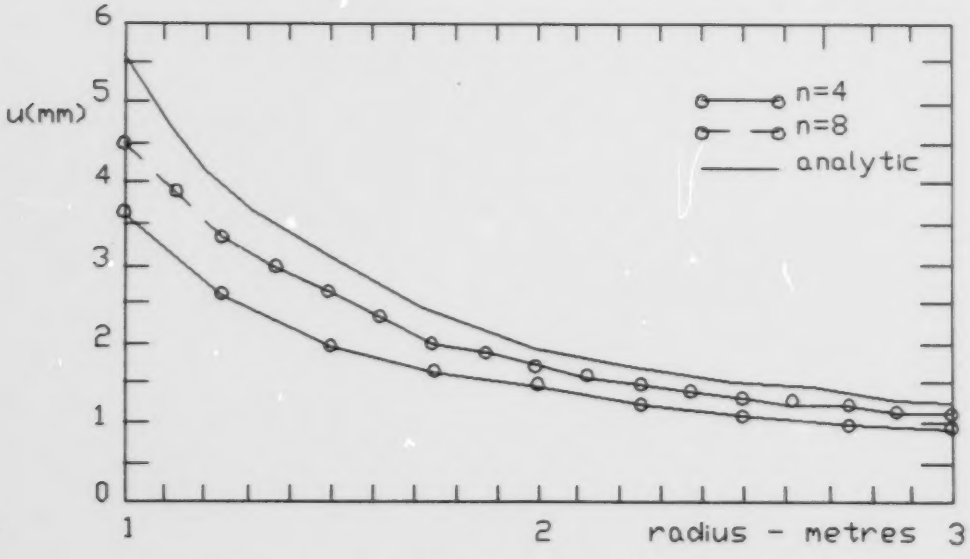

Figure 3-29 Displacements around a circular tunnel

4.0 THREE-DIMENSIONAL FORMULATION (Program MINE3D)

4.1 Introduction

The development of the three-dimensional formulation was primarily based on the boundary element concepts described in Section 2.0 and implemented in MINE2D as discussed in Section 3.0. The computer program MINE3D was developed from the three-dimensional formulation, and this program thus has the following two (2) major features.

1. MINE3D simulates localized regions of plastic yield within an elastic continuum by using both linearly-elastic surface elements and plastic volume elements. Linear strength elements are used to provide greater accuracy for the plasticity analysis.

2. Multiple regions containing different materials can be defined in order to represent conditions such as backfill within orebodies.

The formulation and implementation of these features in MINE3D are discussed in this section.

The development of MINE3D also required a significant variation from the conventional boundary element formulation in order to optimize the code for solving large-scale problems in three dimensions. In particular, MINE3D utilizes a "grid" of parallelepipeds to construct 3-D element geometries. By limiting the shapes of the elements, larger problem sizes could be generated than would be possible using arbitrarily-shaped boundary elements. The details of this geometric structure and the problem size limitations of this approach are also described.

An important factor to the practical utilization of MINE3D was found to be the current computer hardware facility for data storage and speed of both accessing and processing data. Different hardware systems were investigated, and these findings are presented.

Finally, verification testing of MINE3D is described. This testing verifies the accuracy of MINE3D for plasticity and multiple material analyses.

4.2 Overview of Basic Equations

Let D be an infinite homogeneous and isotropic 3-D elastoplastic medium containing excavations bounded by a surface S. The medium, subjected to a far-field stress, is almost everywhere in an elastic state, and zones in which yielding may take place are

enclosed within a volume V. Figure 4-1 provides an illustration.

A Cartesian system of reference axes x_i (i = 1,3) is selected in the medium, and all subscripts in this section refer to components in that system. Also, as a convention, Einstein notation applies to the subscripts but not to the superscripts (see Appendix VI).

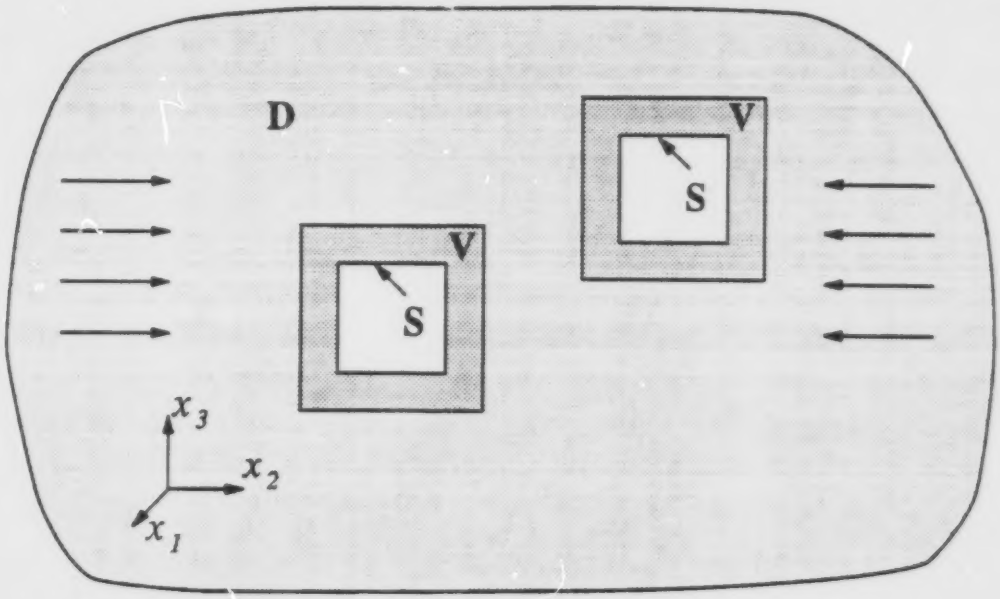

Figure 4-1 Elastic Medium, D, with Local Plastic Regions, V, and Excavations Bounded by S

4.2.1 Equations for Elastoplasticity

In MINE3D, an indirect boundary element method is adopted to solve the problem. The advantage of the indirect approach is that the calculations for the stresses and displacements at interior points of the medium require much less computational effort than that necessary in the direct method.

In the indirect approach, fictitious point force solutions are distributed along the surface S. The intensity $[\phi_i(x)]$ of the distribution is determined so as to satisfy the particular boundary conditions of the problem.

The elastoplastic character of the medium is taken into account using an initial stress formulation. In this framework, the problem is posed as the determination of the solution to an equivalent elastic problem with initial stress field σ°_{ij}. The particular location and magnitude of $\sigma^{\circ}_{ij}(x)$ is unknown beforehand, but it may be determined for a specified yield criterion and flow

rule using the iterative process described in Section 4.4. In the boundary element approach, the initial stress field σ°_{ij} is taken into consideration by means of a distribution of body forces $f_i(x)$ over the volume V such that

$$f_i(x) = \frac{\partial \sigma^{\circ}_{ik}(x)}{\partial x_k} \tag{4.2-1}$$

The basic equations may be written

$$u_i(x) = \frac{1}{2\mu}\left[\int_s G_{ij}(x,\xi)\,\phi_j(\xi)\,dS + \int_v G_{ij}(x,\xi)\,f_j(\xi)\,dV\right] \tag{4.2-2}$$

$$\begin{aligned}\sigma_{ij}(x) &= \int_s T_{ijk}(x,\xi)\,\phi_k(\xi)\,dS \\ &+ \int_v T_{ijk}(x,\xi)\,f_k(\xi)\,DV + \sigma^{F}_{ij}(x) - \sigma^{\circ}_{ij}(x)\end{aligned} \tag{4.2-3}$$

where the kernel functions are given as follows

$$G_{ij}(x,\xi) = \frac{1}{8\pi(1-\nu)}\,\frac{1}{r}\left[(3-4\nu)\,\delta_{ij} + \frac{y_i\,y_j}{r^2}\right] \tag{4.2-4}$$

$$\begin{aligned}&T_{ijk}(x,\xi) = \\ &\frac{1}{8\pi(1-\nu)}\,\frac{1}{r^2}\left[\left(\delta_{ik}\,\frac{y_j}{r} + \delta_{ij}\,\frac{y_i}{r} - \delta_{ij}\frac{y_k}{r}\right)(1-2\nu) + 3\,\frac{y_i\,y_j\,y_k}{r^3}\right]\end{aligned} \tag{4.2-5}$$

In the above formulae,

$\sigma^{F}_{ij}(x)$ - far-field stress state,
ν - Poisson's ratio,
μ - shear modulus of the medium, and

$$y_i = x_i - \xi_i \quad ; \quad r^2 = y_i\,y_i \tag{4.2-6}$$

The tractions $t_i(x)$ at a point x on a surface with outward unit normal $n_i(x)$ are calculated from

$$t_i(x) = \sigma_{ij}(x)\,n_j(x) \tag{4.2-7}$$

The above equations may be used to evaluate stresses and displacements within D and on its boundary S. However, special care must be taken in the computation of boundary values. Indeed, while the displacement field is continuous across S, the tractions, computed from Eq. (4.2-7) using Eq. (4.2-3), jump across boundary S. This feature is an inherent property of the boundary element technique. Values on the boundary must be seen as those obtained from a limiting process as the point x approaches the boundary from

within domain D. This question will be addressed further in Section 4.3.3. Note that, in the code, all quantities are referenced to the global system of reference axes.

4.2.2 Discretization: Parallelepiped Grid

In MINE3D, a finite 3-D grid of nodes is laid over the region of interest. All the nodes in the grid are equally spaced in the three directions of reference of a local system of axes (i,j,k) defined for the grid (Fig. 4-2). Those nodes are used to define elementary parallelepiped (volume) and parallelogram (surface) pieces. Excavation is modeled by removing a desired number of

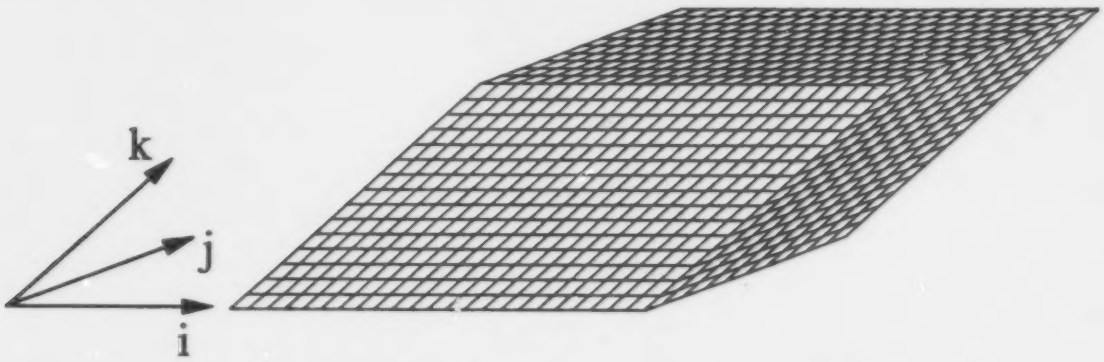

Figure 4-2 Parallelepiped Grid

volume pieces. This generates a surface, S, which is composed of a patchwork of n^S parallelogram pieces S^l, l=1, n^S . These are the surface elements used in the boundary element discretization. The volume V, where yielding may occur, is defined in turn by an assembly of n^V volume pieces V^l, l=1, n^V , referred to in the text as volume elements. With these conventions, Eq. (4.2-2) may be written as

$$u_i(x) = \frac{1}{2\mu}\left[\sum_{l=1}^{n^S} u_i^{S^l}(x) + \sum_{l=1}^{n^V} u_i^{V^l}(x)\right] \qquad (4.2\text{-}8)$$

where

$$u_i^{S^l}(x) = \int_{S^l} G_{ij}(x,\xi)\,\phi_j(\xi)\,dS \qquad (4.2\text{-}9)$$

$$u_i^{V^l}(x) = \int_{V^l} G_{ij}(x,\xi)\,f_j(\xi)\,dV \qquad (4.2\text{-}10)$$

and Eq. (4-3) may be formulated as

$$\sigma_{ij}(x) = \sum_{l=1}^{n^s} \sigma_{ij}^{s^l}(x) + \sum_{lj}^{n^v} \sigma_{ij}\sigma_{ij}^{v^l}(x) + \sigma_{ij}^{F}(x) - \sigma_{ij}^{o}(x) \qquad (4.2\text{-}11)$$

$$\sigma_{ij}^{s^l}(x) = \int_{s^l} T_{ijk}(x,\xi)\,\phi_k(\xi)\,dS \qquad (4.2\text{-}12)$$

$$\sigma_{ij}^{v^l}(x) = \int_{v^l} T_{ijk}(x,\xi)\,f_k(\xi)\,dV \qquad (4.2\text{-}13)$$

4.2.3 Boundary Element Approximation: Linear Elements

In the code, so-called "linear surface elements" are used. The intensity, $\phi_i(x)$ of the distribution of fictitious forces is approximated over those elements by a polynomial function which does vary linearly along the edges of the element. In principle, $\phi_i(x)$ is represented, over surface element l, by a function of the form

$$\phi_i(x) \approx \sum_{m=1}^{4} \phi_i^{l,m}\, h^{l,m}(x) \qquad (4.2.\text{-}14)$$

where $\phi_i^{l,m}$ is the as yet unknown value of the fictitious force at node m of the surface element l, and $h^{l,m}$ is a known shape function.

Similarly, we chose to represent σ_{ij}^{o} over the volume element l by a polynomial function which varies linearly along the edges of the parallelepiped. This function has the form

$$\sigma_{ij}^{o}(x) \approx \sum_{m=1}^{8} \sigma_{ij}^{o\,l,m}\, g^{l,m}(x) \qquad (4.2\text{-}15)$$

where $\sigma_{ij}^{o\,l,m}$ is the value of σ_{ij}^{o} at node m of volume element l, and $g^{l,m}(x)$ is a known shape function.

Note that, in the code, nodal values are unique --- a feature not reflected in the above element-oriented notation. Substitution of Eqs. (4.2-14) and (4.2-15) in Eqs. (4.2-1 and 4.2-9 through 4.2-13) then yields expressions for the surface and volume element contributions to the displacement and stress field, which contain as unknowns the nodal value of the fictitious force intensity and the nodal value of the initial stress. The integrals in Eqs.

(4.2-9 through 4.2-13) have particular properties which will be address in Section 4.3.2.

4.2.4 System of Equations

Assume that the initial stress field $\sigma^{\circ}_{ij}(x)$ is known. (The subject of its determination will be addressed in Section 4.4.) From the previous discussion, it follows that displacements and stresses in the medium are entirely defined from Eqs. (4.2-8) and (4.2-11), provided that the value of the three components of the fictitious forces at the surface element nodes are known. For the problem treated, the three components of either the boundary traction or displacement are known at each of the n^s surface nodes. Application of those boundary conditions, using Eqs. (4.2-7), (4.2-8) and (4.2-11), yields a linear system of $3n^s$ equations with $3n^s$ unknowns which may be solved to determine the three components of ϕ at the n^s surface nodes. These may then be substituted into Eq. (4.2-8) and (4.2-11) to yield expressions for displacements and stresses in the medium.

4.3 Evaluation of Integrals

4.3.1 Saving Scheme: Parallelepiped Grid

The advantage of using the parallelepiped grid approach is evident if one considers the easiness and flexibility it allows as far as data preparation is concerned. However, it has another property which gives MINE3D its particular character. In most 3-D boundary element codes, a large coefficient matrix must be evaluated and a great amount of computer time is involved in the computation of stresses and displacements at points located within the medium.

In MINE3D, a powerful saving scheme is adopted within the scope of matrix storage and computation of stresses and displacement values at all nodes of the grid. The object is to have at hand (i.e. computed and stored) the value at all grid nodes of the integrals involved.

As may be observed from Eqs. (4.2-9) to (4.2-13) and Eqs. (4.2-4) to (4.2-6), integrals corresponding to a particular surface or volume element depend on:

(a) the Poisson's ratio of the medium;

(b) the **relative** location of the grid node at which the integral is computed; and

(c) its orientation (for a surface element).

Supposing that ν is constant for the medium, to cover all cases of

integrals encountered in the stresses and displacement computations, it suffices, therefore, to evaluate the integrals corresponding to one single "reference element" at all the nodes of an "extended" grid whose dimensions are defined by the extremes encountered while considering all possible occurrences of relative locations of grid nodes with respect to elements. Note that the three possible orientations of a surface reference element need to be considered if the node spacing in all three directions of reference of the gird is not the same.

To be on the conservative side, given the maximum number of nodes in the direction of the three axes of the grid as i_{max}, j_{max}, k_{max}, we consider a reference element to be located at the center of an extended grid of dimensions $2*i_{max}-1$, $2*j_{max}-1$ and $2*k_{max}-1$.

Within the parallelepiped grid, each node is surrounded by eight (8) volumes, and tnere are 2^8, or 256, ways in which the volumes may be present. Rather than store all nodal coefficients describing geometries, sets of coefficients for the reference element can be stored. The effect of any node is then the sum of its effects from all adjacent elements. Thus,

$$4 \cdot (2*i_{max} - 1) \cdot (2*j_{max} - 1) \cdot (2*k_{max} - 1)$$

sets of coefficients are required for 4-noded surface elements, and

$$8 \cdot (2*i_{max} - 1) \cdot (2*j_{max} - 1) \cdot (2*k_{max} - 1)$$

sets are required for 8-noded volume elements. Since surface elements can have any one of three orientations, the surface element effect is increased by a factor of 3. The effect of each surface and volume element is considered on six (6) stress components at every node in the grid, and there are three (3) surface solution quantities and six (6) volume quantities. Thus, the effects of the surface quantities are

$$4 \cdot 3 \cdot 6 \cdot 3 \cdot (2*i_{max} - 1) \cdot (2*j_{max} - 1) \cdot (2*k_{max} - 1)$$

and the effects of the volume quantities are

$$8 \cdot 6 \cdot 6 \; (2*i_{max} - 1) \cdot (2*j_{max} - 1) \cdot (2*k_{max} - 1)$$

If the analysis also accounts for displacements, the coefficients additionally required (for three displacement components at any node) are

$$(108 + 144) \cdot (2*i_{max} - 1) \cdot (2*j_{max} - 1) \cdot (2*k_{max} - 1)$$

Thus, the total storage requirement is

$$756 \cdot (2*i_{max} - 1) \cdot (2*j_{max} - 1) \cdot (2*k_{max} - 1)$$

or approximately

$$6000 * i_{max} * j_{max} * k_{max}$$

In the general boundary element approach, allowing elements of arbitrary shape, the influence coefficients are all different. Each elastic surface node n^v has three unique traction components, and their effect is required on three traction components of any other node. Likewise, each plastic volume node n^v has six unique components of stress, and their effect is required on six stress components at any other node. Thus, if it is assumed that surface and volume nodes do not coincide, then there are potentially $(3\ n^s + 6\ n^v)$ unknowns and an equal number of equations to describe their interaction. There are, then $(3\ n^s + 6\ n^v)^2$ unique coefficients in the matrix if no account is taken of common nodes or symmetry.

The coefficients for the parallelepiped grid are calculated for a "box" that encloses all surface and volume nodes. Thus, $(i_{max} * j_{max} * k_{max})$ is not directly related to n^s plus n^v. Nevertheless, a gain in 3-D problem size is clearly achieved by using the parallelepiped grid versus arbitrary elements. This can be seen by comparing the size of the coefficient matrix for the two approaches. As shown in Fig. 4-3, this savings increases dramatically for increasing surface and volume nodes. For example, a 2000-node parallelepiped grid requires approximately 48 Mbytes, whereas the matrix for 2000 surface nodes based on the general approach would require 144 Mbytes.

As a consequence of the parallelepiped scheme, MINE3D dedicates a large amount of computer time in the early stage of its running process to compute those effects. The advantage of this investment becomes clear in the last stage, when stresses and displacements are evaluated at grid nodes.

4.3.2 Numerical Integration

Before solving the system of equations and then computing stresses and displacements in the medium, the integrals of the type exhibited in Eqs. (4.2-9) through (4.2-13) must be evaluated for the reference element at all nodes of the extended grid. In MINE3D, all integrals are evaluated numerically using Gauss quadrature. However, given the character of the kernels (see Eqs. (4.2-4) and (4.2-5)), different tactics are adopted according to whether or not the extended grid node belongs to the reference element.

Off-Element Node - If the node at which the integral is to be evaluated does not belong to the element, the kernel remains bounded throughout the domain of integration and numerical integration can routinely be carried out. In the code, the volume integrals are evaluated using four (4) Gauss points in each of the

three coordinate directions. To evaluate the surface integrals, a refined adaptive technique using four Gauss points is used which takes into account the proximity of the evaluation point with respect to the element (Lachat and Watson, 1976 and Banerjee and Ravendra, 1986).

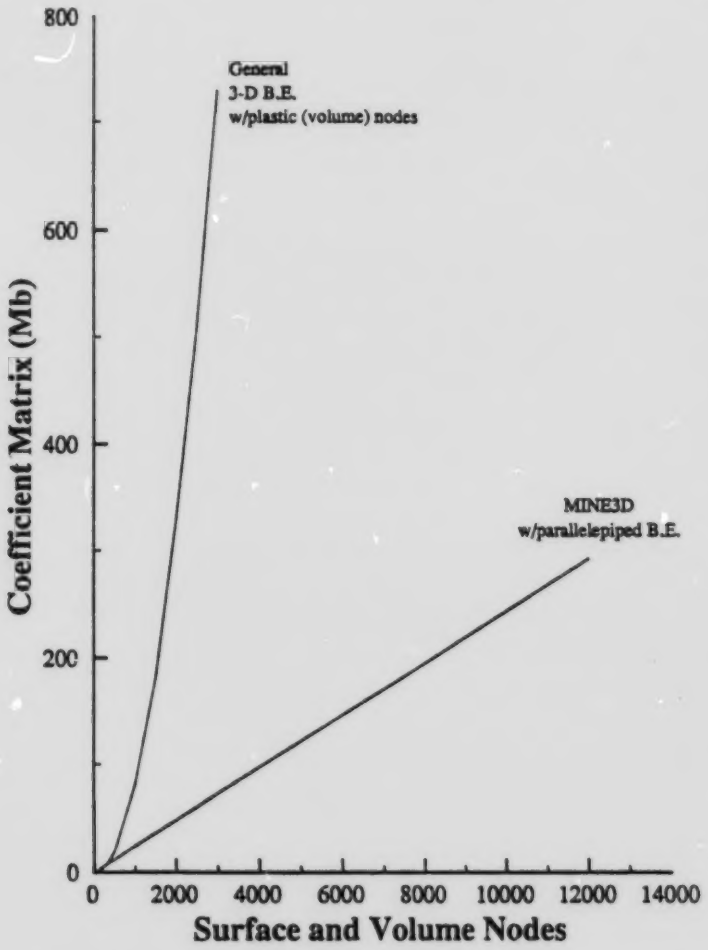

Figure 4-3 Coefficient Matrix Size versus Number of Boundary Element Nodes

Self Effect - Special attention must be given to the case in which the integrals are to be evaluated at one of the element nodes: the so-called self effect. Indeed, the displacement kernal now has a singularity of the order (1/r) at that node, and the stress kernel has a singularity of the order of (1/r). However, the singularity of (1/r) is removable under both the surface and volume integration, while the singularity in ($1/r^2$) of the stress kernel is removable only under the volume integration. Indeed, if we

adopt a polar coordinate system with the origin located at the node and make the corresponding change of variable in the integral, the surface element dS then contains a term in r, and the volume element dV contains a term in r^2 which cancel out the kernel singularity.

As for the surface stress integral, we may decompose it in two terms, as follows:

$$\sigma_{ij^{*l}}(x) = \int_{s^l} T_{ijk}(x,\xi)\,[\phi_k(\xi)-\phi_k(x)]\,dS + \phi_k(x)\int_{s^l} T_{ijk}(x,\xi)\,dS \qquad (4.3\text{-}1)$$

Since the function $\phi(x)$ is continuous along S (recall that a continuous piecewise linear variation has been adopted for $\phi(x)$ along S), the first term in Eq. (4.3-1) is integrable in the normal sense. If we adopt the polar coordinate system mentioned above and make the relevant change of variables, an additional r term emerges from the function $[\phi_k(\xi)-\phi_k(x)]$, which is just what is needed to cancel out the singularity of the kernel.

As for the second part, its singular character is such that its evaluation cannot be incorporated in the extended grid approach because the spatial configuration of elements meeting at the node must be taken into consideration. A particular technique has been used in the code to treat this "singular term"; it will be addressed in Section 4.3.3, Handling of Corners.

In the code, the non-singular surface integrals corresponding to the self effect are evaluated using seven (7) Gauss points in directions r and θ of the polar coordinate axes. For the volume integral, four (4) Gauss points are used in the direction of the global axes. (Seven (7) Gauss points were also tried, but no significant change in value for the integral was observed.)

4.3.3 Handling of Corners

In the boundary element approach, the value of the displacement or traction components at the surface nodes must be obtained to determine the unknowns of the system. The evaluation of boundary displacements offers no difficulty: the displacement field as computed from Eq. (4.2-8) is continuous not only across the boundary S but also along it, as the distribution of fictitious forces is continuous there. Computation of the boundary stresses would offer the same ease if it were not for the terms corresponding to the singular surface stress integral addressed in the preceding section. Evaluation of the stresses at a surface node involves the computation of the singular contribution of all surface elements meeting at the node. This overall singular

contribution may be written

$$D_{ij}(x) = \phi_k(x) \int_{S^x} T_{ijk}(x,\xi)\, dS \qquad (4.3\text{-}2)$$

where $S^x = \sum S^l$, and the summation is carried out over all surface elements meeting at node x. This term has two important properties. First, as a singular Cauchy integral, it is responsible for the jump of the boundary traction across the boundary and, as such, this must be interpreted as the limiting value of the integral when point x approaches the boundary from inside domain D. Second, that term which is finite when the normal to S varies smoothly through x becomes unbounded at a geometric corner. (Its singularity at x is of the order of ln(r); see, for example, Banerjee and Butterfield, 1981, p.126, and cannot be removed at a geometric corner).

In MINE3D, an average normal is defined at each boundary node, and its value is the normalized sum of the normals to the elements meeting at the node. In this way, Eq. (4.2-7) for the boundary traction is well defined, even at points corresponding to geometric corners. Even with this convention, however, boundary tractions (which are otherwise finite along S) are not defined at a geometric corner because the expression for the stresses at that point is unbounded due to the presence of the singular term, Eq. (4.3-2). (Note that this interpretation is different from that found in Banerjee and Butterfield, 1981, p.87.)

In the literature, two main approaches may be found to treat this problem: the multiple independent node concept and the analytical approach (e.g. Banerjee and Butterfield, 1981, p.170). In the first approach, the corner node is replaced by a set of nodes offset along each of the element edges meeting at the node. Each of these nodes has three (3) unknown fictitious forces, and additional equations must be written to determine them. In the second approach, the exact behavior of the stress kernal function is taken into account by means of a series expansion in the vicinity of the corner point.

In MINE3D, a different approach is taken to evaluate the stresses at a boundary node. In this technique, all non-singular terms are evaluated at the node, while the singular term Eq.(4.3-2) is evaluated at a single "offset node" moved within D a small distance with respect to the element's dimensions measured along the average normal at the node. This approximation is done at all surface nodes, and the offset is defined as a constant c times the smallest characteristic length of the elements. For a given grid, the integral Eq.(4.3-2) depends only on the spatial configuration of surface elements at x. This property is taken into consideration, and all integrals involved are evaluated using the 4-point adaptive Gauss quadrature referred to in Section 4.3.2.

As mentioned above, the surface tractions are computed in turn from Eq.(4.2-7), using the average normal at the node. Physically, the approach may be envisioned as a rounding-off process of the corner.

Values for c between 0.01 and 0.005 were investigated. These values are those suggested by Banerjee and Butterfield (1981, pp. 87 and 89) in a 2-D offset approach. Their use may be justified in the special case of a surface node at which 4 elements meet on a plane. In this instance, the unit normal is constant on S^x, and the value of Eq.(4.3-2) is finite at x. The contribution of the integral in Eq. (4.3-2) to the traction at x approached from within D has the well-known following compact form (see, for example, Balas et al., 1989, p. 37):

$$C_{ij}(x) = \int_{s^x} T_{ij1}(x,\xi)\, n_1(x)\, dS = \frac{1}{2}\delta_{ij} \qquad (4.3\text{-}3)$$

Numerical values are presented below for two (2) test runs in which x was located at the center of a configuration of four (4) square elements in the plane.

c	C_{11}	C_{22}	C_{33}
0.01	0.439	0.439	0.437
0.005	0.494	0.494	0.499

Table 4-1 Influence of Corner Offset Factor c

These values clearly converge to the exact solution (i.e., 0.5) when the value of c decreases, and it may be observed that the value corresponding to the normal component of the traction does so more rapidly than those of the tangential components. It is recalled that, at a geometric corner, the singular term Eq. (4.3-2) is unbounded, in which instance a value of c smaller than 0.005 is not recommended.

4.4 Plasticity Formulation

The plasticity formulation in MINE3D assumes an elastic, perfectly plastic solid which conforms to a Mohr-Coulomb yield criterion and non-associated flow rule.

The yield surface is given by

$$f = \sigma_1 - N_\phi \sigma_3 + 2c\sqrt{N_\phi} \qquad (4.4\text{-}1)$$

and the plastic potential function is given by

$$g = \sigma_1 - N_\psi \sigma_3 + 2c\sqrt{N_\psi} \qquad (4.4\text{-}2)$$

where $N_\xi = \dfrac{1+\sin\xi}{1-\sin\xi}$ $[\xi = \phi \quad \psi]$

c	=	cohesion,
ϕ	=	friction angle,
ξ	=	dilation angle,
σ_1	=	major principal stress, and
σ_3	=	minor principal stress.

The strain increments are assumed to be composed of elastic and plastic parts:

$$\begin{aligned} \Delta e_1 &= \Delta e_1^e + \Delta e_1^p \\ \Delta e_3 &= \Delta e_3^e + \Delta e_3^p \end{aligned} \qquad (4.4\text{-}3)$$

The plastic strain rates are given by the non-associated flow rule:

$$\begin{aligned} \dot{e}_1^p &= \gamma \frac{\partial g}{\partial \sigma_1} = \gamma \\ \dot{e}_3^p &= \frac{\gamma \partial g}{\partial \sigma_3} = -\gamma N_\psi \end{aligned} \qquad (4.4\text{-}4)$$

where γ is the multiplier which must be determined from the stress state.

Multiplying by Δt , Eq. (4.4-4) becomes

$$\begin{aligned} \Delta e_1^p &= \gamma \Delta t \\ \Delta e_3^p &= -\gamma N\psi \, \Delta t \end{aligned} \qquad (4.4\text{-}5)$$

The incremental principal elastic stresses are given by:

$$\begin{aligned} \Delta\sigma_1 &= (K+\frac{4}{3}G)\,\Delta e_1^e + (K-\frac{2}{3}G)\,(\Delta e_2^e + \Delta e_3^e) \\ \Delta\sigma_3 &= (K+\frac{4}{3}G)\,\Delta e_3^e + (K-\frac{2}{3}G)\,(\Delta e_1^e + \Delta e_2^e) \end{aligned} \qquad (4.4\text{-}6)$$

Substituting Eqs. (4.4-3) and (4.4-5) into Eq. (4.4-6),

$$\Delta\sigma_1 = (K+\frac{4}{3}G)(\Delta e_1 - \gamma\Delta t) + (K-\frac{2}{3}G)(\Delta e_3 + \gamma N_\phi \Delta t) + (K-\frac{2}{3}G)\Delta e_2^*$$

$$\Delta\sigma_3 = (K+\frac{2}{3}G)(\Delta e_1 - \gamma\Delta t) + (K-\frac{4}{3}G)(\Delta e_3 + \gamma N_\phi \Delta t) + (K-\frac{2}{3}G)\Delta e_2^* \quad (4.4\text{-}7)$$

Determining the initial elastic principal stresses by σ_1^I, σ_2^I and σ_3^I the corrected (for plasticity) stresses σ_1, σ_2 and σ_3 are given by

$$\sigma_i^I - \sigma_i = \Delta\sigma_i^I - \Delta\sigma_i \quad (4.4\text{-}8)$$

where i = 1, 2 or 3.

The initial principal stress increments are given by

$$\Delta\sigma_1^I = (K+\frac{4}{3}G)\Delta e_1 + (K-\frac{2}{3}G)(\Delta e_2 + \Delta e_3)$$

$$\Delta\sigma_2^I = (K+\frac{4}{3}G)\Delta e_1 + (K-\frac{2}{3}G)(\Delta e_1 + \Delta e_3) \quad (4.4\text{-}9)$$

$$\Delta\sigma_3^I = (K+\frac{4}{3}G)\Delta e_3 + (K-\frac{2}{3}G)(\Delta e_1 + \Delta e_2)$$

By substituting Eqs. (4.4-7) and (4.4-9) into Eq. (4.4-8) and noting that $\Delta e_2 = \Delta e_2^*$,

$$\sigma_1 = \sigma_1^I - \gamma\Delta t\left[(K+\frac{4}{3}G) - (K-\frac{2}{3}G)\,N_\phi\right]$$

$$\sigma_3 = \sigma_3^I - \gamma\Delta t\left[(K+\frac{2}{3}G) - (K-\frac{4}{3}G)\,N_\phi\right] \quad (4.4\text{-}10)$$

or, simplifying,

$$\sigma_1 = \sigma_1^I - \gamma\Delta t(\alpha_1 - \alpha_2 N_\phi)$$

$$\sigma_3 = \sigma_3^I - \gamma\Delta t(\alpha_2 - \alpha_1 N_\phi) \quad (4.4\text{-}11)$$

where $\alpha_1 = K+\frac{4}{3}G$, and $\alpha_2 = K-\frac{2}{3}G$.

Equation (4.4-10) gives the new principal stresses in terms of the trial initial stress, the material constants, and the multiplier, γ . The γ value can be found since σ_1 and σ_3 lie on the yield surface (if a non-admissible stress state is detected). This is done by substituting (Eq. 4.4-10) into the equation for the yield surface (Eq. 4.4-1) and equating to zero:

$$\gamma \Delta t = \frac{\sigma_1^I - N_\phi \sigma_3^I + 2c\sqrt{N_\phi}}{\alpha_1(1+N_\phi N_\psi) - \alpha_2(N_\phi + N_\psi)} = \frac{f(\sigma_1^I,\ \sigma_3^I,\ c,\ N_\phi)}{\gamma} \qquad (4.4\text{-}12)$$

where $\gamma = \alpha_1(1+N_\phi N_\psi) - \alpha_2(N_\phi + N_\psi)$.

Substituting Eq. (4.4-12) into Eq. (4.4-11) yields the corrected principal stress components:

$$\sigma_1 = \sigma_1^I - (\alpha_1 - \alpha_2 N_\psi)\frac{f(\sigma_1^I,\ \sigma_3^I,\ c,\ N_\phi)}{\gamma}$$

$$\sigma_3 = \sigma_3^I - (\alpha_2 - \alpha_1 N_\psi)\frac{f(\sigma_1^I,\ \sigma_3^I,\ c,\ N_\phi)}{\gamma} \qquad (4.4\text{-}13)$$

Although σ_2 , the intermediate principal stress does not enter in the calculations for γ , a correction must be made to the initial estimate, σ_2^I because it is calculated on the assumption that all strains are elastic (Eq. (4.4-9)).

The stress increment corresponding to the plastic strains Δe_1^P and Δe_3^P must be subtracted from σ_2^I to give σ_2 . The correction is

$$\sigma_2 = \sigma_2^I - \frac{\alpha_2(1-N_\psi)\ f(\sigma_1^I, \sigma_3^I, c, N_\phi)}{\gamma} \qquad (4.4\text{-}14)$$

This correction equals zero where the dilation angle is 0.0.

MINE3D first determines the σ_{xx}, σ_{yy}, σ_{zz}, σ_{xy}, σ_{xz} and σ_{yz} elastic stresses and converts them to principal stresses. These values are then substituted into the equation for the yield surface (Eq. 4.4-1). If,

f<0, then the direction cosines of the principal stresses are found and the plastic corrections are made (Eq. 4.4-13 and 4.4-14) to require conformity to the yield surface.

f>0, then no corrections are necessary.

The principal stresses are then resolved back to the x,y,z global axes by the direction cosines determined previously. The plastic correction is stored for evaluation in the solution procedure (see Section 4.7).

4.5 Multiple Materials

The presence within the medium of finite subdomains with different material properties is also taken into account in the model. These inclusions may be used to represent regions of backfill in the excavation.

In MINE3D, each inclusion is considered as an independent domain with its own set of surface and, if appropriate, volume elements. Stresses and displacements are then described in the inclusion and on its boundary by relevant equations of the type as Eq. (4.2-2) and (4.2-3). The elements are again defined by means of the parallel-epiped grid, a process which generates twin nodes and twin surface elements at the interface between different materials.

The interaction with the rest of the medium is made by requiring continuity of the three components of traction and the three components of displacement at the twin nodes. Imposition of the continuity conditions allows for the determination of the six unknown components of the fictitious forces at the twin nodes.

4.5.1 Principle of Solution

MINE3D devotes a great amount of computer time to evaluate the integrals present in the expressions for stresses and displacements at the grid nodes. To avoid computation of new integrals for the inclusions, it was decided to allow the shear modulus to differ, but to adopt the same Poisson's ratio for all materials. Because the Poisson's ratio is the only material property present in the kernels of the integrals (see Eqs. (4.2-4) and (4.2-5)), all values computed and stored in the reference element context could thus be used in the evaluation of stresses and displacements in the inclusions. The continuity conditions at the interfaces are imposed by using an iterative procedure in which the infinite medium solution provides boundary conditions for the inclusions, and vice versa. The principle is, starting with an initial guess for the tractions at the interface boundaries of the infinite medium, to find the solution for this medium. With this solution, displacements are computed at the twin nodes. These values are used to impose boundary conditions for the inclusions. Their respective solution is found and used to evaluate tractions at their twin nodes - tractions which, with a change of sign, are imposed as boundary conditions for the infinite medium. This procedure is repeated until convergence is achieved (i.e. until no more change is observed, at a pre-set accuracy, in the value of the

fictitious forces involved).

While, in most applications, the boundary conditions for the infinite medium are of the "traction imposed" type, those for an inclusion usually are mixed: displacements are imposed along that part of the inclusion boundary which corresponds to an interface while, along the remaining part in contact with the void, tractions are specified. Displacements and stresses have different orders of magnitude; to avoid numerical problems associated with the solution to a system of equations generated by mixed boundary conditions, all displacement relations (Eq. 4.2-2) are multiplied by 2μ .

4.6 Sequential Mining

Sequential mining has been introduced in the code to calculate the stresses and displacements at progressive stages of the mining operation. The input is prepared for a sequence of mining steps. At each new step, existing excavations are enlarged, new ones created, and backfill set in place. Also, regions in which plastic behavior is expected are created or updated. The output solution provides global (rather than incremental) values for stresses and displacements at each step.

Each new step is viewed as a modification of the former one. This eases the input process and speeds up intermediate calculations by providing at the new step "good" first guesses for unknowns involved in the iterative processes based on values obtained at the former step.

4.6.1 Mining Steps and Plasticity

When all materials in the medium behave elastically, the solution at a particular mining step may be determined independently. For the case in which plasticity is involved, the mining history must be taken into consideration. To illustrate this dependence on history, consider a one-dimensional model involving an elasto-plastic rod and an elastic spring, as illustrated in Fig. 4-4.

In the figure, compression and contraction are taken as positive. There are three stages: the initial stage, A, at which the rod is unstressed; the intermediate stage, B, at which the rod is placed in contact with a spring prestressed to σ_B and the final stage, C, at which contact is made with a spring prestressed to σ_C . We now investigate two loading histories: (1) from A to C directly; and (2) from A through B to C.

In the first case, the elastoplastic rod is progressively loaded, as a result of the unloading of the spring, until the state of equilibrium is reached correspondingly to the solution $(\sigma_1, \varepsilon_1)$ at

point 1 on the diagram. In the second case, the state of equilibrium, O, is reached first, at which point it is imagined that the spring is instantaneously removed and replaced by another spring prestressed to σ_C . The solution at the end of the loading path is now given by $(\sigma_2, \varepsilon_2)$ at point 2.

The loading path is approximated by an incremental process used to follow the mining history. In MINE3D, the mining steps play the role of load increments, and plastic information is transmitted

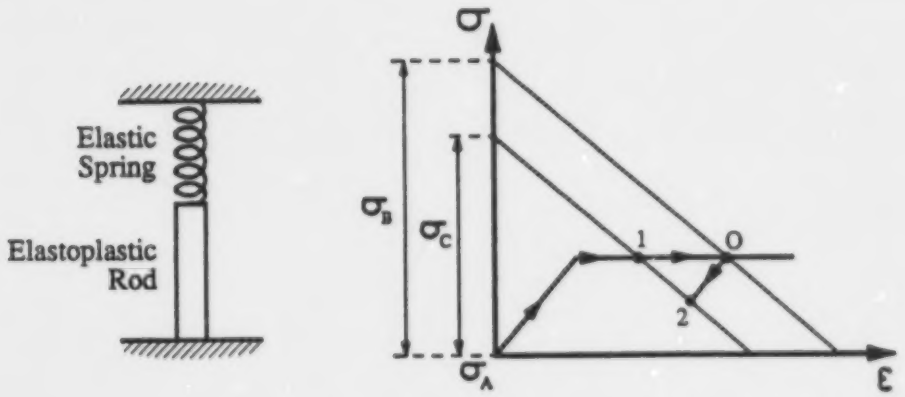

Figure 4-4 Loading History for an Elastic Spring and Elastoplastic Rod

between steps by taking as a first guess for the plastic initial stress field at a new step the value obtained at the end of the former step, e.g. start at $(\sigma_0, \varepsilon_0)$ rather than $(\sigma_A, \varepsilon_A)$.

4.7 Solution Process

In the model, several components are represented, such as excavations, plastic zones and multiple materials. Each of these components, when brought into the context of sequential mining, generates unknowns which must be determined to allow evaluation of stresses and displacements in the medium.

Conditions to be imposed for the determination of the unknowns were discussed in previous sections. The techniques used to meet those conditions were also addressed: plasticity and material coupling are taken into account through iterative procedures and, thus, the final task is to determine the solution to a linear system of equations.

4.7.1 Algorithm of Resolution

The components have been treated individually previously. It is now assumed that they are all present. The general algorithm of resolution is outlined below.

FOR EACH MINING STEP

1. Guess the initial plastic stress.

   The value of σ°_{ij} at the nodes of the volume elements defined for a given step is selected based on the value obtained at the previous mining step, if it is available. If not, the value for σ°_{ij} is set to zero.

2. Solve for fictitious forces.

   Including the assigned value of σ°_{ij} , three equations are set up for each of the surface nodes which express the fact that three components of traction or displacement are imposed at the node. At a "single" surface node, the value imposed is known beforehand, and corresponds to a boundary condition for the overall problem. At a "twin" node, the value imposed is computed using an iterative procedure devised to ensure continuity of tractions and displacements across the interface (see Section 4.5). The resulting system of equations is solved, providing values for the fictitious forces. The method of solution is addressed in the following section.

3. Compute initial plastic stress correction.

   For each volume node, the stresses are computed using both the values for the guess at σ°_{ij} and those for the associated fictitious forces. If the yield criterion is violated at the node, the stresses are brought back to the yield curve by means of the flow rule as discussed in Section 4.4. The corresponding plastic stress correction is calculated and stored.

4. Check for convergence.

   If the value of the plastic stress correction falls below a pre-set tolerance at all volume nodes, the solution is obtained. Otherwise, the initial stress field is updated, and the procedure is repeated, beginning at Step 2.

4.7.2 Method of Solution: Successive Overrelaxation (SOR)

The linear system of equations is solved using the "successive overrelaxation" method (see, for example, Dahlquist and Bjorck, 1974, p.192). This iterative method reduces to the Gauss-Seidel method when the relaxation parameter is selected as one.

The solution procedure for multiple materials discussed in Section 4.5 has the advantage of being independent of the method adopted to solve the system of equations. In MINE3D, rather than solve for stresses and displacements in each material separately, as discussed in Section 4.5, the "multi-material loop" is interlaced in the "SOR loop." One single set of equations is solved by SOR using an initial guess for the fictitious forces (recall that there are $3n^s$ equations, where n^s is the total number of surface nodes). At each of the twin nodes, the tractions or displacements imposed at one node are those transmitted by the other in the pair (a change of sign is involved for the tractions); these values are updated at each SOR iteration. Overall boundary conditions are imposed at the other surface nodes. The advantage of using the interlaced solution approach versus the separated solution approach has not been demonstrated.

4.8 Energy Release

4.8.1 Case 1: Elastic Host Rock

We wish to determine the energy balance which results from excavation of new mined volume and placement of backfill. Salamon (1984) determined the basic energy balance equations which are presented below. Consider the problem of energy changes in moving from the State I to State II excavation geometry as shown in Fig. 4-5. The primary components which describe the energy transfer in the body (in Salamon's terminology) are listed below.

1. energy source terms - these terms include any energy available upon excavation.

   (a) W - the work done by external and body forces through displacements of the rockmass

   (b) U_m - the strain energy content of the volume of rock (V_m) which is mined in moving from State I to State II. U_m becomes available upon excavation.

2. expended energy terms - these terms include energy stored or lost through deformation of support.

   (a) U_c - the increase in stored strain energy in the rock mass

(b) W_s - the work done on compression of rock support

3. "released" or unaccounted for energy.

W_r - the amount of energy which remains unaccounted for after energy balance; can be considered a surplus energy

Energy Balance

The energy balance can be obtained by subtracting the energy expended from the energy sources, resulting in the released energy:

$$W_r = (W + U_m) - (U_c + W_s) > 0 \qquad (4.8\text{-}1)$$

where $W + U_m$ = source terms,
$U_c + W_s$ = dissipated or expended terms, and
W_r = released energy.

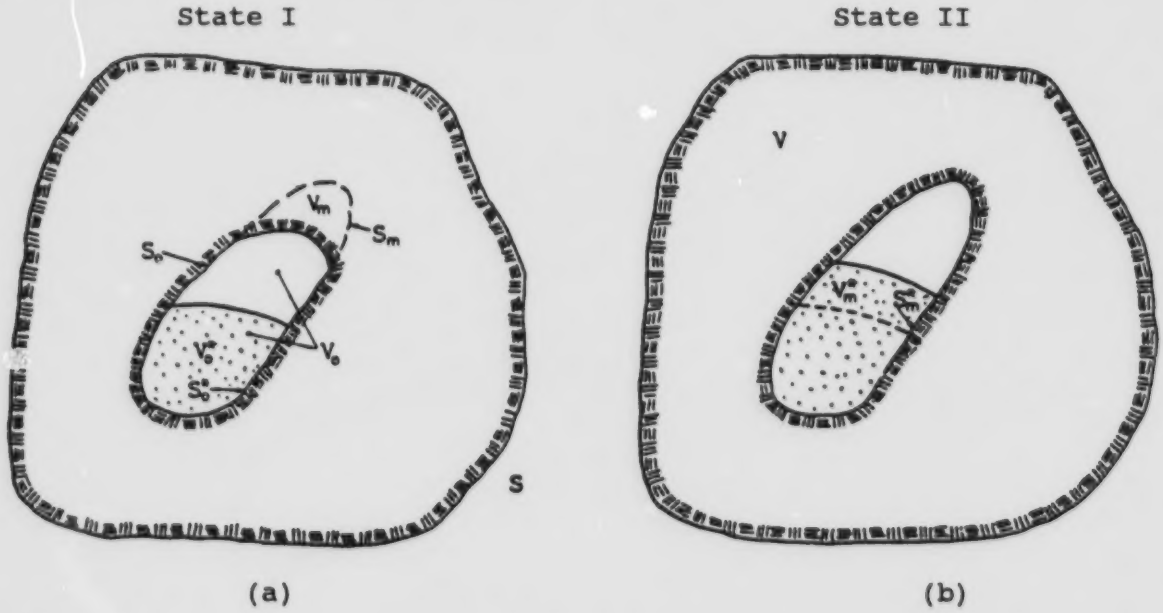

Figure 4-5 Mining Configuration and Notations in the Reference State, i.e. in State I (a) and After Additional Mining, i.e. in State II (b) (Salamon, 1984)

Since U_m is not available to strain rock or support,

$$W \geq U_c + W_s \qquad (4.8\text{-}2)$$

and, since $U_m > 0$, it follows that

$$(W + U_m) > (U_c + W_s) \qquad (4.8\text{-}3)$$

Finally,

$$W_r \geq U_m > 0 \qquad (4.8\text{-}4)$$

When an excavation is created rapidly, energy is given off in the form of seismic waves which will be damped by some inelasticity in the rock. This kinetic energy, denoted W_k, is a portion of the released energy:

$$W_r = U_m + W_k \qquad (4.8\text{-}5)$$

where $W_k = W - (U_c + W_s) \geq 0$.

Expressions for the Energy Components

There are two primary energy components from which most of the others are derived. These are (again using Salamon's terminology) as follows.

1. U^{ii} - strain energy stored in a volume V if the induced stresses were to act on the originally unstrained body

2. U_m - strain energy content of the volume V_m prior to its excavation (i.e., in State I)

Referring to Fig. 4-5, V_m is the volume of rock excavated in going from State I to State II. S_m is the new surface which is exposed when going from State I to State II. The energy components are given by:

$$U^{ii} = \frac{1}{2}\int_{S_m} T_i^{(P)}\, u_i^{(i)}\, dS - \frac{1}{2}\int_{S^*} R_i^{(P)}\, u_i^{(P)}\, dS \qquad (4.8\text{-}6)$$

and

$$U_m = \frac{1}{2}\int_{S_m} T_i^{(P)}\, u_i^{(P)}\, dS \qquad (4.8\text{-}7)$$

where super P refers to primitive or pre-existing state,
super i refers to induced by further mining,
sub i refers to vector components,
T_i is the traction acting at a point on surface S_m ,
u_i is the displacement at a point on the surface S_m or S^* ,
and
R_i is the traction acting at a point on the backfill surface S^* where the surface and fill are in contact.

Note: The integral energy terms corresponding to the infinite surface is taken to be zero, as the body is considered to be weightless.

Some definitions are required regarding the notion of "induced" components. The displacement and traction at any point in the body can be expressed as:

$$u_i = u_i^{(P)} + u_i^{(I)} \qquad T_i = T_i^{(P)} + T_i^{(I)}$$

where $u_i^{(P)}$, $T_i^{(P)}$ are the pre-existing components (pre-existing to the current mining state),

and

$u_i^{(I)}$, $T_i^{(I)}$ are the "induced" components due to the current mining state.

MINE3D currently provides the values u_i, T_i at any state - i.e. the total displacements and tractions. The induced components can be found by simply subtracting those from the previous mining step.

The surface S_0 defines the excavations. A portion of this surface, S_0^* may be in contact with backfill. When the excavation is advanced, a new volume (V_m) is extracted, exposing new surface (S_m). If the backfill is advanced, it will be in contact with new surface S_m^* . On all exposed surfaces (the tractions), $T_i = 0$. On all surfaces (S_m^*), tractions R_i are applied to the fill.

In MINE3D, the backfill is modeled as a Mohr-Coulomb material, and the internal failure is assumed here to be accounted for in the boundary deformations of the opening. The total work done in compression of the backfill (W_s) is given by

$$W_s = \frac{1}{2} \int_{S^*} R_i^{(I)} \, u_i^{(I)} \, dS + \int_{S_0^*} R_i^{(P)} \, u_i^{(I)} \, dS \qquad (4.8\text{-}8)$$

where the integral $\frac{1}{2}\int_{S^*} R_i^{(I)} u_i^{(I)} dS$

is taken over the entire backfilled surface, the integral

$$\int_{S_0^*} R_i^{(P)} u_i^{(I)} dS$$

is taken over the filled surface which was present prior to the present mining step,

and $S^* = S_0^* + S_m^*$

This expression determines the work done on compression of the backfill by contact forces for the present mining step.

Relationship Between Energy Components

Salamon (1984) showed that

$$U_c = U^{(II)} + 2U^{(P_I)} \qquad (4.8\text{-}9)$$

where $2U^{(P_i)} = \int_{S_m} T_i^{(P)} ds - \int_{S^*} R_i^{(i)} u_i^{(P)} dS$.

If support is not present,

$$U_c = U^{(ii)} + 2U_m \qquad (4.8\text{-}10)$$

Now, the work done by external forces, W, becomes

$$W = U_c + W_s + \frac{1}{2}\int_{S_m} T_i^{(P)} u_i^{(i)} dS + \frac{1}{2}\int_{S^*} R_i^{(i)} u_i^{(i)} dS \qquad (4.8\text{-}11)$$

The released energy is

$$W_r = U_m + \frac{1}{2}\int_{S_m} T_i^{(P)} u_i^{(i)} dS + \frac{1}{2}\int_{S^*} R_i^{(i)} u_i^{(i)} dS \qquad (4.8\text{-}12)$$

and

$$W_k = \frac{1}{2}\int_{S_m} T_i^{(P)} u_i^{(i)} dS + \frac{1}{2}\int_{S^*} R_i^{(i)} u_i^{(i)} dS \qquad (4.8\text{-}13)$$

4.8.2 Case II: Elastic Host Rock Mass, Excavation Occurs in Plastic Material.

There are two potential methods for determining the energy change associated with excavation, backfilling and yield in the rock mass. The first is to treat the elastic host rock mass separately from the inelastic rock mass, as shown in Fig. 4-6. Here, a surface, S_i , separates the elastic host rockmass from the internal yielding material. This surface will move with excavation as the elastic-plastic boundary changes. The second method is to attempt to determine the total energy change in the body from the boundary tractions and displacements, as done in the previous section, but to perform the summations of energy in an incremental fashion, as the solution iterations are performed. Both approaches are discussed here.

4.8.2.1 Outline of Method in Which Elastic and Plastic Regions Treated Separately

This discussion follows that given in Section 3.10 of this report, and is the basis for the formulation in MINE2D.

Elastic Host Rockmass - Figure 4-6 illustrates a yielding material in contact with an elastic host rock. The boundary between the material is defined as S_i , with the boundary at infinity given by S .

The energy exchange can be determined by treating the surface S_o as an internal boundary in the problem. The work done from external forces acting through displacements at S_i is given by W_{host} when excavation occurs inside boundary S_i . Use the convention that excavation occurs in moving from State I to State II. The work delivered to the interior region by the surrounding mass is given by

$$W_{host}^{I-II} = \frac{1}{2} \int_{S_i} T_i^{(P)} u_i^{(i)} dS \qquad (4.8\text{-}14)$$

where T_i are the traction components on surface S_i ,
u_i are the displacement components on surface S_i ,
superscript P refers to the earlier state, and
superscript i refers to induced state.

A positive sign for this term means energy stored in the host and lost to the internal region. This is the standard case.

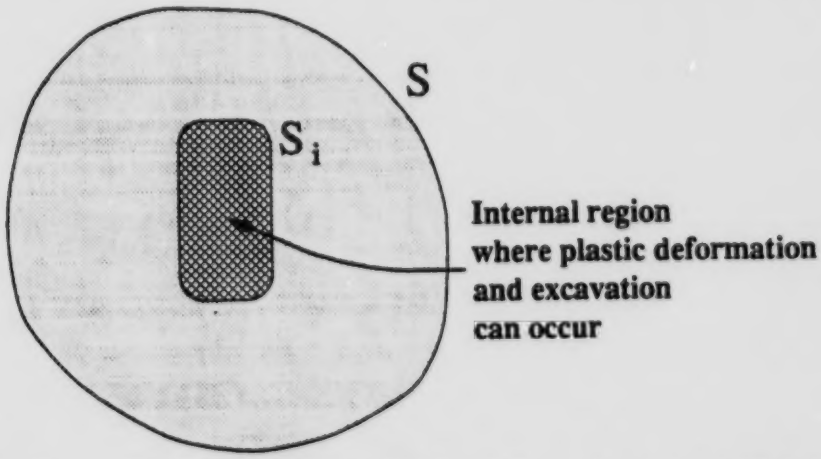

Figure 4-6 Boundary Description for Case In Which Yielding Material Can Occur (surface S is the infinite boundary; S_i occurs between the yielding region and elastic host rock)

Internal Region - The internal region is bounded by surface S_i , and is subdivided into volume elements, each with identical volume V_i (Fig. 4-7). The stress and strain tensors are known for every node point in the mass, as well as the displacement components.

Excavations of any of these elements can occur by creating internal boundaries, S_o . Using the same terminology as Salamon (1984), the excavation has a volume V_m , and exposes fresh surface, S_m . The excavations may be backfilled, with the surface of contact being S_o^* . If new volume is mined, the additional contact surface for the fill is S_m^* , as illustrated in Figure 4-8.

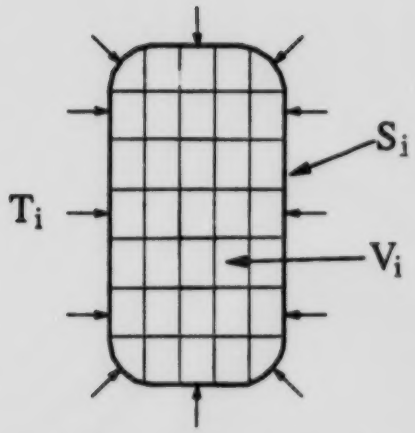

Figure 4-7 Internal Discretized Region Loaded at Boundary by Elastic Host Rock

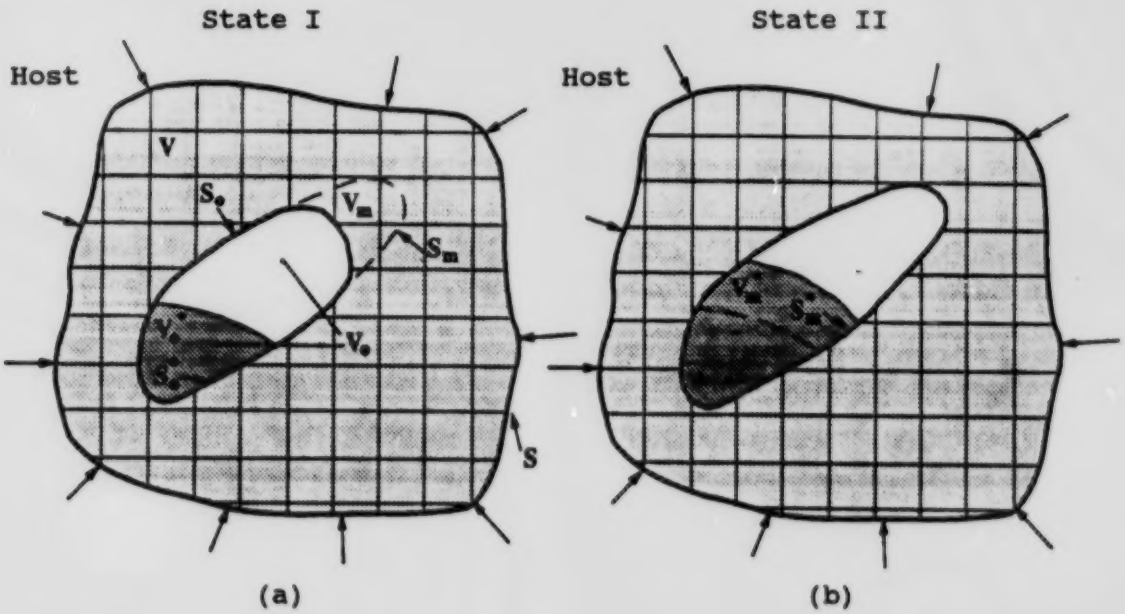

Figure 4-8 Mining Configuration and Notations in the Reference State, i.e. in State I (a), and after additional mining, i.e. in State II (b), Within the Yielding Region (adapted from Salamon, 1984)

The total elastic stored strain energy in the interior region can be found at any state from the strain energy density function ϕ :

$$U_{el} = \int_v \phi(\sigma)\, dV \qquad (4.8\text{-}15)$$

where σ = current total stress, and

$$\phi(\sigma) = \frac{[\sigma_1^2+\sigma_2^2+\sigma_3^2-2\nu(\sigma_1\sigma_2+\sigma_2\sigma_3+\sigma_3\sigma_1)]}{2E}$$

The stored strain energy freed in extracting volume V_m is U_m , and is calculated from the State I stresses in volume V_m :

$$U_m = \int_{V_m} \phi(\sigma^I)\, dV \qquad (4.8\text{-}16)$$

The total energy available to do work on the mass is derived from the host and that freed from U_m :

$$U_{source} = W_{host} + U_m \qquad (4.8\text{-}17)$$

Energy Expended

Energy is expended in several ways:

1. straining of the rock mass in the host and interior region, denoted by U_c ; and

2. loading and deforming of backfill, W_b .

Change in Stored Strain Energy - The change in strain energy stored in the interior region can be found by summing the strain energy for each volume element:

$$U_c^{I\text{-}II} = \int_v \phi(\sigma^{II})\, dV - \int_v \phi(\sigma^I)\, dV \qquad (4.8\text{-}18)$$

Work in Deforming Backfill - The work expended in deforming the backfill can be found from the tractions and deformations at the backfill-interior region interface (Fig. 4-9):

$$W_b^{I\text{-}II} = \int_{S_i} R_i^{(P)} u_i^{(1)}\, dS + \frac{1}{2}\int_{S_i} R_i^{(1)} u_i^{(1)}\, dS \qquad (4.8\text{-}19)$$

where $S^* = S_o^* + S_m^*$, S_o^* being the surface which was previously filled and S_m^* being the newly-filled surface which was loaded when V_m is mined,
R_i is the contact reaction between fill and interior, and
u_i is the contact displacement.

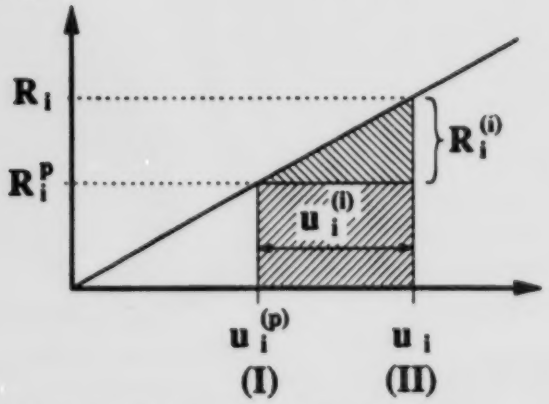

Figure 4-9 Illustration of Work Done on Compression of Backfill(W_b^{I-II} is the hatched area.)

Plastic Work Terms Due to Irreversible Strain in Interior - The plastic work is found from

$$W_{p^1} = \frac{1}{2} \int_{V_1} \Delta e_i^P \, (\sigma_i^{II} + \sigma_i^I) \, dV \qquad (4.8\text{-}20)$$

where $\Delta e_i^{(P)}$ = principal plastic stress,
σ_i = principal stress component, and
V_i = volume of yielding elements.

Total Expended Energy -

$$U_{expended} = U_c + W_b + W_{p^1} \qquad (4.8\text{-}21)$$

Energy Release --- The "released" energy term is the difference in source and expended:

$$W_r = (W + U_m) - U_{expended} \qquad (4.8\text{-}22)$$

4.8.2.2 Outline of Method Using Only Boundary Values

Implementing the first method in a three-dimensional boundary element approach is quite difficult. The elastic-plastic boundary surface changes with excavation, making the process of finding the boundary and determining its shape and its traction and deformation

conditions a rather difficult procedure. Instead, a less rigorous method (used in MINE3D) can be used to determine the gross energy change resulting from excavation.

This method uses the same calculation procedure as outlined previously in the elastic rock mass case, and assumes that the energy change can be determined from boundary deformations and tractions. In the elastic case, the tractions and displacements are determined after equilibrium for each excavation step. The assumption is made that the force displacement relation for the rock mass at the boundary in linear (i.e., the factor 1/2 in the equations for energy components $U^{(ii)}$ and U_{ij} . For a yielding material, the MINE3D program iteratively adjusts the stresses at each volume element so that they conform to the yield surface. These iterations are performed elastically, resulting in a series of elastic stress corrections for each node. A calculation of the energy components can also be made on an incremental basis and summed as the surface nodes come to equilibrium. The form of the basic integrals are the same, with the exception that they are summed over the iteration steps. For example, Eq. (4.8-6) can be expressed as:

$$U^{(ii)} = \sum_{\substack{n-1, \\ iterations}} \left[\int_{S_\sigma} T_i^{(p)} U_i^{(i)} \, dS - \int_{S_\sigma} R_i^{(p)} U_i^{(p)} \, dS \right] \qquad (4.8\text{-}23)$$

The assumption of linearity over the entire mining step is not made, and the energy calculation may follow a non-linear force-displacement characterization.

This approach assumes that: (1) strains are small since the conversion of volume to surface integrals requires a symmetric strain tensor; and (2) the body comes to equilibrium at each excavation step. It is also assumed that the stress iterations conform to the actual deformation path. It is not known how accurately this is done since the true excavation process during blasting involves dynamic processes. Only very simplistic problems (e.g. circular tunnel in yielding material) can be solved analytically, so detailed confirmation of the program results is not possible.

4.9 Verification Analyses

This section presents the results of several analyses which were conducted to verify the various components of MINE3D. Three test series were performed. The first was a model of a square-shaped tunnel, and the second a model of two rectangular drifts separated by a weak pillar. These problems are similar to those conducted with MINE2D. The third was on analysis of a destress slot in a large crown pillar. This problem approximates conditions of the crown pillar at Creighton Mine.

Verification of MINE3D is demonstrated by comparison of analysis results to analytical solutions, where appropriate, and to solutions from another numerical method - namely, the explicit finite difference method, first using the two-dimensional program FLAC (Itasca, 1990), and then the three-dimensional program 3DEC (Itasca, 1991).

4.9.1 Square-shaped Drift

A 6m x 6m square-shaped drift was modeled with MINE3D by selecting the drift length to be at least 2.5 times greater than the drift width. A calculation plane was chosen through the drift midway between the ends so that results were representative of those assuming plane strain symmetry and could be compared to FLAC.

Four model discretization conditions were evaluated. These conditions involved using progressively more elements along the boundary of the excavation, as shown by Figs. 4-10(a) through (d). The additional field-point nodes comprising the parallelepiped grid are also shown on these figures.

Both elastic and plastic analyses were performed. The material properties and field stresses used for the analyses are summarized in the table below.

Material Properties		Field Stresses	
Young's modulus	E = 1000 MPa	elastic	plastic
Poisson's Ratio	ν = 0.30	σ_1 = 5 MPa	σ_1 = 9 MPa
Cohesion	C = 5 *MPa*	σ_2 = 5 MPa	σ_2 = 9 MPa
Friction Angle	ϕ = 0	σ_3 = 5 MPa	σ_3 = 9 MPa
Dilation Angle	δ = 0		
Tensile Strength	T = 0		

Table 4-2 Properties Used in MINE3D Analysis Examples

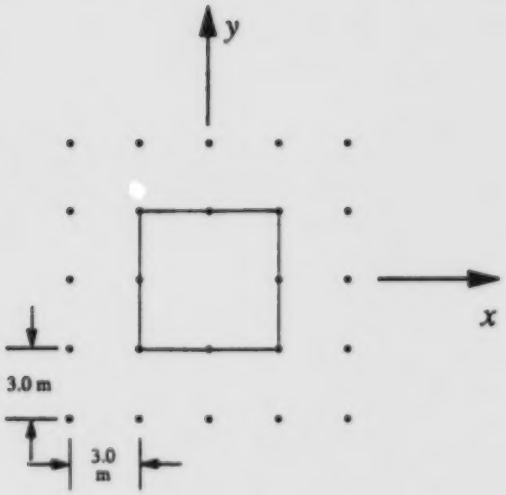

a) 2 elements on a side
(4 elements at 6m/elements
in Z-direction)

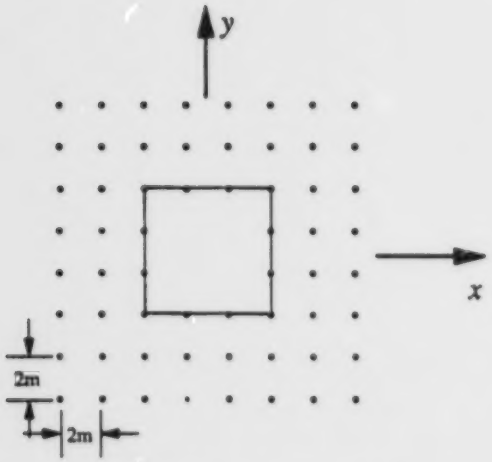

b) 3 elements on a side
(7 elements at 4m/element
in Z-direction)

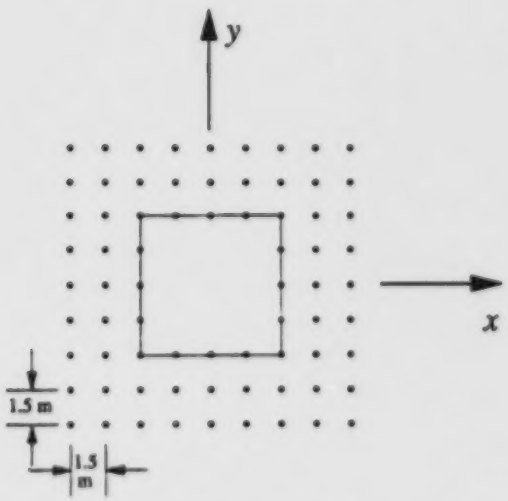

c) 4 elements on side
(8 elements at 3m/element
in Z-direction)

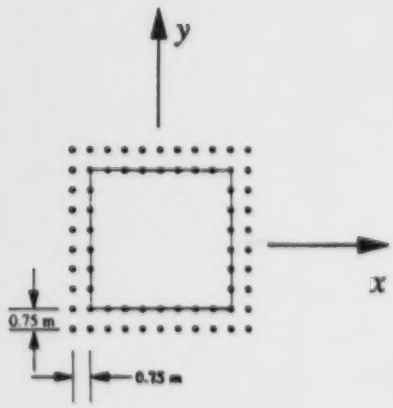

d) 8 elements on a side
(10 elements at 1.5m/element
in Z-direction)

Figure 4-10 MINE3D Models for Square-Shaped Drift

Results for the elastic analysis were first verified by comparing the calculated tangential boundary stresses around the tunnel periphery to a closed-form solution given by Greenspan (1944). This solution is for the problem of a small square-shaped ovaloid in a uniformly-loaded plate. For this solution, the corners are rounded to avoid the infinite tangential stresses at sharp corners.

Two solutions provided by Greenspan are used for the comparison. The first is for the case of an applied stress parallel to a side of the square hole. The ratio of tangential stress, σ_t, to applied stress, σ_x is given by the equation

$$\frac{\sigma_t}{\sigma_x} = \frac{0.981 - 2.967 \cos 2\beta}{1.401 + \cos 4\beta} \qquad (4.9\text{-}1)$$

where β is the angle measured from the direction of the applied stress to the point on the tunnel periphery where σ_t is calculated.

The second solution is for the case in which the applied stress is parallel to the diagonal of the square hole. In this case, the ratio σ_t/σ_x is given by

$$\frac{\sigma_t}{\sigma_x} = \frac{0.981 - 1.606 \cos 2\beta}{1.401 - \cos 4\beta} \qquad (4.9\text{-}2)$$

The comparison between MINE3D results and the analytical solutions is shown in Fig. 4-11. For the first case, models with 4 elements on a site and 8 elements on a side are tested. As Fig. 4-11(a) shows, the agreement between results improve as the number of elements is increased. The discrepancy between results is greatest at the corners, as shown in both Figs. 11(a) and (b). This is attributed to the corner offset logic used in MINE3D. The results suggest that more than 8 elements along a side are required to calculate stresses at the corners with good accuracy.

The difficulty with the analysis at corners is common for numerical calculations and most techniques perform the stress calculation at some interior point which is offset from the corner. In the explicit finite difference method, for example, the stress calculation is located at an element centroid and not at an exterior gridpoint.

For this problem, plasticity will initiate at the corners because this is where the deviatoric stresses are greatest. Since it is not possible to check the stress calculation directly on the corner, in order to verify the plasticity calculation in MINE3D, it is first necessary to demonstrate that the corner stress calculation matches that produced by another numerical technique which uses a corner offset calculation, such as the explicit finite difference technique. This is shown by comparison of the MINE3D

elastic analysis to that made with FLAC.

In FLAC, constant strain elements are used with strain calculations based upon incremental displacement gradients calculated at gridpoints (i.e., element nodes). This scheme differs from the linear strength elements used in MINE3D. The FLAC model is shown in Figure 4-12. This simulation utilizes two lines of symmetry so that only one-quarter of the square-shaped drift is modeled. The FLAC elements are square, with a side dimension of 0.75 m. The exterior boundaries of the FLAC model are located at a distance from the opening of ten times the size of the drift. This is sufficient to minimize the influence of the boundary conditions on the calculated displacements and stresses around the drift.

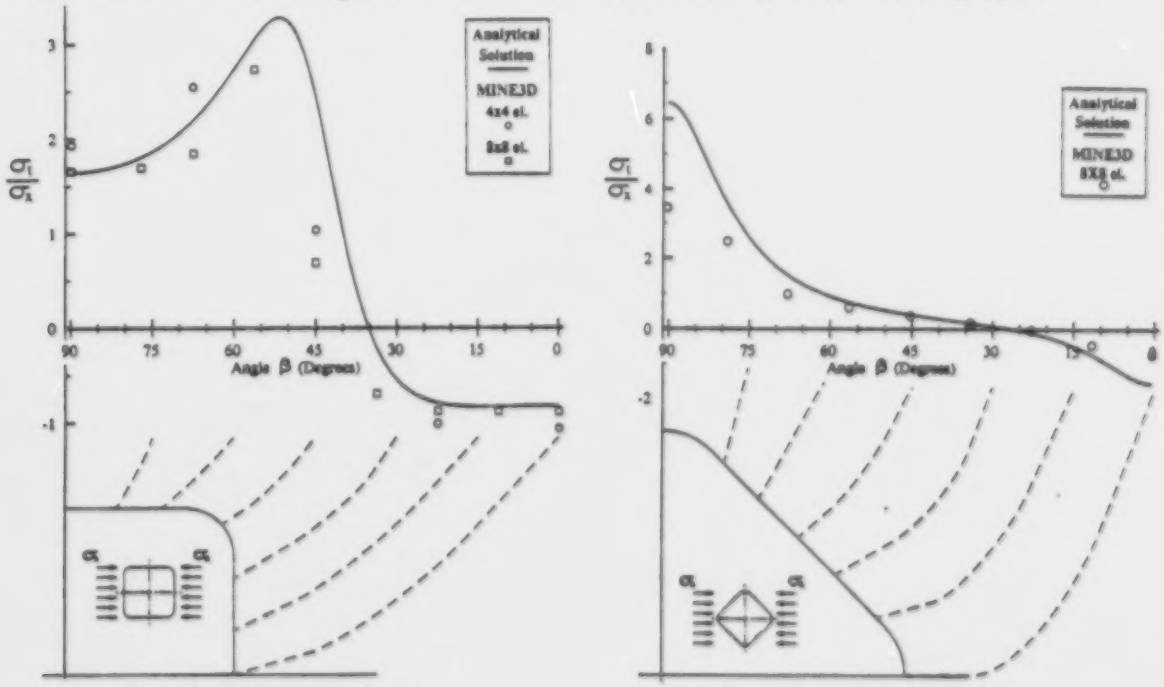

(a) Applied Stress Parallel to Side

(b) Applied Stress Parallel to Diagonal

Figure 4-11 Tangential Boundary Stress Around Tunnel Periphery

Figures 4-13 through -17 compare the calculated stresses and displacement form MINE3D and FLAC. As these figures show, the comparison between MINE3D and FLAC improves as the number of elements along a side is increased in the MINE3D model. The analyses indicate that at least four elements on a side are required to achieve a reasonable agreement between the two models.

For the plastic analysis, the MINE3D model shown in Fig. 4-10(c) was used with plastic volume elements created within the two rows of nodes surrounding the surface nodes of the 4x4 element drift.

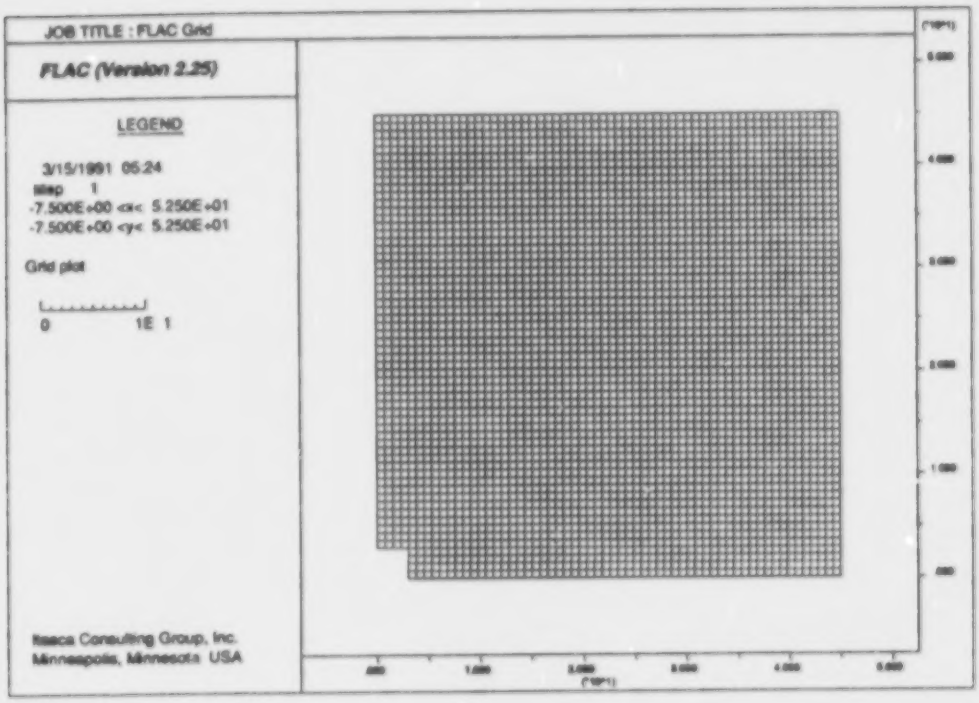

(a) FLAC Grid

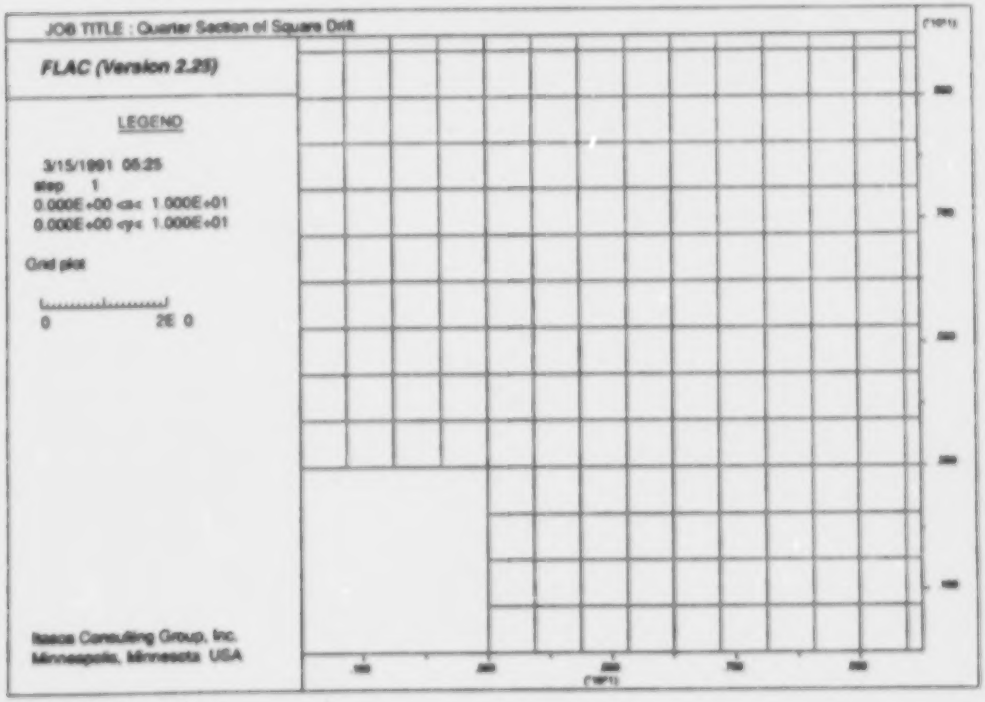

(b) Close-Up View

Figure 4-12 FLAC Model of Square Drift

A frictionless material behavior with a cohesion of 5 MPa wasassigned to the volume elements. The in-situ stress level was set to 9 MPa, isotropic and in compression. This was sufficient to develop a plastic region which surrounded the drift.

Figures 4-18 through 4-22 present the results of this analysis. Stresses and displacements from both elastic and plastic simulations at the selected stress level are shown. The agreement between MINE3D and FLAC is reasonable for the plastic analysis, although not as good as that for the elastic case. The disparity in results primarily reflects the differences between locations for stress calculations in the two codes. For example, in Figs. 4-18 and 4-19 the stresses calculated on the drift surface are exact in MINE3D for the given boundary conditions and plastic failure rule -- σ_1 =0 and σ_3 = -10 Mpa. The FLAC stresses are calculated at the centroid of the element adjacent to the opening and average the effect of the stress gradient around the opening. A finer FLAC mesh would be required to approach the MINE3D results.

The displacement calculations, as shown in Figs. 4-20 through -22, indicate that a somewhat greater plastic displacement occurs in the FLAC model than in the MINE3D model. In the FLAC model, however, plasticity only occurs in the zones adjacent to the corners and does not completely encompass the opening. A better comparison of the effect of plasticity is made in the second test series.

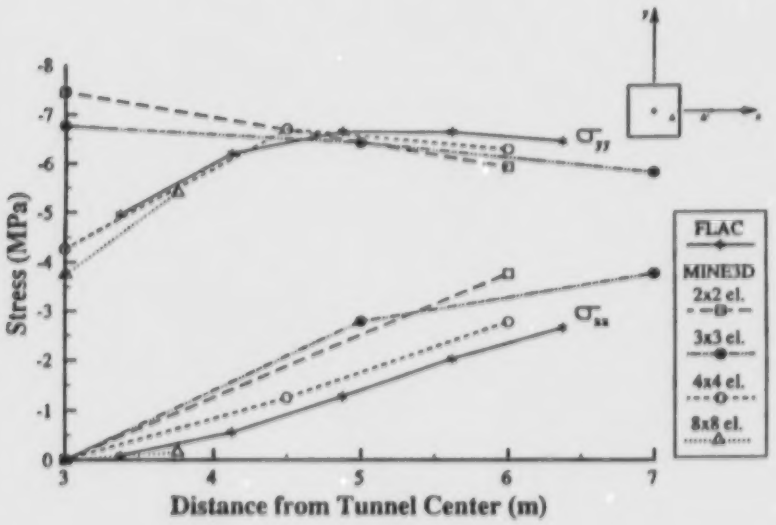

Figure 4-13 Stresses Along A - A'

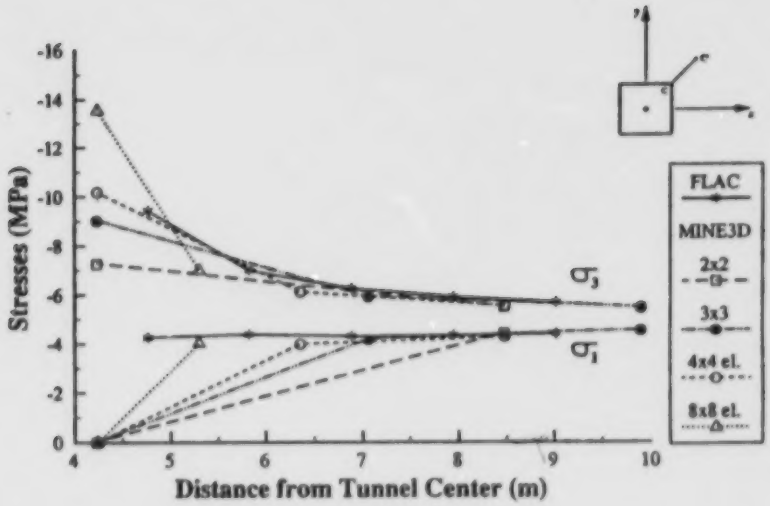

Figure 4-14 Stresses Along C-C'

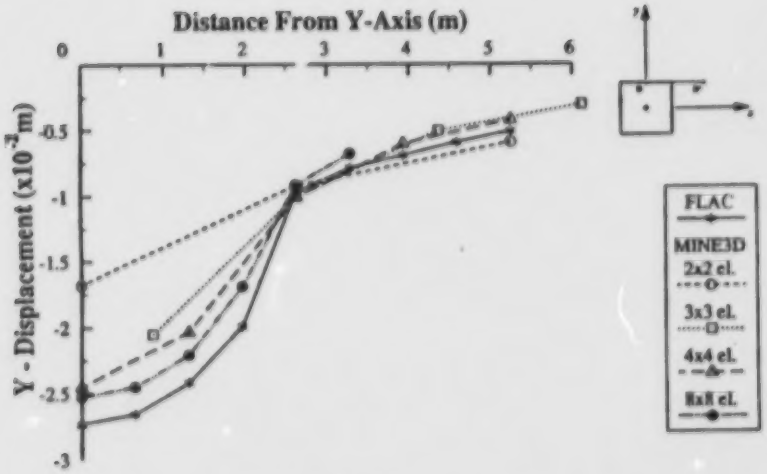

Figure 4-15 Y-Displacements Along B - B'

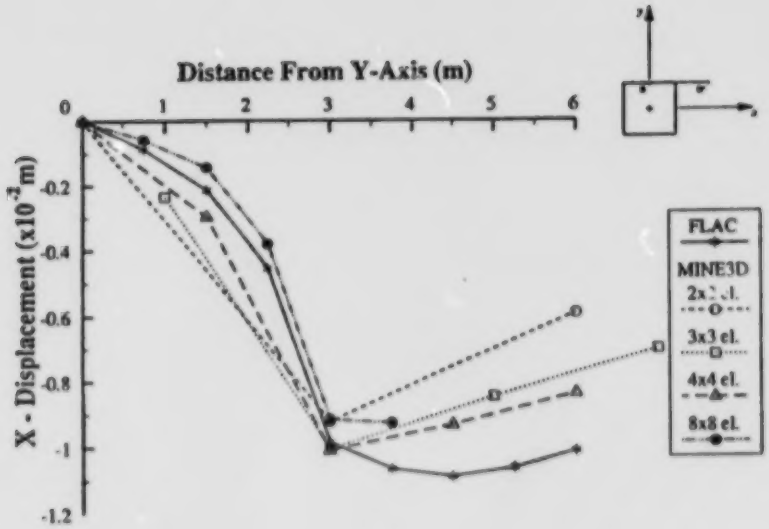

Figure 4-16 X-Displacements Along B - B'

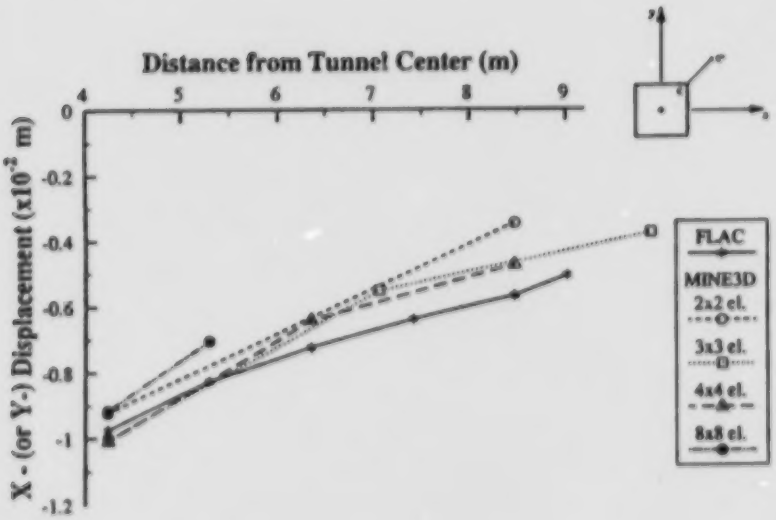

Figure 4-17 Displacements Along C - C'

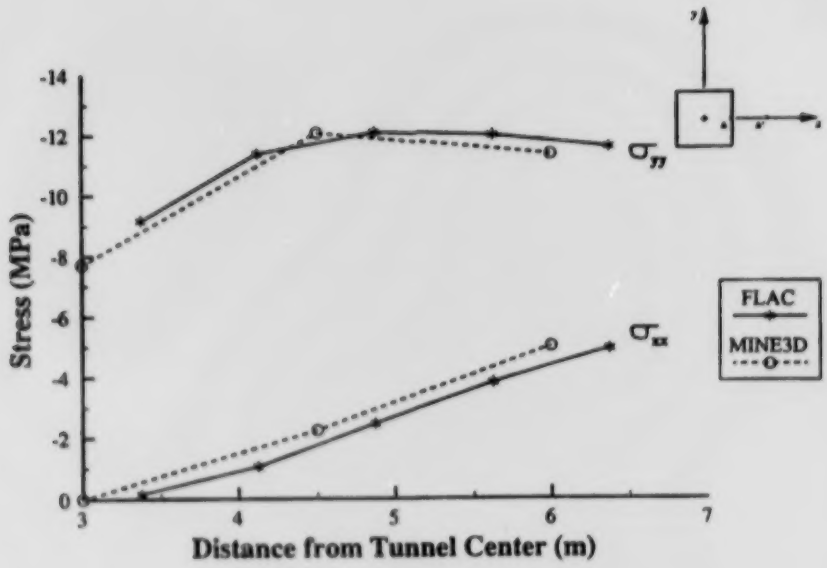

(a) Elastic Analysis

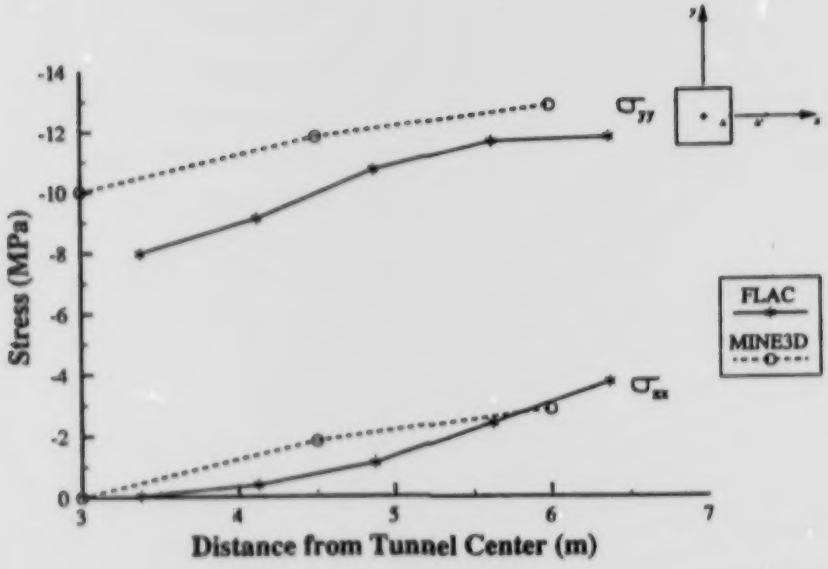

(b) Plastic Analysis

Figure 4-18 Stresses Along A - A'

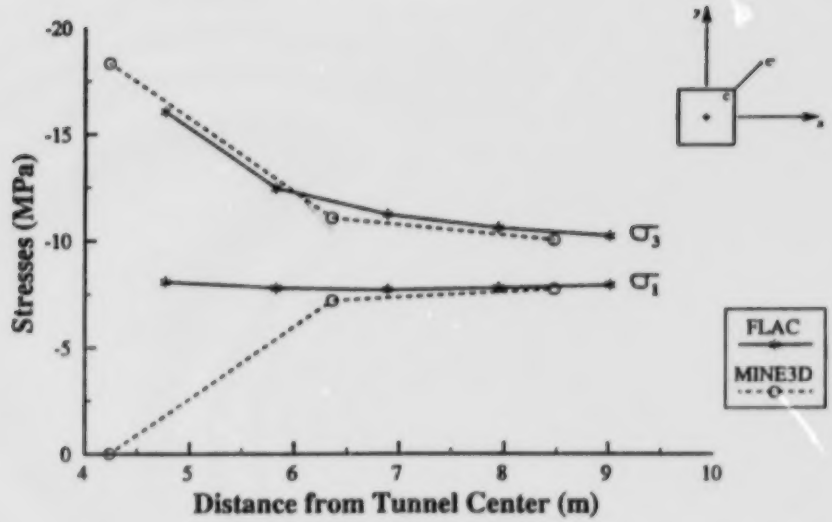

(a) Elastic Analysis

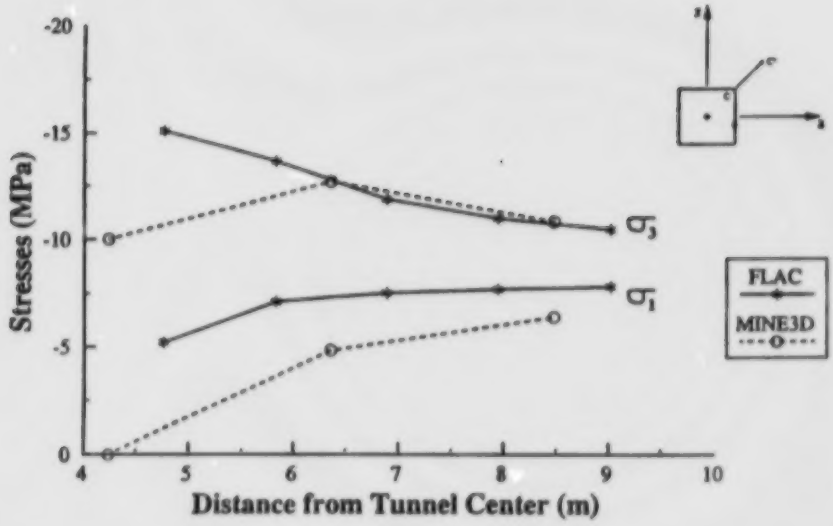

(b) Plastic Analysis

Figure 4-19 Stresses Along C - C′

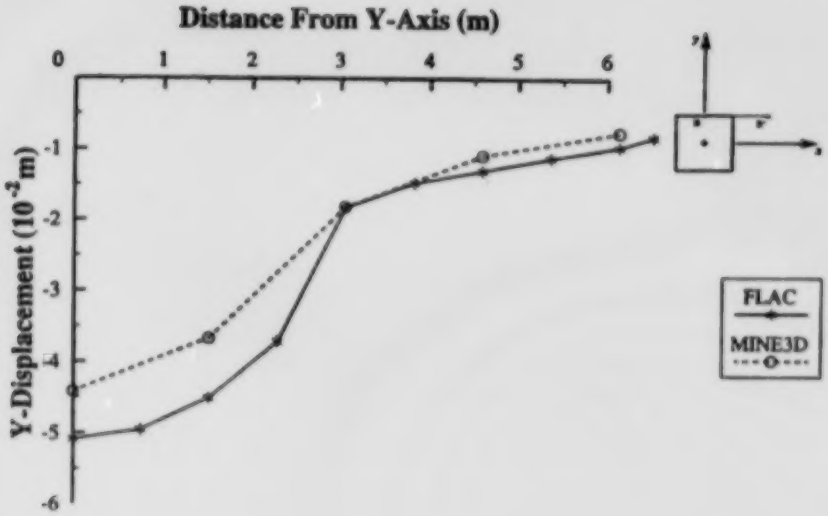

(a) Elastic Analysis

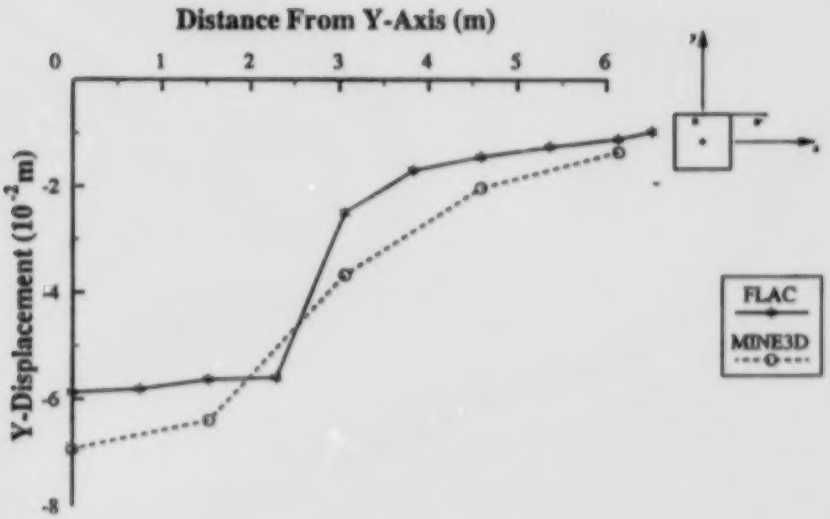

(b) Plastic Analysis

Figure 4-20 Y-Displacements Along B - B'

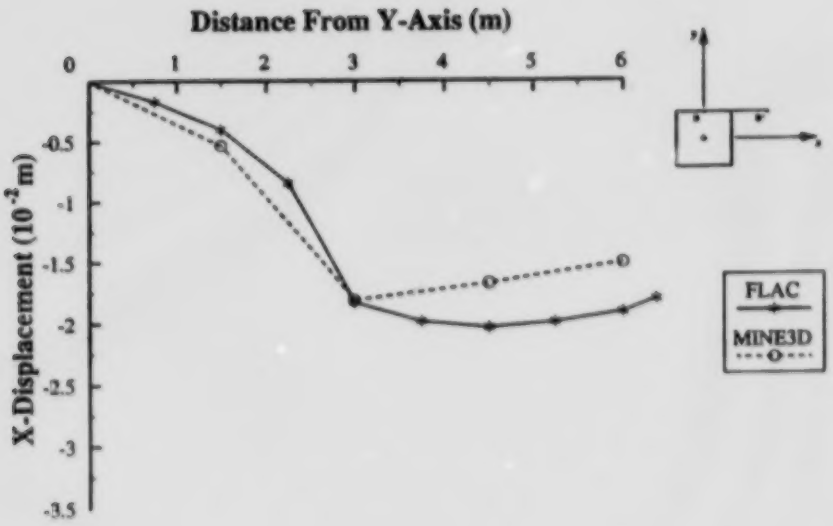

(a) Elastic Analysis

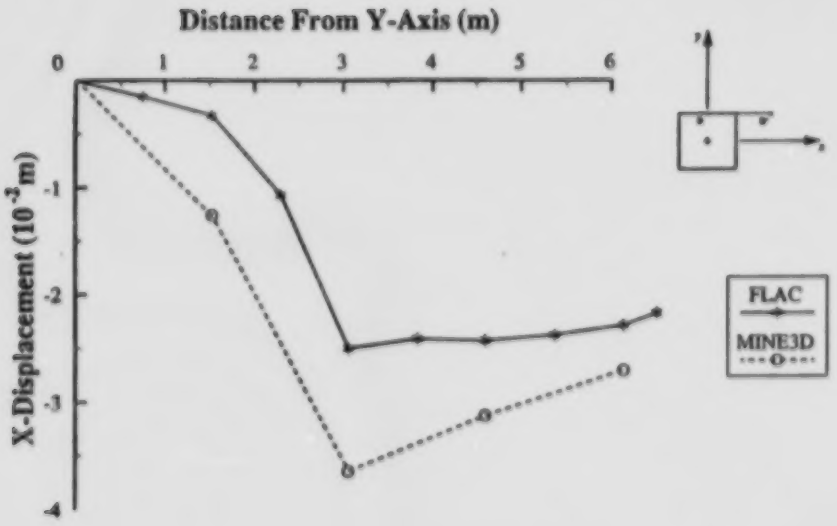

(b) Plastic Analysis

Figure 4-21 X-Displacements Along B - B′

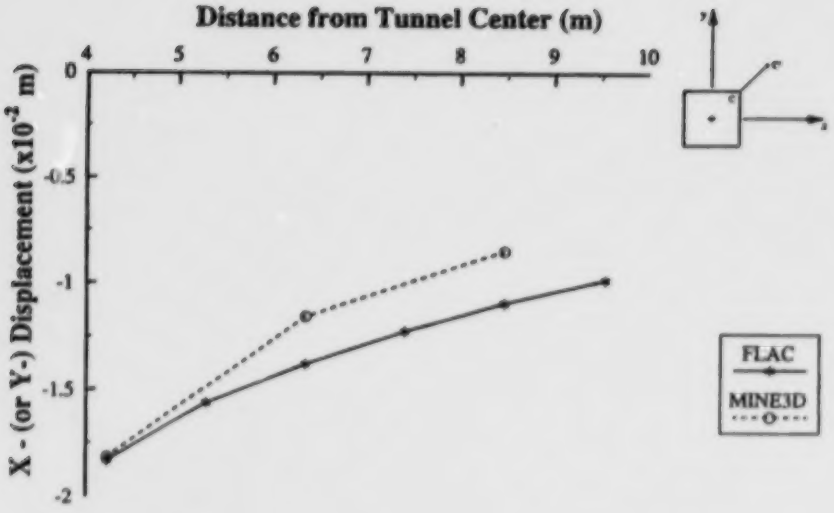

(a) Elastic Analysis

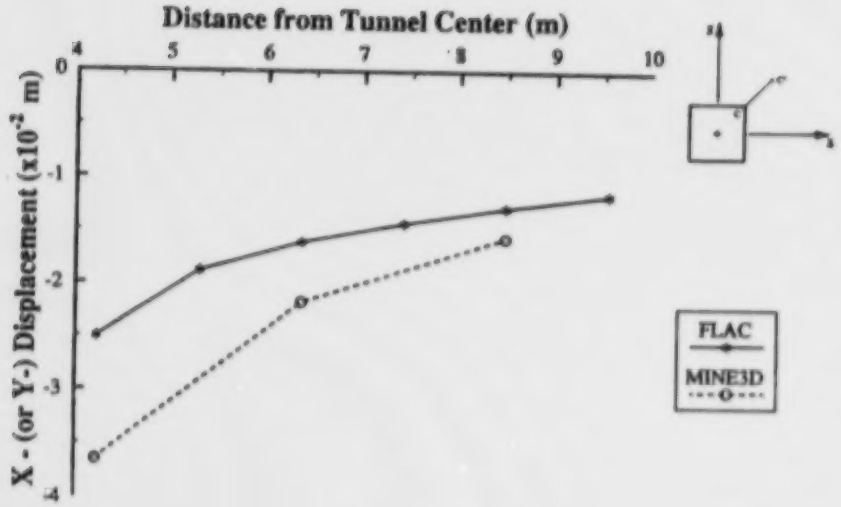

(b) Plastic Analysis

Figure 4-22 Displacements Along C - C'

4.9.2 Rectangular Drifts Separated By a Weak Pillar

Two rectangular drifts separated by a weak pillar are analyzed for the second verification test. The drifts are 6 m wide, 9 m high, and 24 m in length. The pillar is 6 m wide (see Fig. 4-23). The MINE3D model consists of a grid of 13x9x9 nodes. The node spacing is 1.5 m in the i- and j- directions and 3 m in the k-direction.

A series of three tests were performed to evaluate the plasticity and multiple region logic. These tests are described as follows.

A. Both stopes are "mined" simultaneously with the pillar region and allowed to fail. (Plastic volume elements are defined in the pillar region only.)

B. Mining is performed in two steps. Stope 1 is mined first, and Stope 2 second. The pillar region is allowed to fail.

C. Mining is performed in three steps: (1) Stope 1 is mined in Step 1; (2) Stope 2 is mined and Stope 1 is filled in Step 2; and (3) Stope 2 is filled and the pillar is mined in Step 3. The pillar region is allowed to fail.

The material properties listed in Table 4-2 are used for the virgin rock. The fill material is assumed to be elastic, with a Young's modulus of 100 MPa and Poisson's ratio of 0.3. The field stresses are isotropic, with a magnitude of 9 MPa.

The FLAC model for this test is illustrated in Fig. 4-24. A horizontal line of symmetry is taken through the center of the two drifts, and only the upper half of the drifts/pillar problem is modelled. Three regions are defined in the model corresponding to the two stopes and the pillar. These regions are alternately changed to null regions to represent excavation, or changed to a material with plastic behavior corresponding to the weak pillar or elastic behavior corresponding to the fill. These regions are shown in Fig. 4-24(b) through (d).

The comparison between MINE3D and FLAC results are given in Figs. 4-25 through 4-27 for the first test series. Both elastic and plastic analyses are compared for the two codes. Figure 4-25 shows a comparison on maximum principal stress in the pillar as a result of removing both stopes simultaneously. Figures 4-26 and -27 display the displacements induced by the excavation. The stress comparison is quite good for this test. The displacements, particularly at the nodes along the pillar region, do not compare as well.

The softer response in Flac is considered to be related to the difference in the condition of the elements used to calculate the incremental displacement fields. FLAC utilizes an approach known

as mixed-discretization (Marti and Cundall, 1982), which has been shown to provide an accurate calculation for displacement fields as plastic collapse is approached. The eight-noded volume elements used in MINE3D may provide an excessive number of kinematic constraints on the stress field (e.g. Sloan and Randolph, 1982). This may be improved by use of higher-order elements; however, the use of such elements was not feasible within present computer memory constraints (see discussion in Section 4.10). If the application of MINE3D is for problems with only localized regions of plastic yield, the restriction on the displacement field is not considered unreasonable.

The results for the second test series are given in Figs. 4-28 through 4-30. The comparison is similar in agreement to that seen from the first series. This test shows the influence on the stress state in the pillar and displacements of the stopes due to the sequential excavation.

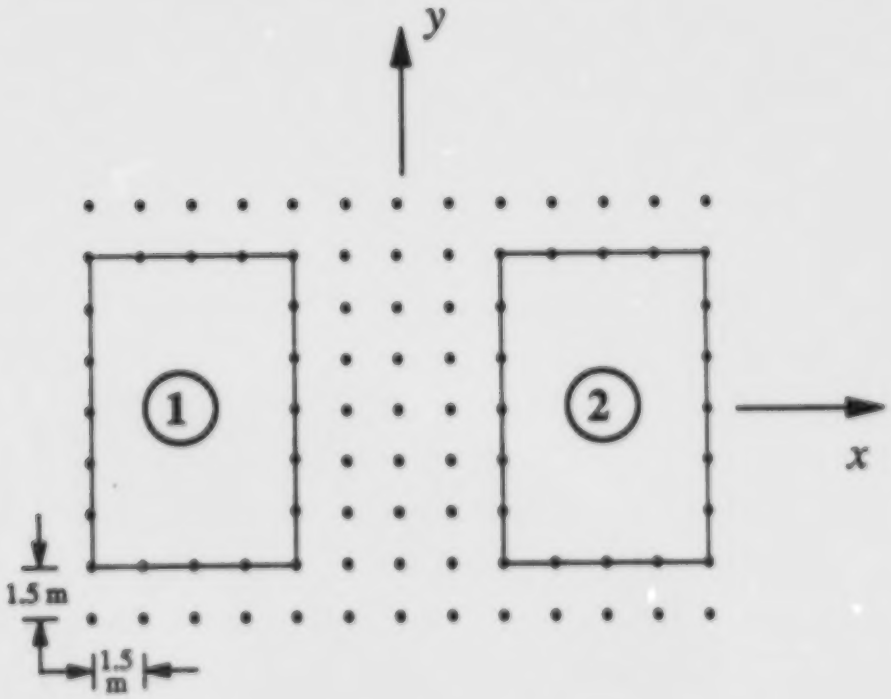

Figure 4-23 Pillar Between Two Stopes (pillar height 9m, width 6m, length 24m)

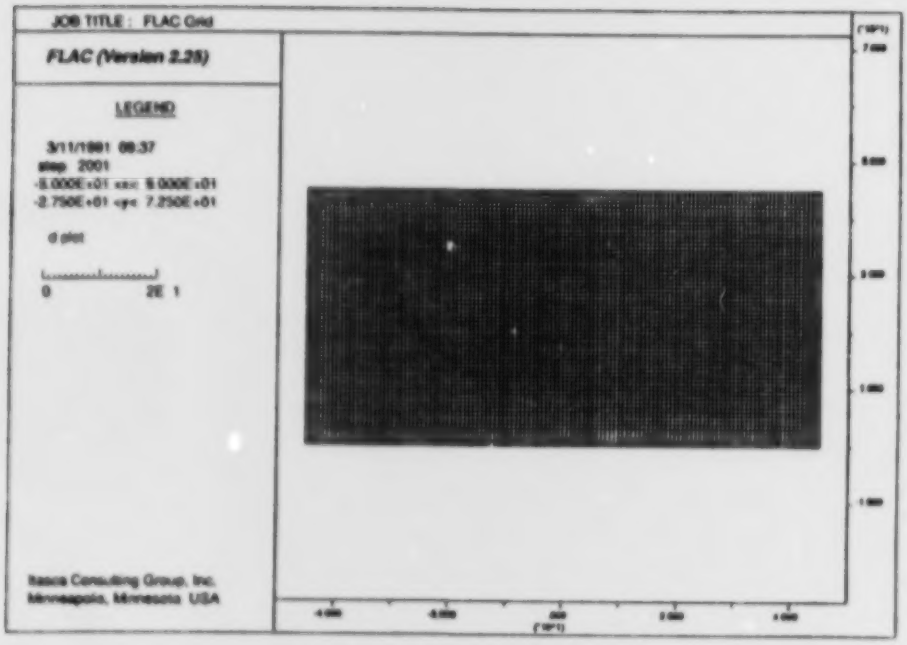

(a) FLAC Grid

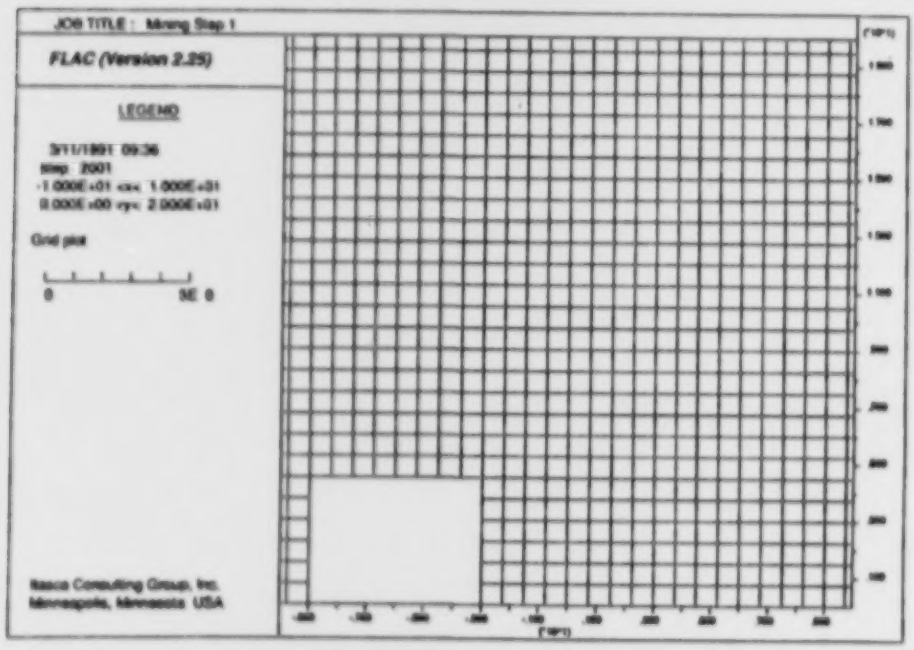

(b) Mining Step 1

Figure 4-24 FLAC Model of Rectangular Drifts Separated by a Weak Pillar

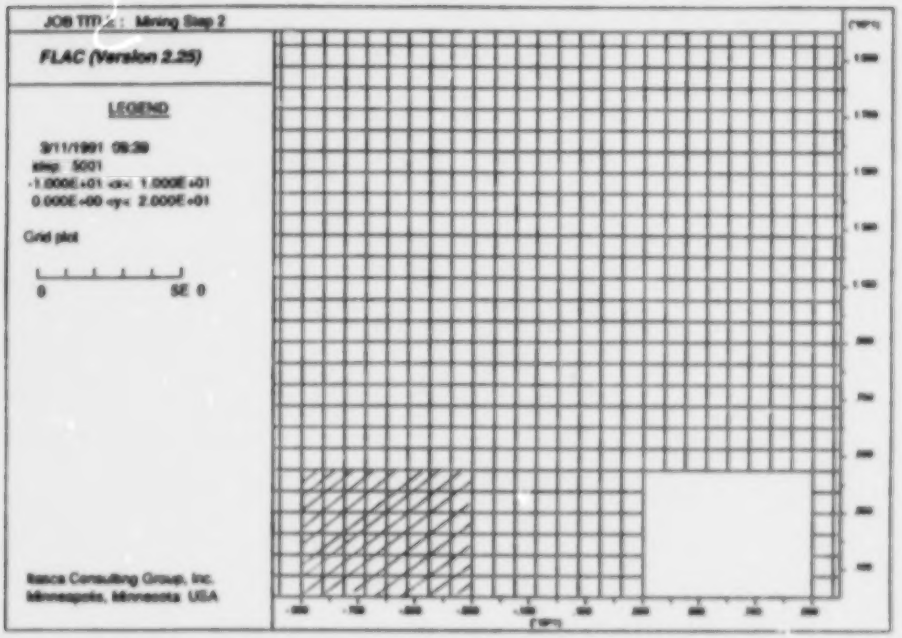

(c) Mining Step 2 (hatched area is filled region)

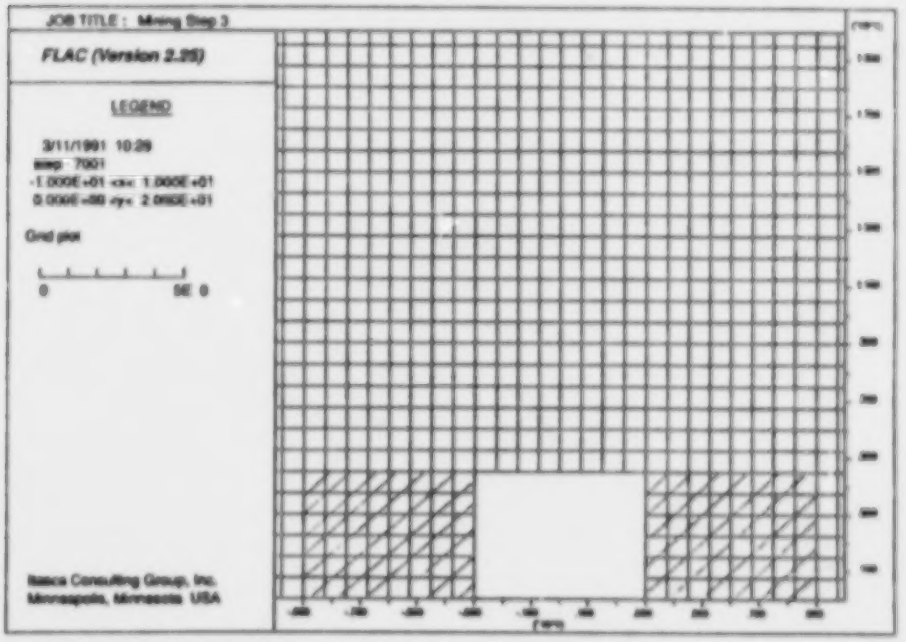

(d) Mining Step 3 (hatched area is filled region)

Figure 4-24 FLAC Model of Rectangular Drifts Separated by a Weak Pillar (continued)

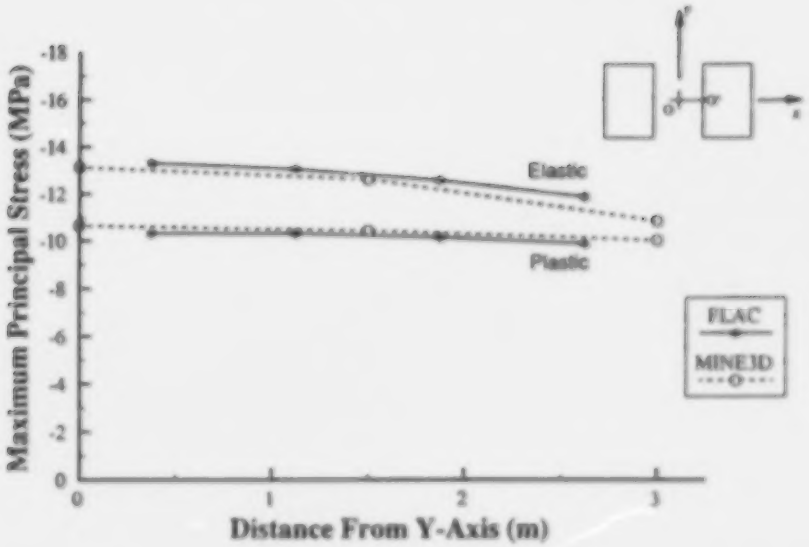

Figure 4-25 Stresses Along O - O'

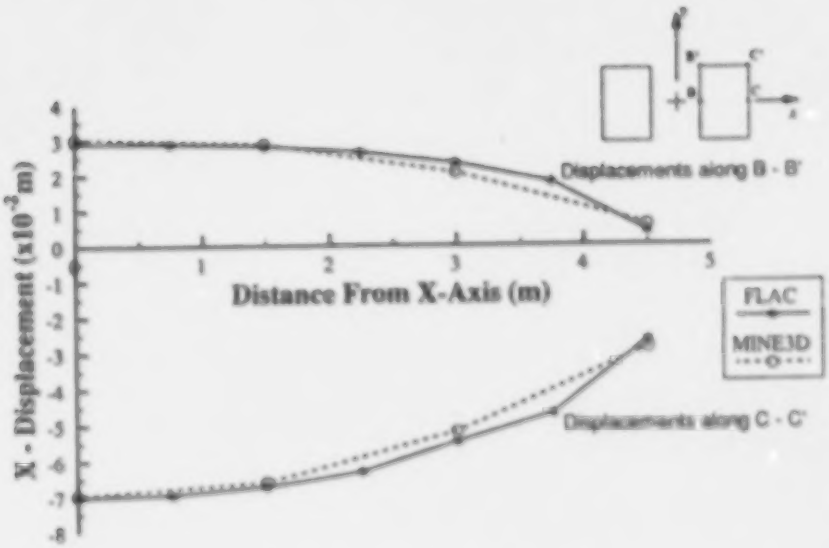

(a) Elastic Analysis

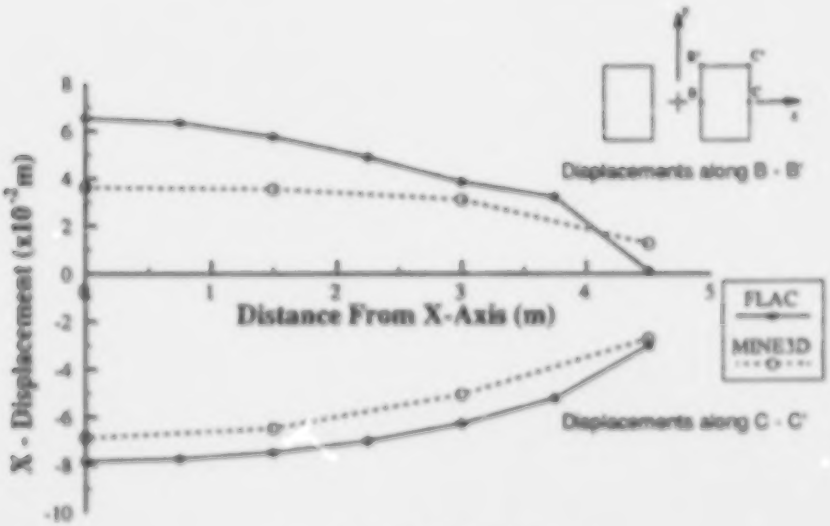

(b) Plastic Analysis

Figure 4-26 Displacements Along B - B' and C - C'

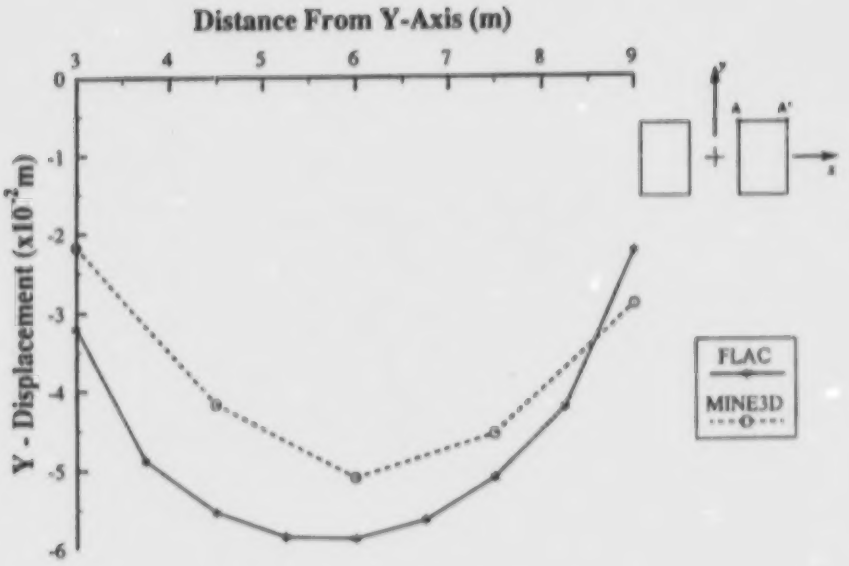

(a) Elastic Analysis

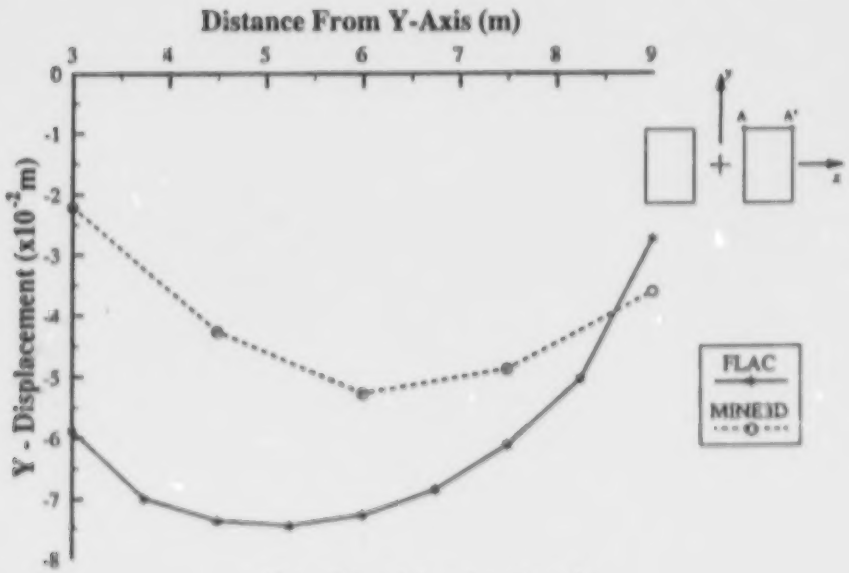

(b) Plastic Analysis

Figure 4-27 Displacements Along A - A'

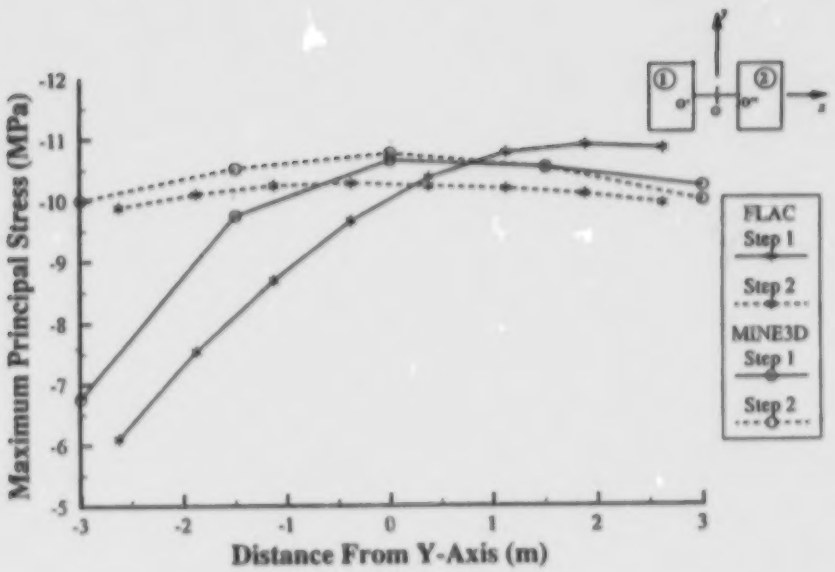

Figure 4-28 Stresses Along O′- O" for Two Mining Steps

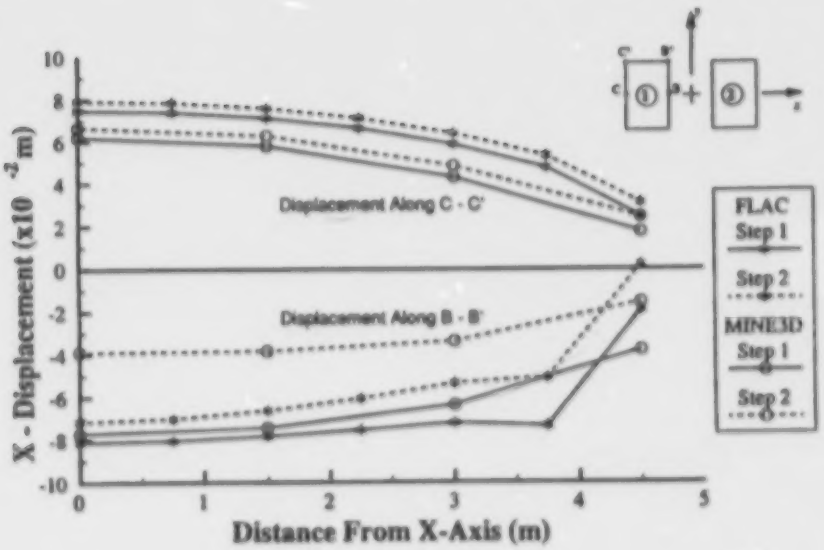

Figure 4-29 Displacements Along B - B′ and C - C′ for Two Mining Steps

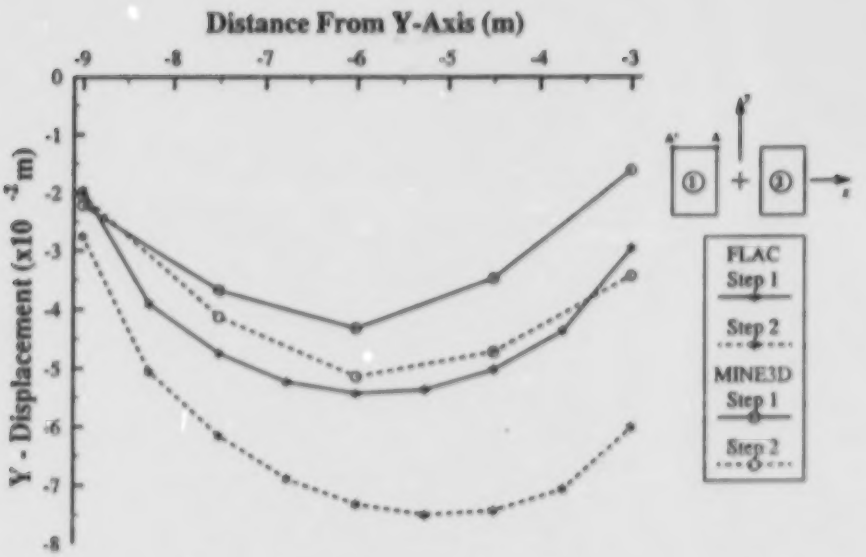

Figure 4-30 Displacements Along A - A' for Two Mining Steps

In the third test series, the ability of MINE3D to simulate both local plastic failure and stress build-up in fill material are verified. For this test, the effect of pillar failure on stress change in the fill material is a path-dependent process. Stresses in the two stopes evolve differently due to the change in displacement that occurs in each stope for each mining step.

MINE3D solves the global problem at each step for total displacements and stresses. In order to simulate stress build-up correctly, the displacement increment following fill emplacement must be calculated to provide the displacement boundary condition at the fill/rock interface. The incremental displacement calculation is verified with this test.

Figures 4-31 and 4-32 present plots of stress change and displacement in the stopes for the different mining steps. The stress plots in Fig. 4-31 show the different stress build-up in the two stopes assuming either elastic or plastic pillar response. In general, the stresses in the MINE3D analysis indicate a similar path-dependent response as do those in the FLAC analysis. The difference in stress magnitudes are primarily due to the smaller stope displacements resulting in the MINE3D run than in the FLAC run when the pillar fails.

The failure in the pillar is indicated by the plastic node plots in Fig. 4-33. These results coincide with those produced by the FLAC analysis.

The displacement in the rock at each step is illustrated in Fig. 4-34. Total displacements are shown on these plots. The incremental displacement starting at the end of step 1 provides the displacement boundary conditions for stope 1, and that starting at the end of step 2 provides the boundary condition for stope 2.

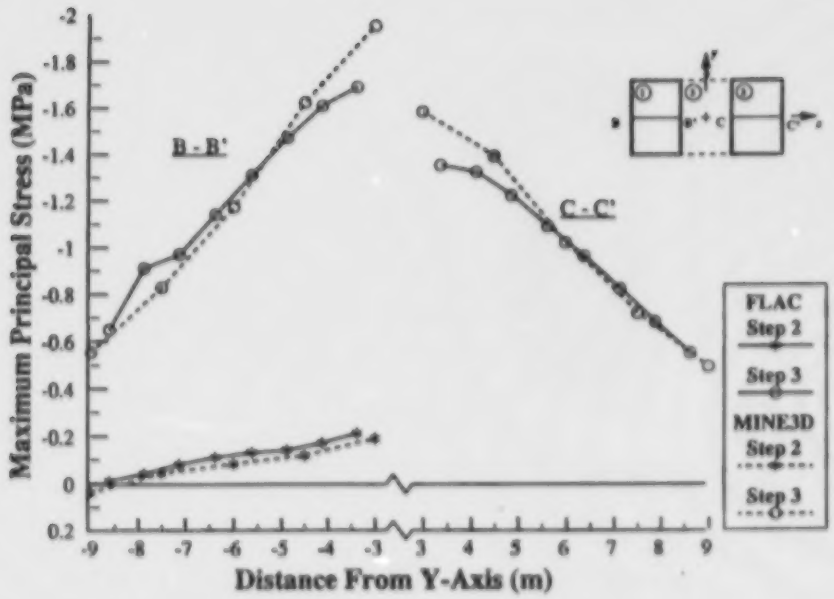

(a) elastic analysis

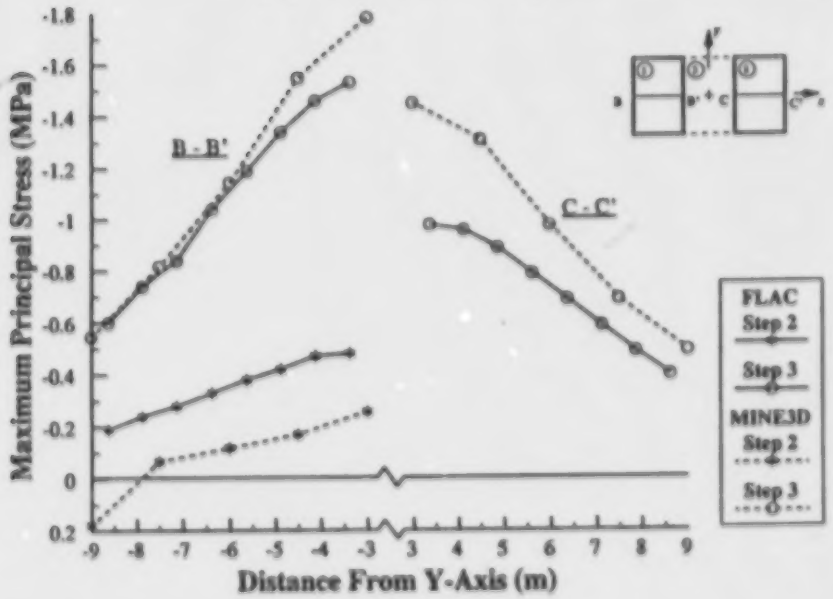

(b) plastic analysis

Figure 4-31 Stresses Along B - B′ and C - C′ in Stopes 1 and 2

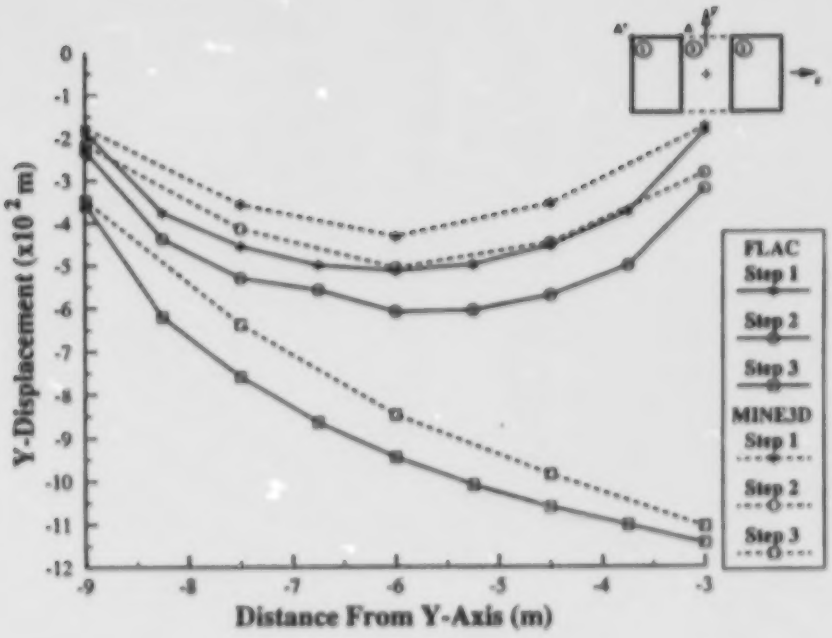

(a) elastic analysis

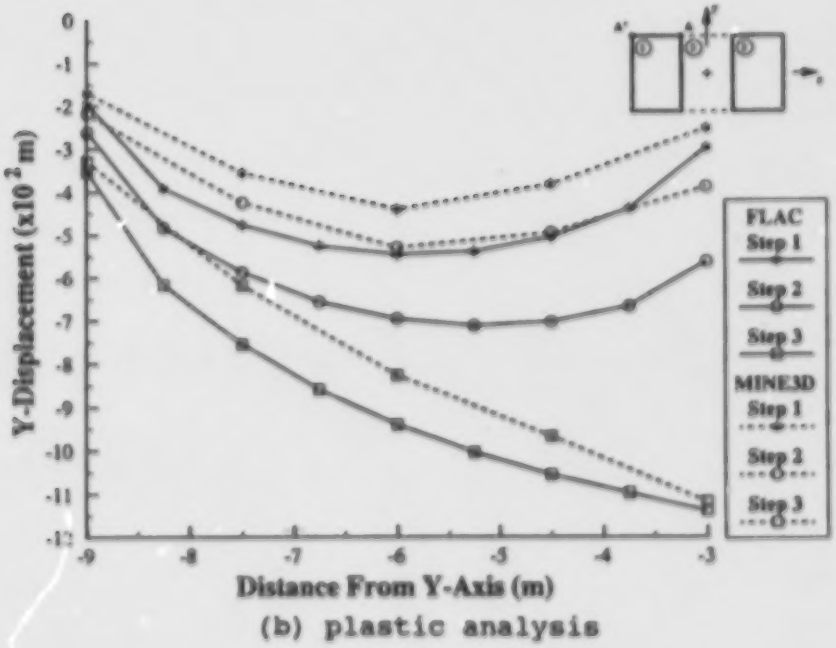

(b) plastic analysis

Figure 4-32 Displacements Along A - A′ in Stope 1

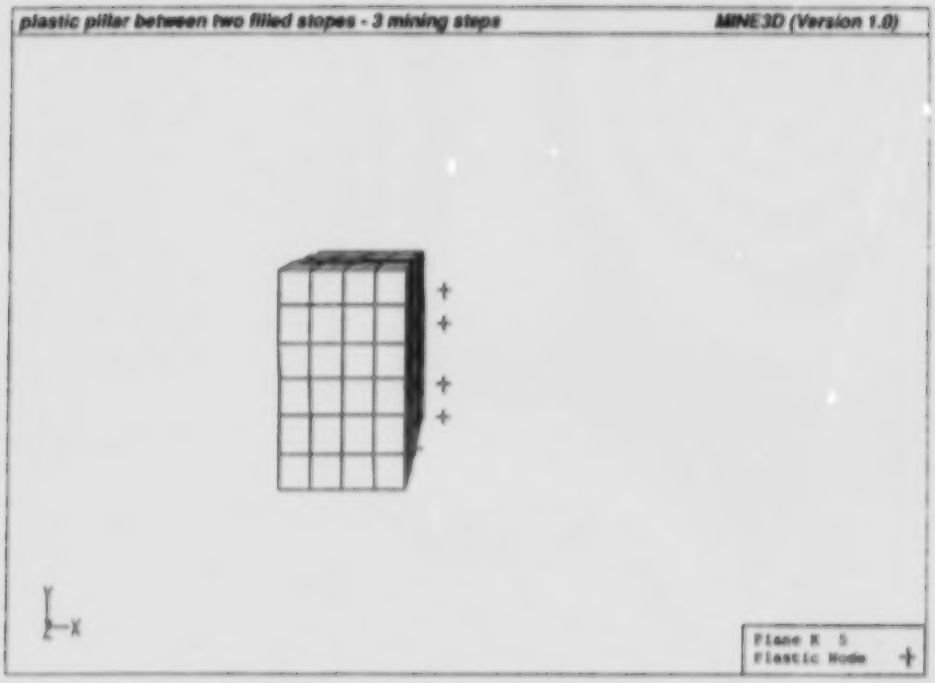

(a) Mining Step 1

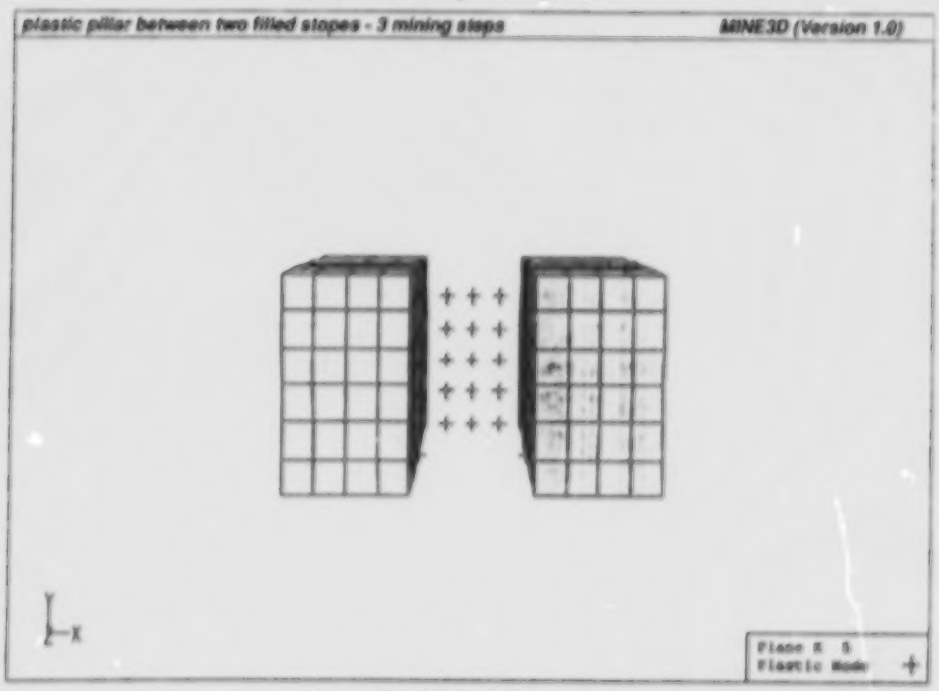

(b) Mining Step 2

Figure 4-33 Volume Nodes where Failure Limit has been Reached

(a) Mining Step 1

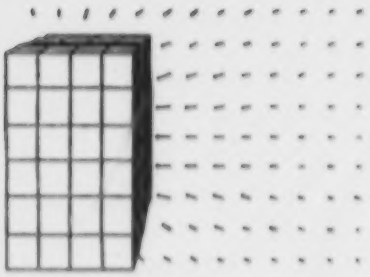

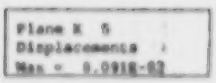

(b) Mining Step 2

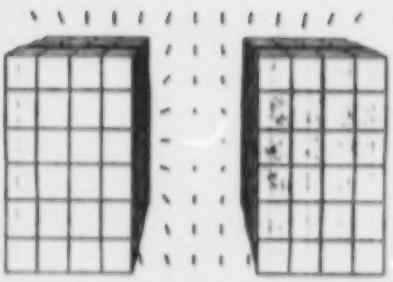

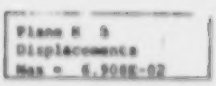

(c) Mining Step 3

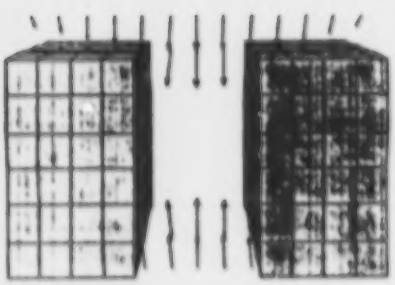

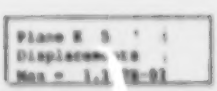

Figure 4-34 Total Displacement Vectors at End of Each Mining Step

4.9.3 Destress Slot in Large Crown Pillar

The third test problem is an idealized model of a destress slot in a large crown pillar. The analysis involves the calculation of stresses and displacements induced by the excavation of the slot and the previously mined ore blocks above and below the crown pillar.

Because of computer run time constraints, as discussed below, only an elastic analysis was performed for this test. The following elastic properties were used:

Young's modulus	68 GPa (9.86×10^6 psi)
Poisson's ratio	0.25

The far-field stress state was:

σ_{11} = 93.5 MPa (13,545 psi) (horizontal, normal to slot)
σ_{22} = 93.5 MPa (13,545 psi) (horizontal, parallel to slot)
σ_{33} = 60.0 MPa (8,670 psi) (vertical)

The MINE3D model dimensions approximated the conditions at the 6600-6700 level ore block at Creighton Mine. The slot width in the model is 6.1m (20 ft), the length is 73.2m (240 ft), and the height is 42.7m (140 ft). The mined ore blocks above and below the crown pillar are modeled as two rectangular polyhedra with dimensions 182.9m (600 ft) by 73.2m (240 ft) by 30.5m (100 ft). Figure 4-35 presents the MINE3D model. The model is defined within a parallelepiped grid consisting of 31x13x18 nodes. The node spacing is 6.1 m (20 ft) in the i-, j- and k- directions. This model contains 2,434 surface elements and 2,440 surface nodes. The size of the parallelepiped grid was the minimum size sufficient to encompass the mining region. This model requires approximately 75 Mbytes for storage of the nodal coefficients. Unfortunately, the solution time for this model was over seven days on the SUN SPARCStation 2 computer. The run time is primarily influenced by the time required for access of virtual memory to store and retrieve the coefficients. (This problem is discussed further in Section 4.10.)

As indicated in Fig. 4-35, the slot does not extend completely from the lower mining block to the upper block. A continuous slot would require the use of re-entrant corner nodes in the model. Re-entrant corners pose a particular problem in boundary elements because the fictitious point force solution is infinite at such corners. Corner offsets, as discussed in Section 4.3.3, can be used to move the corner calculation so that this effect is minimized. The optimum corner offset for reentrant corners has not been studied at present. For this calculation, because of the excessive solution time required, reentrant corners were eliminated from the model, to avoid the problem completely, by leaving a 6 m space between the slot and the upper and lower blocks.

The 3DEC model used for this comparison is shown in Fig. 4-36. Figure 4-36(a) shows the outer boundary of the model which has dimensions of 600m by 600m by 600m. The model is subdivided into 15 joined blocks (i.e., blocks are "glued" together). The inner three blocks represent the mined region, as shown in Fig. 4-36(b). Compare this figure to Fig. 4-35. The blocks in the 3DEC model are subdivided into 24,000 finite difference tetrahedral zones. Figure 4-36(c) shows a close-up view of the zoning in the crown pillar region (surrounding blocks are hidden for better viewing). The solution time for this 3DEC model was approximately eight hours on an 80386 microcomputer with Weitek coprocessor.

The results from the two models are compared in Figs. 4-37 through 4-40. Displacement vectors along a horizontal plane and a vertical plane are compared in Figs. 4-37 and 4-38. Both directions and magnitudes of displacements compare quite well.

Maximum principal stress contours from MINE3D are compared to principal stress vector plots from 3DEC in Figs. 4-39 and 4-40. Although the plots are of different type, they both show the same form of stress redistribution around the slot and also calculate similar areas of stress concentrations. The values of peak stress do not compare closely, but this is more a function of the difference in stress calculation locations in the two models.

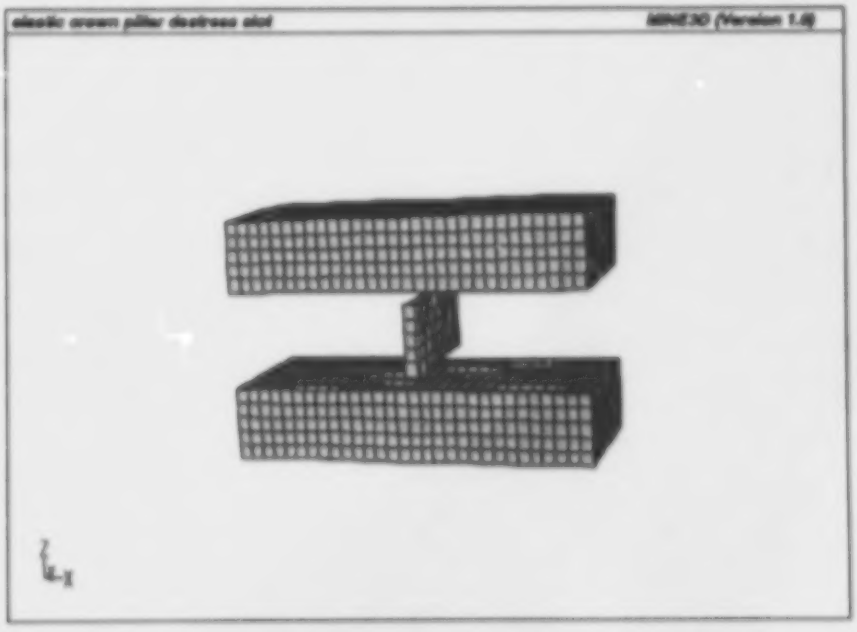

Figure 4-35 MINE3D Model of Destress Slot in Large Crown Pillar
NOTE: The non-uniformity in the element plotting is due to integer truncation in the graphical output routine.

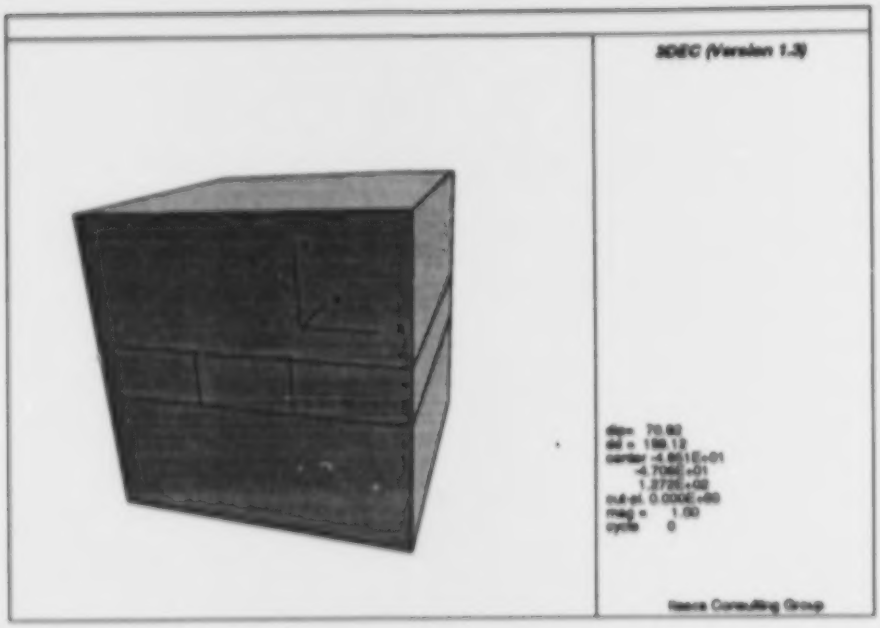

(a) Model Boundary

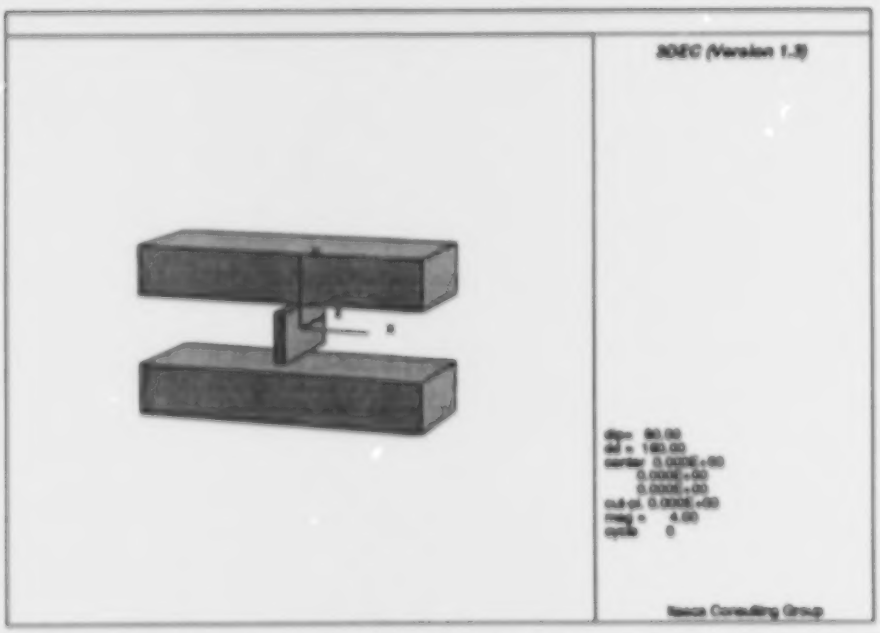

(b) Destress Slot and Upper and Lower Mining Blocks
(Surrounding blocks are hidden from view.)

Figure 4-36 3DEC Model of Destress Slot in Large Crown Pillar

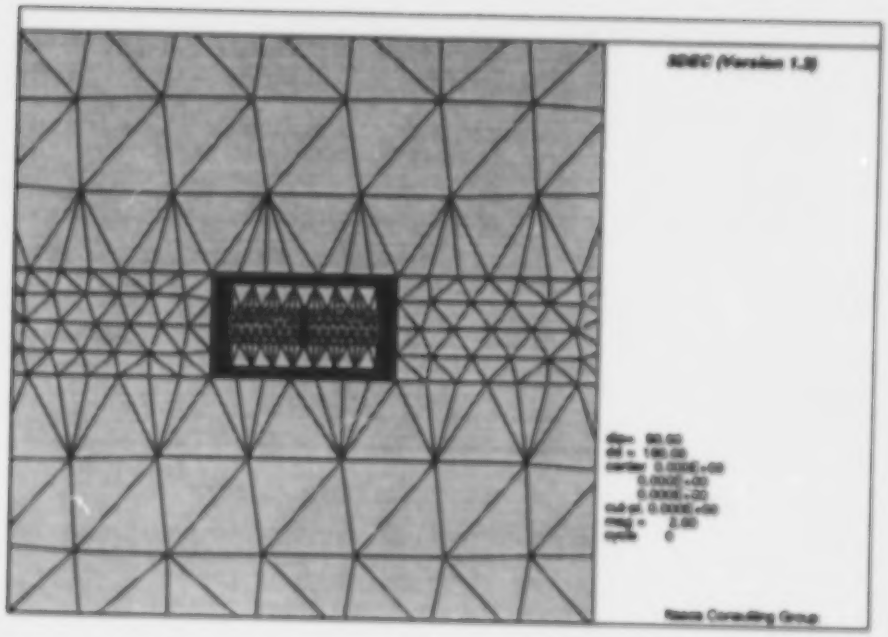

(c) Close-Up of Crown Pillar Region Showing Model Zoning

Figure 4-36 3DEC Model of Destress Slot in Large Crown Pillar (continued)

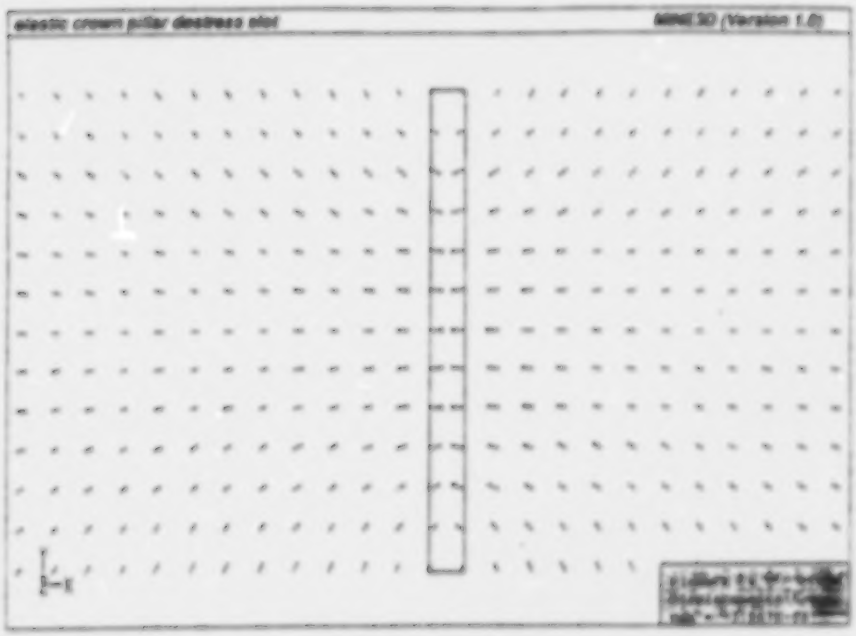

(a) MINE3D Model

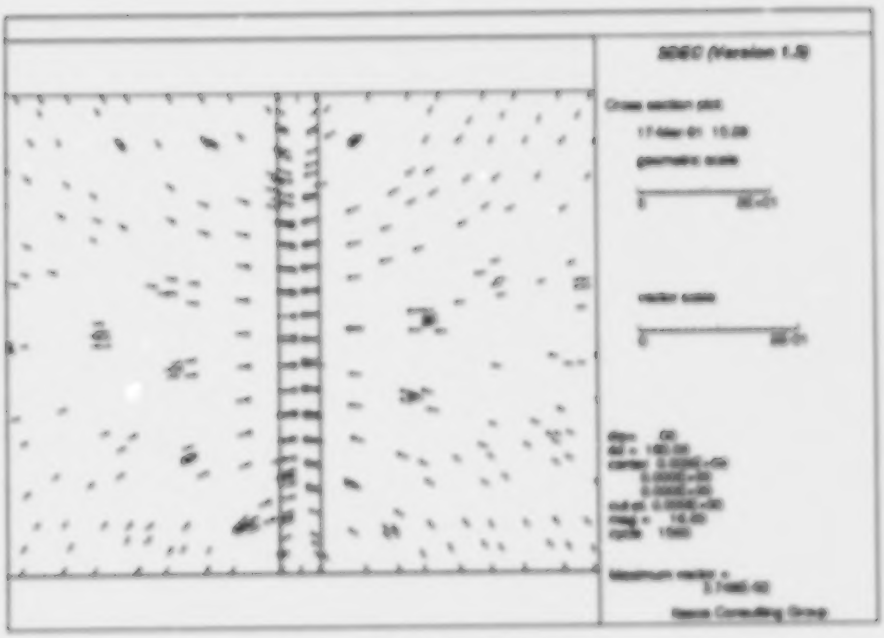

(b) 3DEC Model

Figure 4-37 Displacement Vectors on Horizontal Plane Through Destress Slot

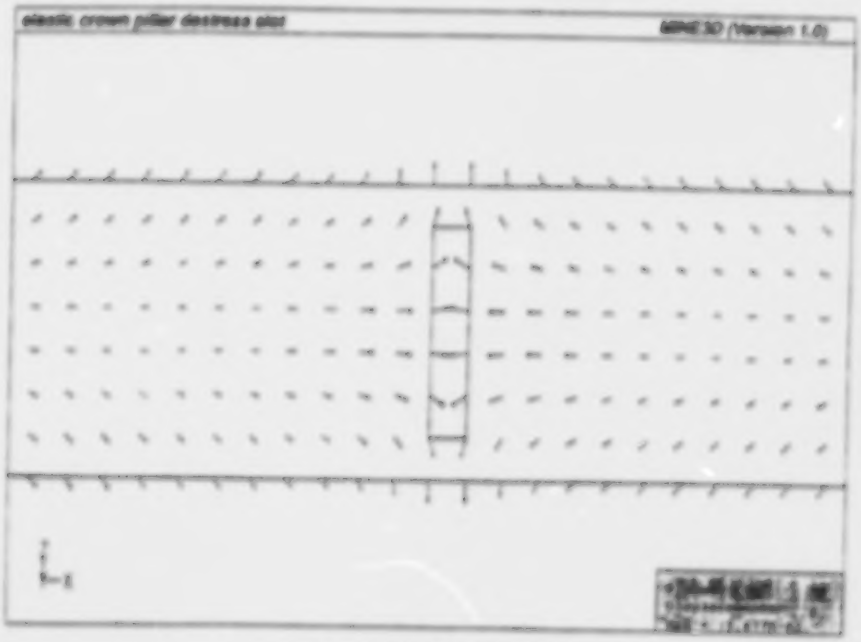

(a) MINE3D Model

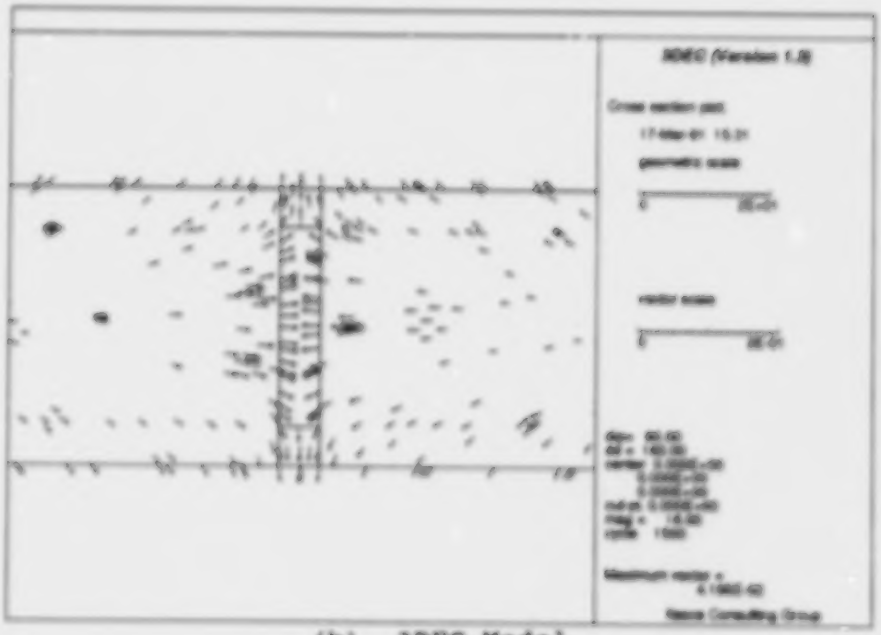

(b) 3DEC Model

Figure 4-38 Displacement Vectors on Vertical Plane Through Destress Slot

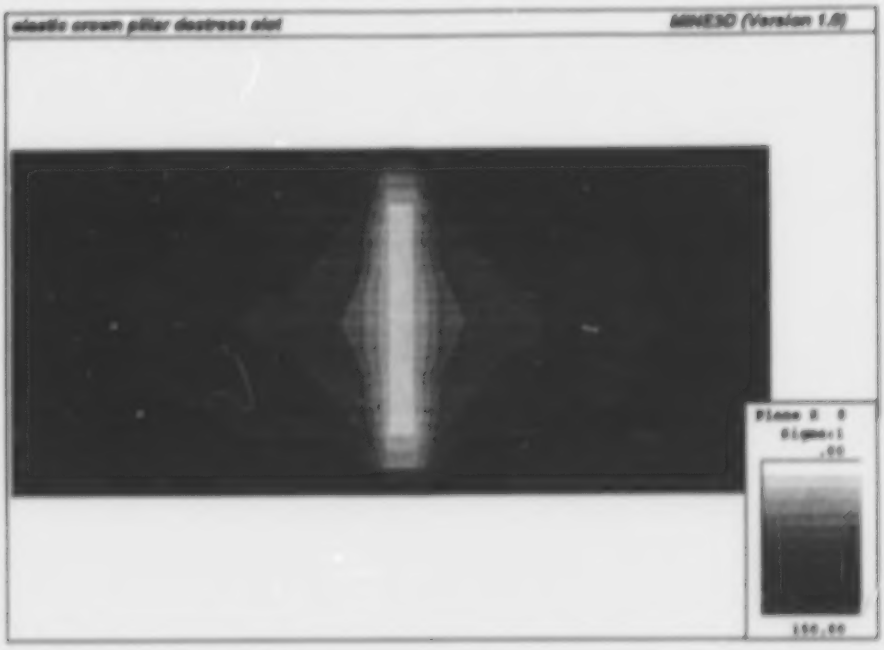

(a) MINE3D Model

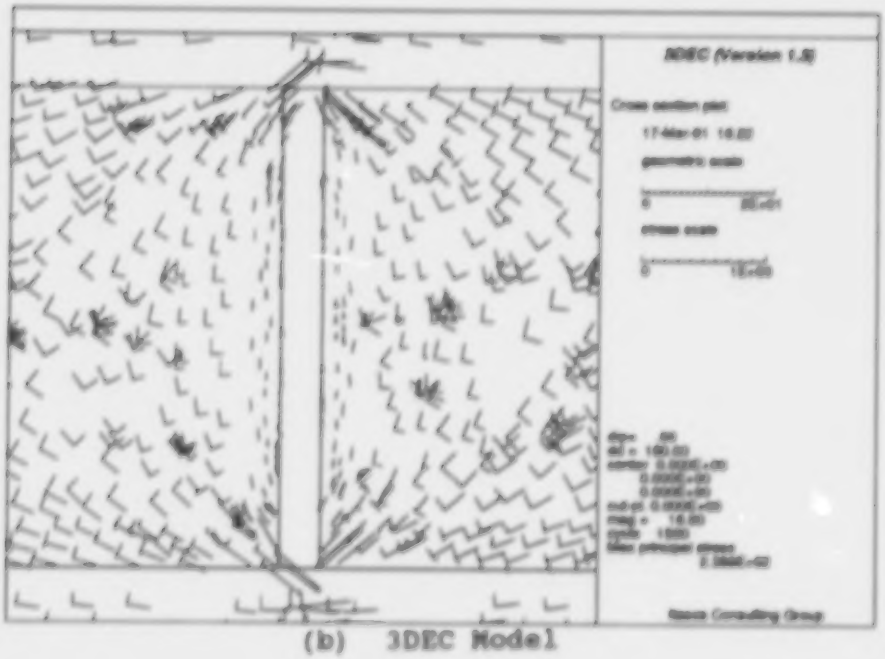

(b) 3DEC Model

Figure 4-39 Principal Stresses on Horizontal Plane Through Destress Slot

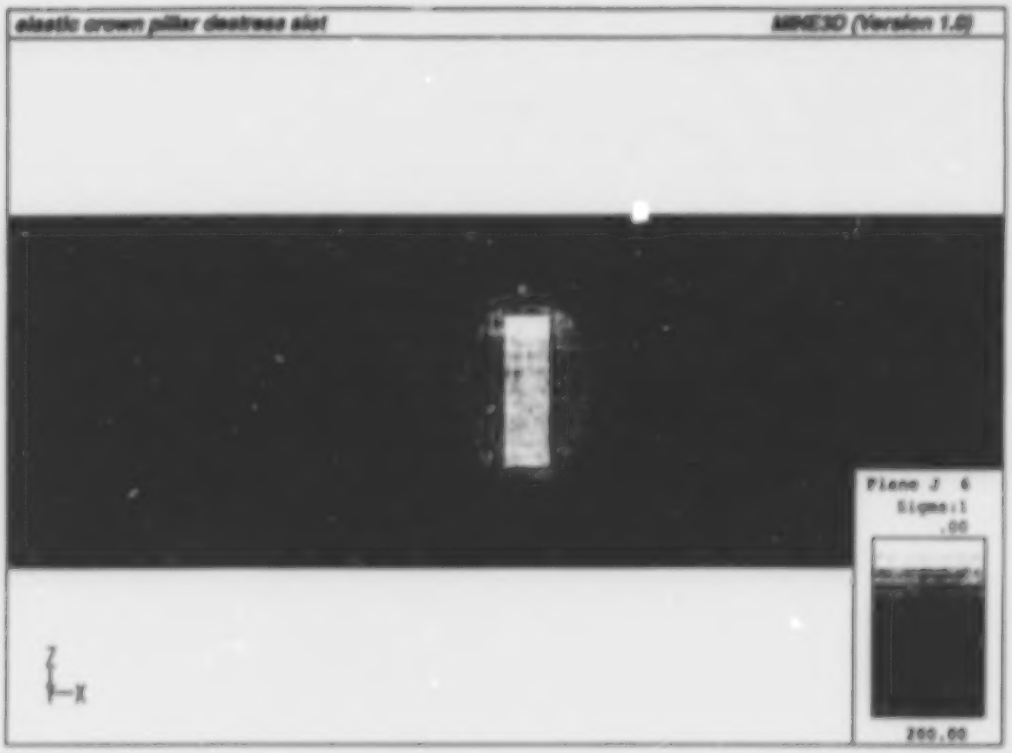

(a) MINE3D Model

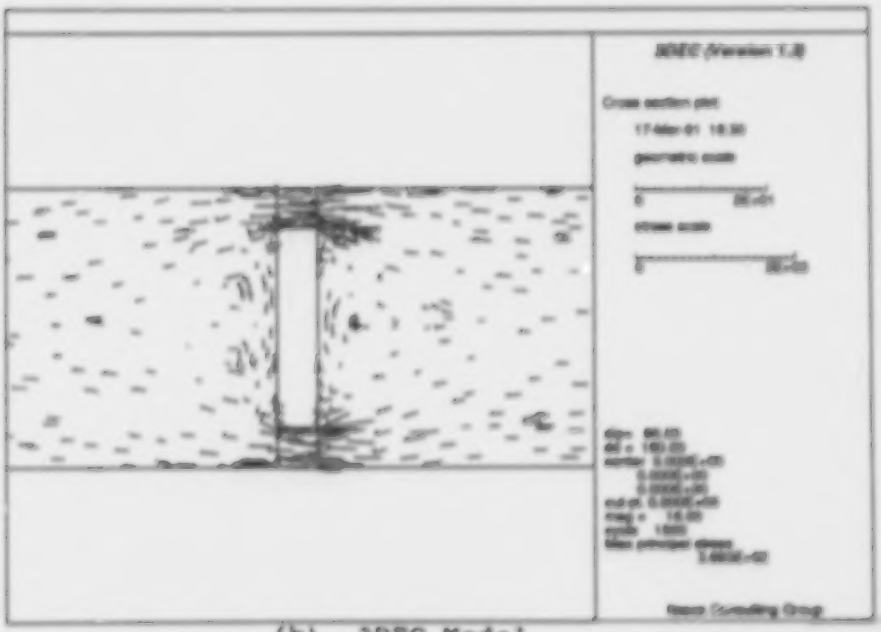

(b) 3DEC Model

Figure 4-40 Principal Stresses on Vertical Plane Through Destress Slot

4.10 Computer Hardware and Run Time Assessment

As discussed in Section 4.3.1, a parallelepiped grid scheme was selected in an attempt to solve as large a three-dimensional problem as possible with the boundary element approach. The requirements for MINE3D (i.e., to simulate local plastic failure and to model multiple materials) impose conditions which necessitate the assembly and storage of significantly more boundary element coefficients than for conventional boundary elements codes. This requirement places a severe restriction on problem size.

A major emphasis of this project was to investigate various methods to optimize MINE3D and test different computer hardware options to increase run time efficiency. The results of this study are presented below.

4.10.1 Coefficient Storage Requirements

There are important differences between MINE3D and conventional boundary element codes which only analyze problems in elasticity. This can best be demonstrated by comparing MINE3D to BEM3D, which is a three-dimensional boundary element code that uses constant strength surface elements for elastic analyses (Wiles, 1988). BEM3D employs planar, quadrilateral-shaped surface elements with a single (three-component) traction vector calculated for each element. Displacements are not calculated with the code.

This differs from MINE3D, where the requirement to model plasticity necessitates the use of linear strength elements and the calculation of four (six-component) stress tensors per element: one at each of the four surface nodes associated with the element.

The difference in storage requirements for the two codes is clearly seen from the following comparison of stress influence coefficients.

For BEM3D, the stress influence coefficients are required for each

n	surface elements with
3	traction components calculated from each of
3	element tractions at each of all other
n	elements at
4	bytes per number, or a total of

36	n^2 bytes of storage.

This requirement was discussed previously in Section 4.3.1.

If the quadrilateral constant-strength elements from BEM3D were extended to linear surface elements, then the stress coefficients are required for each of

n	surface elements with
4	nodes, for which are calculated
6	stress components for each of
3	nodal tractions at each of
4	nodes at each of all other
n	elements with
4	bytes per number, or a total of
1152	n^2 bytes of storage.

By using parallelepiped geometry, the storage requirement is substantially reduced, as described previously in Section 4.3.1. Now, the stress influence coefficients are required for each specified point (N) in space. Thus, the requirement is for

6	stress components for each of
3	nodal tractions at each of
4	nodal points at one of
3	possible orientations at one of
8N	possible spatial distances along the parallelepiped grid at
4	bytes per number, or a total of
6912	N bytes of storage.

The storage in this case is related to the total number of nodes (N) within the parallelepiped grid and not the number of surface elements.

For the destress slot verification test described in Section 4.9.3, the parellelepiped grid was composed of 7254 nodes and 2434 surface elements. If BEM3D were used for this analysis with the same number of surface nodes, the storage requirement for stress influence coefficients would be 213 Mbytes. If BEM3D utilized linear elements, the requirement would be 6824 Mbytes. With MINE3D, the storage requirement for stress coefficients was 50 Mbytes.

In addition to the stress coefficients, there are also surface element displacement coefficients, volume stress coefficients, and volume displacement coefficients required in MINE3D. All of these coefficient arrays are of similar size to the surface stress coefficient array. For example, the surface displacement coefficient array for the destress slot model required approximately 25 Mbytes in MINE3D.

In addition to coefficient storage, there is also a contrast in the number of calculations involved with a solution. Both BEM3D and

MINE3D use the same iterative solution technique. However, for each iteration step, BEM3D calculates for each of

n	elements,
3	traction components based on the
3	traction components at each of the other
n	elements, or a total of

9	n^2 calculations.

For MINE3D, the stress calculation involves

n	elements with
4	nodes per element, for which are calculated
6	stress components from each of
3	traction components at each of the
4	nodes at each of all other
n	elements, or a total of

288	n^2 calculations.

Thus, the number of calculations by MINE3D is at least 32 times more than that by BEM3D. In addition, MINE3D must make displacement calculations and plasticity (volume) calculations in each iteration loop.

4.10.2 Run Time Evaluation

Unfortunately, with the parallelepiped approach, the influence coefficients are accessed non-sequentially. This can greatly influence model run time. For small problems where coefficient array storage can be handled primarily by computer memory, most of the run time is spent in computations. As discussed above the time required to solve a system of equations using an iterative approach is a function of n^2 (n = number of elements) times the number of iterations.

However, for large problems, the computer disk drive is primarily used for array storage (i.e., for typical hardware systems with up to 16 Mb memory). In this case, the run time performance is mainly tied to the efficiency of disk IO and the virtual memory system. It has been found that the performance of virtual memory systems degrades significantly (and abruptly) with increased array size. Figure 4-41 shows a comparison of MINE3D run times (in terms of iteration rate) on three different computers: (1) an IBM-compatible 80386 microcomputer with Weitek coprocessor, 16 Mbytes memory and 120 Mbyte drive; (2) a Sun SPARCStation 1+ with 8 Mbytes memory and 200 Mbyte drive; and (3) a Sun SPARCStation 2 with 16 Mbytes memory and 860 Mbytes drive. The effect of virtual memory performance is clearly seen for all three computers. For example, for the Sun SPARCStation 2, as the number of surface nodes

increases from 1789 to 2080 for two different test problems, the iteration rate jumps from 8 min/iteration to 160 min/iteration, or a factor of 20 increase. Based on computation time alone, this increase should only be factor of 1.4. In the range where performance rate does not drop off, the SPARCStation 2 was found to be two times faster than the SPARCStation 1+ and 5 times than the 80386 with Weitek.

It was also observed that for large problems (i.e., with coefficient arrays greater than roughly 25 Mbytes) 90% and more of the total run time was spent by the system in disk I/O swapping virtual memory.

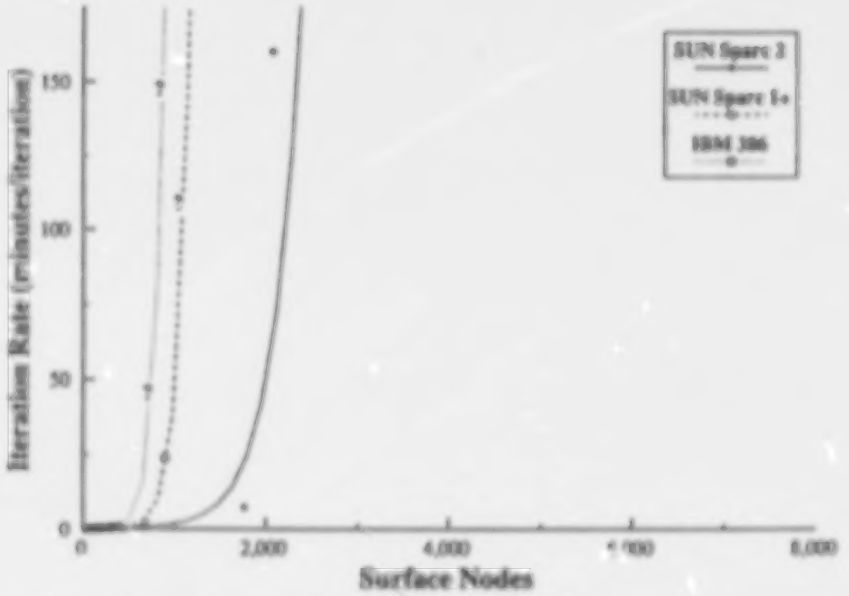

Figure 4-41 Comparison of MINE3D Iteration Rate Versus Number of Surface Nodes for Different Computer Systems

4.10.3 Speed Enhancement Studies

Several techniques were evaluated to reduce the drop-off in performance rate for disk access. Two different ways were evaluated to handle the large arrays: either by using virtual memory, or by writing the arrays in direct access files. On the Sun SPARCstation 1+, the direct access file approach was found to be approximately three times faster than using virtual memory for arrays greater than roughly 25 Mbytes. Also, approximately 70% of the total run time was spent in reading the direct access files. For smaller arrays, the difference in speed was found to decrease.

Unfortunately, the direct access files version of MINE3D performed very poorly on the Sun SPARCstation 2, and ran nearly six times

slower than the virtual memory version. Approximately 98% of the run time was spent in file access. The reason for the poor performance is not understood, but apparently may be related to changes in the operating system on the SPARCstation 2 from that on the SPARCstation 1+.

A considerable effort has been made to order the influence coefficient arrays to ensure that neighboring array elements are used sequentially as much as possible. Intermediate value calculations have been moved outside of loops wherever feasible.

In order to minimize the problem with disk thrashing which results from the non-sequential disk access for influence coefficients, an investigation was made into blocking of multiple coefficient records. This revealed that blocks of 1000 records are required to achieve hit rates above 80%. The extra overhead of the block reads results in a net loss of performance. Additional methods have been considered, such as statistically analyzing the frequency of coefficient usage and placing more commonly used records in core memory, but these have not been investigated.

Another technique which appears promising is to invert the element calculation loop. Currently, the stresses at the element nodes are calculated by calling the required coefficients. It may be possible that by reading a block of influence coefficients and then performing all calculations which utilize these coefficients, the disk access can be reduced. This approach has not been tested.

Ultimately, the key to improving calculations is to find either faster disk hardware or software logic which reduces the disk IO time.

4.11 Conclusions and Recommendations

A three-dimensional boundary element program has been developed for the special purpose of solving problems pertaining to bulk mining in massive orebodies. Program MINE3D has two major distinguishing features: (1) the capability to simulate localized zones of plastic yield which are defined within an elastic infinite body; and (2) the ability to define multiple regions of different material types, thus permitting the simulation of backfill emplacement. MINE3D is formulated such that sequential calculations can be made in order to simulate progressive mining steps involving excavation and backfill. The complete stress state, total displacements and energy release at each step are calculated so that an evaluation can be made of the effect of each mining step. The plasticity influence on stress history is remembered in order to include load path dependency in the solution.

Unfortunately, the computational price that must be paid to utilize

these features in the boundary element method is enormous. As shown in the discussion in Section 4.10, the size of the influence coefficient arrays that must be created in order to perform a plasticity analysis if conventional quadrilateral-shaped elements are used is substantially greater than that for an elasticity analysis. In order to reduce array sizes to a manageable level, a parallelepiped geometry was imposed in the boundary element formulation. By restricting the element geometry, the number of elements which can be modelled within the same storage requirement as that for arbitrary elements is increased dramatically. The nature of bulk mining is such that regularly-shaped excavations are the norm, and the vast majority of problems can be simulated with elements which are restricted to equal-sized parallelepipeds.

As shown by Figure 4-3, using parallelepipeds changes the coefficient storage relation from a quadratic function of the number of boundary element nodes to a linear function. Although this results in greatly reduced storage requirements, the coefficient array size is still large. For three-dimensional problems in bulk mining, the total number of elastic surface elements and plastic volume elements can easily exceed 10,000, and for full mine-scale analysis over 100,000 elements can be required for typical problems. Even with the parallelepiped approach, coefficient arrays can be of the order of 200 Mbytes and higher.

The reason for the great number of boundary elements is the requirement in plasticity analysis to have a fine nodal discretization in the region of anticipated plasticity. As demonstrated in Section 4.9, the grid of volume elements must be sufficiently fine to calculate the stress gradient and plastic deformation accurately. Although the parallelepiped geometry provides a substantial reduction in the coefficient arrays, the number of parallelepiped elements needed for plasticity problems is still large, because the element geometry is uniform throughout the entire modelled region. The approach does not directly permit varying the parallelepiped grid spacing. Consequently, the element spacing required for modelling the localized plasticity accurately must be used throughout the entire model.

In addition to coefficient array size restrictions, plasticity in the boundary element method also imposes a considerable increase in the number of calculations required for problem solution as compared to that for elastic-only boundary elements. As described in Section 4.10, the number of calculations for each solution iteration step is increased by at least a factor of 72 for all the required stress components for the plastic solution. Additionally, displacement calculations and plasticity adjustment calculations are also required.

The storage requirement and calculation intensity necessitates the operation of MINEJD on a computer system with facility for large memory for array storage and rapid access of array coefficients.

Unfortunately, as shown by the study discussed in Section 4.10.2, current computer hardware systems typically available to mining organizations are not capable of providing sufficient memory for array storage without a substantial degradation in performation rate for disk access. A considerable effort was made to try to enhance the array access speed by optimizing the ordering of the arrays in software. This effort, to date, has not provided a sufficient increase in speed to warrant the practical solution of problems containing more than roughly 2,000 surface nodes (see Figure 4.41).

Collectively, these factors pose a fundamental dilemma to the application of a three-dimensional boundary element code with plasticity. While in principle MINE3D can simulate problems associated with bulk mining in massive orebodies, the practical application of this program to actual mining conditions is severely restricted. For example, the destress slot model created in Section 4.9.3 is highly idealized and simplified. Even then, the solution time for this model was more than one week, and this was an elastic problem only. The inclusion of plastic volume elements may be expected to increase the solution time by at least a factor of 2 to 3.

Consequently, this makes the application of MINE3D to a field-scale analysis prohibitive. Months of computer run time would be required on the present systems available in order to perform a series of computations to verify the code for field-scale analysis.

Furthermore, until this dilemma is resolved, it is not warranted to pursue other improvements to the MINE3D program. Two specific areas which were identified to require further study are: (1) the investigation of higher-order elements to resolve the apparently overly-stiff response of the volume elements during plasticity; and (2) the resolution of numerical stability problems associated with reentrant corners. In addition, the inclusion of other features in MINE3D, such as displacement discontinuity logic to simulate discrete fault-slip, is not justified, because such features merely add to the coefficient array storage and number of calculations per iterations.

It is clear that if MINE3D is to be used on a practical basis, either extremely faster disk hardware or larger core memory must be found or a substantial effort be made to develop software logic which reduces disk access time. While some improvements can still be made to reduce the storage requirement in MINE3D to some degree (e.g., additional symmetry constraints may be imposed), this savings is not considered sufficient to enhance solution speed (including array access by more than roughly a factor of 2 or 3.

8.0 REFERENCES

Abramowitz, M. and Stegun, I.A., 1970. Handbook of Mathematical Functions, Dover Publications Inc., New York, New York, U.S.A.

Balas, J., J. Sladek and V. Sladek, 1989. "Stress Analysis by Boundary Element Methods," Studies in Applied Mechanics."

Banerjee, P.K. and Butterfield, R., 1981. Boundary Element Methods in Engineering Science, McGraw-Hill Book Company (UK) Limited, London.

Banerjee, P.K., and Raveendra, S.T., 1986. "Advanced Boundary Element Method for Two and Three-Dimensional Problems of Elastoplasticity," Int. J. Num. Meth. in Engng., 985-1002.

Crouch, S., 1976. "Analysis of stresses and displacements around underground excavations: an application of the displacement discontinuity method", Dept. Civil Engineering., U. of Minnesota, Minneapolis, Minnesota, USA.

Dahlquist, G. and Bjorck, A., 1974. Numerical Methods. Englewood Cliffs, New Jersey: Prentice-Hall.

Greenspan, M., 1944. "Effect of a Small Hole on the Stresses in a Uniformly Loaded Plate," Q. J. Appl. Math., 60-71 (April).

Herget, G., 1987, "Stress assumptions for underground excavations in the Canadian shield", Int. J. Rock Mech. and Min. Sci. & Geo. Abs., V. 24, No. 1, p. 95-97.

Hoek, E. and Brown, E.T., 1980. Underground Excavations In Rock, The Institution of Mining and Metallurgy, London.

Hornbeck, R.W., 1975. Numerical Methods, Quantum Publishers Inc., New York.

Itasca Consulting Group, Inc., 1990. FLAC Version 2.25 User Manual, Minneapolis, Minnesota.

Itasca Consulting Group, Inc., 1987. FLAC - Fast Lagrangian Analysis of Continua (Version 2.00), Minneapolis, Minnesota.

Itasca Consulting Group, Inc., 1991. 3DEC Version 1.30 User Manual, Minneapolis, Minnesota.

Jaeger, J.C. and Cook, N.G.W., 1976. Fundamentals of Rock Mechanics, Chapman and Hall, a Halsted Press Book, John Wiley & Sons Inc., New York, New York, U.S.A.

Johnson, W. and Mellor, P.B., 1973, Engineering Plasticity, Van Nostrand Reinhold Company, London.

Koiter, W.T., "Stress-strain relations, uniqueness and variational theorems for elastic plastic materials with singular yield surface", Q. J. of Applied Mathematics, vol. 11, 1953.

Lachat, J.C., and Watson., J.O., 1976. "Effective Numerical Treatment of Boundary Integral Equations: A Formulation for Three-Dimensional Elastostatics," Int. J. Num. Meth. in Engng., 991-1005.

Landrault, D., 1989, Field monitoring program, Year three interim report on field work for the project "Simulation of Bulk Mining at Depth with Backfill in Ontario Mines", DSS File No. 14SQ.23440-6-9033.

MacDonald, P., Wiles, T. and Villeneuve, T., 1988. "Rock mechanics aspects of vertical retreat mining at 2000-m depth at Creighton mine Canada", Conf. on Applied Rock Engrg., Inst. Min. and Metallurgy, London, England. p. 151-157.

Marti, J., and Cundall, P.A., 1982. "Mixed Discretization Procedure for Accurate Solution of Plasticity Problems", Int. Journal of Numerical Methods in Engineering, No. 6.

Oliver, P.H., Wiles, T. and MacDonald, P., 1987, "Rockburst control measures at INCO's Creighton mine", Proc. 6th Conf. on Ground Control in Min., West Virginia, USA.

Ryder, J.A., 1988. "Excess shear stress in the assessment of geologically hazardous situations", J.S. African Inst. Min. and Metallurgy, p. 27-39.

Salamon, M.D.G., 1984. "Energy considerations in rock mechanics: fundamental results", S. African Inst. Min. and Metallurgy, p. 233-246.

Sloan, S. W., and Randolph, M.F., 1982. "Numerical Prediction of Collapse Loads Using Finite Element Methods," Int. J. Num. & Analy. Meth. in Geomech., p47-76.

Timoshenko, S.P. and Goodier, J.N., 1970. Theory of Elasticity, McGraw-Hill Book Company, New York.

Wiles, T. and Curran, J., 1982. "Use of 3-D displacement discontinuity elements for modelling", Proc. 4th Conf. Num. Methods in Geomechanics, Edmonton, Alberta, Canada. p. 103-111.

Wiles, T. D., 1988. "Accuracy and Applicability of Elastic Stress Analysis Methods in Mining," Proc. of the 15th Canadian Rock Mechanics Symposium, Toronto, Ontario.

Wiles, T. and P. MacDonald, 1988. "Correlation of stress analysis results with visual and microseismic monitoring at Creighton mine", Comp. and Geotech. V.5 p. 105-121.

Wiles, T. D., 1989b, Non-linear modelling of mining at great depth: a case history at Creighton mine", Int. Symp. Rock Mechanics, Pau, France, V 2, p. 621-628.

Zienkiewicz, O.C., 1977. The Finite Element Method, McGraw-Hill Book Company (UK) Limited, London.

6.0 APPENDICES

APPENDIX I	POINT FORCE APPLIED IN AN INFINITE MEDIUM
APPENDIX II	DISTRIBUTED FORCES IN AN INFINITE MEDIUM
APPENDIX III	COORDINATE TRANSFORMATION
APPENDIX IV	SHAPE FUNCTIONS FOR LINEAR VARIATION
APPENDIX V	CORNERS AND EDGES OF POTENTIAL FUNCTIONS
APPENDIX VI	INDICIAL NOTATION
APPENDIX VII	GREEN'S FUNCTION - DISPLACEMENT DISCONTINUITY

APPENDIX I POINT FORCE APPLIED IN AN INFINITE MEDIUM

APPENDIX I - POINT FORCE APPLIED IN AN INFINITE MEDIUM

The effect at x_i of a point force P_i applied at the point ξ_i for two-dimensional plane strain elasticity, is given by

$$c_{111}(x,\xi) = B_1/r^4[\ -(3-2\nu)u_1^3 - (1-2\nu)u_1u_2^2\ ]$$

$$c_{221}(x,\xi) = B_1/r^4[\ -(1-2\nu)u_1^3 - (1+2\nu)u_1u_2^2\ ]$$

$$c_{121}(x,\xi) = c_{211}(x,\xi) = B_1/r^4[\ -(1-2\nu)u_2^3 - (3-2\nu)u_1^2u_2\ ]$$

$$c_{112}(x,\xi) = B_2/r^4[\ -(3-2\nu)u_2^3 - (1-2\nu)u_2u_1^2\ ]$$

$$c_{222}(x,\xi) = B_2/r^4[\ -(1-2\nu)u_2^3 - (1+2\nu)u_2u_1^2\ ]$$

$$c_{122}(x,\xi) = c_{212}(x,\xi) = B_2/r^4[\ -(1-2\nu)u_1^3 - (3-2\nu)u_2^2u_1\ ]$$

where

$$B_i = P_i/[4\pi(1-\nu)]$$
$$r^2 = u_i^2$$
$$u_i = (x_i-\xi_i)$$

APPENDIX II DISTRIBUTED FORCES IN AN INFINITE MEDIUM

APPENDIX II - DISTRIBUTED FORCES IN AN INFINITE MEDIUM

The effect at x_i of a point force P_j distributed at constant intensity on the line segment defined by the end points

$$\xi_1^1,\ \xi_2^1 = \xi_3^1$$
$$\xi_1^2,\ \xi_2^2 = \xi_3^2$$

is given by the integrals of the expressions in appendix I as follows

$$C_{ijk}(x) = \int_{\xi_1^1}^{\xi_1^2} c_{ijk}(x,\xi)\, d\xi_1$$

The required integrals are evaluated as follows:

$$2\int y^3/r^4\,dx = xy/r^2 + \int y/r^2\,dx$$

$$2\int y^2x/r^4\,dx = -y^3/r^2$$

$$2\int yx^2/r^4\,dx = -xy/r^2 + \int y/r^2\,dx$$

$$2\int x^3/r^4\,dx = y^2/r^2 + 2\int x/r^2\,dx$$

$$\int y/r^2\,dx = \tan^{-1}(x/y)$$

$$2\int x/r^3 dx = \ln(r^3)$$

where ln represents a natural logarithm and for clarity x has been substituted for u_1 and y has been substituted for u_2. This also requires that

$$\int d\xi_1 = -\int du_1$$

The effect at x_i of a point force P_i distributed at linear intensity

$$P_i = a + b\xi_1$$

is given by the integrals of the expressions in appendix I as follows

$$Cs_{ijm}(x) = a\int_{\xi_1^j}^{\xi_1^i} c_{ijm}(x,\xi)\, d\xi_1 + b\int_{\xi_1^j}^{\xi_1^i} c_{ijm}(x,\xi)\,\xi_1 d\xi_1$$

The additional integrals are evaluated as follows:

$$\int xy^3/r^4 dx = y\int y^2 x/r^4 dx$$

$$\int x^2y^3/r^4 dx = y\int yx^2 x/r^4 dx$$

$$\int x^3y/r^4 dx = y\int x^3/r^4 dx$$

$$\int x^4/r^4 dx = \int x^2/r^2 dx - \int y^2x^2r^4 dx$$

$$\int x^3/r^3 dx = x\int y/r^3 dx$$

The effect at x_i of a point force P_i distributed at constant intensity on the triangle defined by the corner points

$$\begin{matrix} \xi_1^1, & \xi_2^1 \\ \xi_1^2, & \xi_2^2 \\ \xi_1^3, & \xi_2^3 \end{matrix}$$

is given by the integrals of the expressions in appendix I as follows

$$CD_{ij\alpha}(x) = \sum_{p=1}^{3} \int_{\xi_2^p}^{\xi_2^q} \int_{\xi_1^p}^{\xi_1^q} c_{ij\alpha}(x,\xi)\, d\xi_1 d\xi_2$$

such that when p equals one, two and three, q equals respectively two, three and one. To evaluate these integrals define each side of the triangle as

$$y = Dx + E$$

where the constants D and E can be determined as in appendix IV and for clarity x has been substituted for u_1 and y has been substituted for u_2. This requires that

$$\iint d\xi_1 d\xi_2 = \iint du_1 du_2$$

Then

$$r^2 = Ax^2 + Bx + C$$

where

$$A = D^2 + 1$$

$$B = 2DE$$

$$C = E^2$$

The required integrals are evaluated as follows:

$$2\iint x^3/z^4\,dx\,dy = \int [\ xy/z^3 + \tan^{-1}(y/x)\ ]\,dx$$

$$2\iint x^3/z^4\,dx\,dy = \int [\ -xy/z^3\ ]\,dx$$

$$2\iint xy^2/z^4\,dx\,dy = \int [\ -xy/z^3 + \tan^{-1}(y/x)\ ]\,dx$$

$$2\iint y^3/z^4\,dx\,dy = \int [\ x^2/z^3 + \ln(z^2)\ ]\,dx$$

Now, specializing for the side of the triangle and substituting for y, the remaining integrals are evaluated as follows:

$$E\int 1/z^3\,dx = \tan^{-1}[(2Ax+B)/(2E)]$$

$$2A\int x/z^3\,dx = \ln(z^2) - B\int 1/z^3\,dx$$

$$A\int x^2/z^3\,dx = x - B\int x/z^3\,dx - C\int 1/z^3\,dx$$

$$A\int x^3/z^3\,dx = x^2/2 - B\int x^2/z^3\,dx - C\int x/z^3\,dx$$

$$\int \tan^{-1}(y/x)\,dx = x\tan^{-1}(y/x) + E\int x/z^3\,dx$$

$$\int \ln(x^2)\,dx = x \ln(x^2) - 2A\int x^2/x^2\,dx - B\int x/x^2\,dx$$

APPENDIX III COORDINATE TRANSFORMATION

APPENDIX III - COORDINATE TRANSFORMATION

The coordinate transformations are given by

$$x_i' = A_{ij}(x_j - x_j^*)$$

where A_{ij} represent direction cosines for the x_i' axis and x_j^* represents the origin of the local coordinate system.

The transformation from local to global coordinates is easily found as

$$x_i = A_{ij}x_j' + x_i^*$$

by noting that

$$A_{ij}^{-1} = A_{ji}$$

STRESS TRANSFORMATION

The components of stress, parallel to the global coordinate axes, acting on the plane whose normal is defined by the direction of the local axes x_i' are given by

$$X_{ik} = A_{ij}\sigma_{kj}$$

where σ_{kj} are the components of stress in global coordinates. The components of stress, parallel to the local coordinate axes are found from

$$\sigma_{ij}' = A_{jk}X_{ik}$$

then substituting for X_{ik}

$$\sigma_{ij}' = A_{jk}A_{ij}\sigma_{kj}$$

The transformation from local to global coordinates is determined by using the inverse of A_{ij} giving

$$\sigma_{ij} = A_{ik}A_{jl}\sigma'_{kl}$$

STRAIN TRANSFORMATION

The displacements in terms of a local coordinate system defined by x_i' can be found by applying the coordinate transforms used above

$$u_i' = A_{ik}u_k$$

The strain components in terms of the local coordinate system can be found by applying the chain rule for partial derivatives as follows

$$\frac{\partial u_i'}{\partial x_j} = \frac{\partial u_i'}{\partial x_k}\frac{\partial x_k}{\partial x_j}$$

Noting that

$$\frac{\partial x_k}{\partial x_j} = a_{jk}$$

and substituting for the displacements in terms of global coordinates, it can be found that

$$\frac{\partial u_i'}{\partial x_j} = A_{ik}\frac{\partial u_k}{\partial x_l}A_{jl}$$

Substituting these into the strain-displacement relations in terms of local coordinates

$$\epsilon_{ij}' = (u_{i,j}' + u_{j,i}')/2$$

it can be found that

$$\dot{e}_{ij} = A_{ik}A_{jl}(u_{k,l} + u_{l,k})/2$$

or

$$\dot{e}_{ij} = A_{ik}A_{jl}\dot{e}_{kl}$$

The transformation from local to global coordinates is determined by using the inverse of A_{ij} giving

$$\dot{e}_{ij} = A_{ki}A_{lj}\dot{e}_{kl}$$

It can be observed that these transforms are identical to those for transformation of stresses.

APPENDIX IV SHAPE FUNCTIONS FOR LINEAR VARIATION

APPENDIX IV - SHAPE FUNCTIONS FOR LINEAR VARIATION

The required function has the form

$$P(\xi) = a_0 + a_1\xi_1$$

where the constants a_0 and a_1 can be determined by evaluation of this equation at the known points ξ_1^p where $P(\xi^p)$ takes on the value P^p, giving

$$P^p = a_0 + a_1\xi_1^p$$

This can be expanded into matrix form for the case of two independent unknowns, as follows

$$\begin{bmatrix} 1 & \xi_1^1 & \xi_2^1 \\ 1 & \xi_1^2 & \xi_2^2 \\ 1 & \xi_1^3 & \xi_2^3 \end{bmatrix}$$

The matrix can be inverted to give the constants a_0 and a_1

$$\begin{bmatrix} P^1 \\ P^2 \\ P^3 \end{bmatrix} = \begin{bmatrix} 1 & \xi_1^1 & \xi_2^1 \\ 1 & \xi_1^2 & \xi_2^2 \\ 1 & \xi_1^3 & \xi_2^3 \end{bmatrix} \begin{bmatrix} a_0 \\ a_1 \\ a_2 \end{bmatrix}$$

The first row of the inverted matrix defines the vector N^{0p} such that

$$a_0 = \sum_{p=1}^{n} N^{0p} P^p$$

where for this example M equals three. The remaining rows of the inverted matrix defines the vectors N^{ip} such that

$$a_i = \sum_{p=1}^{n} N_i^{ip} P^p$$

and hence the expression

$$P(\xi) = a_0 + a_1\xi_1$$

becomes

$$P(\xi) = \sum_{p=1}^{n} \left(\delta^{qp} + \sum_i N_i^{(p)}(\xi_j)\right) P^p$$

For the case of a surface boundary element (straight line segment) used in two-dimensional analysis, there is only one independent variable ξ_1 and therefore two known values of P^p must be supplied. For surface boundary elements used in three-dimensional analysis and internal elements used in two-dimensional analysis (planar triangles), there are two independent variable ξ_1 and ξ_2 and therefore three known values of P^p must be supplied. For internal elements used in three-dimensional analysis (tetrahedron), there are three independent variable ξ_1, ξ_2 and ξ_3 and therefore four known values of P^p must be supplied.

APPENDIX V CORNERS AND EDGES OF POTENTIAL FUNCTIONS

APPENDIX V - CORNERS AND EDGES OF POTENTIAL FUNCTIONS

The equation of line through (x_1,y_1,z_1) and (x_2,y_2,z_2) with direction (a,b,c) is given by

$$(x-x_1)/a = (y-y_1)/b = (z-z_1)/c$$

$$a=x_2-x_1 \quad b=y_2-y_1 \quad c=z_2-z_1$$

The equation of plane through (x_3,y_3,z_3) with normal direction (a,b,c) is given by

$$ax + by + cz = ax_3 + by_3 + cz_3$$

The intersection of the line and plane at the point (x−,y−,z−) is given by

$$(x_4-x_1)/a = (y_4-y_1)/b = (z_4-z_1)/c$$

$$= a(x_3-x_1) + b(y_3-y_1) + c(z_3-z_1) = d$$

The equation of a line through (x_3,y_3,z_3) and (x_4,y_4,z_4) is given by

$$(x-x_4)/A = (y-y_4)/B = (z-z_4)/C$$

where the direction (A,B,C) can be found as

$$A = x_3-x_4=x_3-x_1 - ad$$
$$B = y_3-y_4=y_3-y_1 - bd$$
$$C = z_3-z_4=z_3-z_1 - cd$$

APPENDIX VI INDICIAL NOTATION

APPENDIX VI - INDICIAL NOTATION

A_i are the components of the vector A_1, A_2, $\cdots$, where i varies from 1 to 2 in two dimensions, and from 1 to 3 in three dimensions.

A_{ij} are the components of the tensor A_{11}, A_{12}, A_{21}, $\cdots$, where both i and j vary over their complete range.

$A_{i,j}$ represents the differentials $\partial A_i/\partial x_j$.

$A_i = B_{i,j}C_j$ represents the sum of the products of the components of the tensor B with the vector C such that $A_i = B_{i1}C_1 + B_{i2}C_2 + \cdots$, where j varies over its complete range.

$A_i = B_{i,j}$ represents the sum of the differentials of the components of B with respect to x such that $A_i = \partial B_i/\partial x_1 + \partial B_i/\partial x_2 + \cdots$, with j varying over its complete range.

APPENDIX VII GREEN'S FUNCTION - DISPLACEMENT DISCONTINUITY

APPENDIX VII - GREEN'S FUNCTION - DISPLACEMENT DISCONTINUITY

The effect at x_i of a discontinuity in displacement Γ_i, applied at the point ξ_i for two-dimensional plane strain elasticity, is given by (Wiles and Curran, 1982)

$$
\begin{aligned}
g'_{11}(x,\xi) &= D_1/(2G)\,[\,-(1-2\nu)\zeta_2/r^2 - 2\zeta_2\zeta_1^2/r^4\,] \\
g'_{21}(x,\xi) &= D_1/(2G)\,[\,-(1-2\nu)\zeta_1/r^2 - 2\zeta_2^2\zeta_1/r^4\,] \\
g'_{12}(x,\xi) &= D_2/(2G)\,[\,\ (1-2\nu)\zeta_1/r^2 - 2\zeta_1\zeta_2^2/r^4\,] \\
g'_{22}(x,\xi) &= D_2/(2G)\,[\,-(3-2\nu)\zeta_2/r^2 + 2\zeta_1^2\zeta_2/r^4\,]
\end{aligned}
$$

$$
\begin{aligned}
c'_{111}(x,\xi) &= 2D_1/r^6\,[\ 3\zeta_1^3\zeta_2 - \zeta_1\zeta_2^3\,] \\
c'_{221}(x,\xi) &= 2D_i/r^6\,[\ 3\zeta_2^3\zeta_1 - \zeta_2\zeta_1^3\,] \\
c'_{121}(x,\xi) &= c'_{211}(x,\xi) = c'_{112}(x,\xi)
\end{aligned}
$$

$$
\begin{aligned}
c'_{112}(x,\xi) &= D_2/r^6\,[\,-\zeta_1^4 - \zeta_2^4 + 6\zeta_1^2\zeta_2^2\,] \\
c'_{222}(x,\xi) &= D_2/r^6\,[\,-\zeta_1^4 + 3\zeta_2^4 - 6\zeta_1^2\zeta_2^2\,] \\
c'_{122}(x,\xi) &= c'_{212}(x,\xi) = c'_{221}(x,\xi)
\end{aligned}
$$

where

$$
\begin{aligned}
D_i &= \Gamma_i/[4\pi(1-\nu)] \\
r_2 &= \zeta_i^2 \\
\zeta_i &= (x_i-\xi_i)
\end{aligned}
$$